Ammonia monitor based on intermodulated CO_2 laser photoacoustic Stark spectroscopy

ISh SS2009

J. J. A. M. Sauren

Ammonia monitor based on intermodulated CO_2 laser photoacoustic Stark spectroscopy

STELLINGEN

behorende bij het proefschrift

Ammonia monitor based on intermodulated CO_2 laser photoacoustic Stark spectroscopy

van

J.J.A.M. Sauren

[1]

Door gebruik te maken van zowel het Stark effect als intermodulatie technieken, is het mogelijk via fotoakoestische detectie ammoniak op een relatief eenvoudige wijze in de buitenlucht te meten. *Dit proefschrift.*

[2]

Een dun metalen stripje, aan één kant ingeklemd in een blok, kan als geluidsbron in fotoakoestische experimenten gebruikt worden voor de bepaling van de gevoeligheid van fotoakoestische meetmicrofoons als functie van de druk . *Dit proefschrift.*

[3]

Theoretisch is bewezen dat Photothermische technieken honderd keer gevoeliger zijn dan Photoacoustische technieken (F.Lepoutre, J.de Physique, 688, (1985)).
Sub-ppbv detectie van atmosferisch ammonia moet daarom in de toekomst eerder van de eerste dan van de tweede techniek verwacht worden.

[4]

In gepulste photoacoustische experimenten kan door het plaatsen van een parabolische akoestische reflector de detectiegevoeligheid met een orde van grootte verhoogd worden.
I.Carrer, L.Fiorina, E.Zanzottera, 7th International Topical Meeting on Photoacoustics and Photothermal Phenomena, Conference Digest, 401-402 (1991).

[5]

Voor fotoakoestische metingen van sporengassen waarin gebruik wordt gemaakt van resonante fotoakoestische meetcellen met hoge versterkingsfactoren Q (Q>50), is het noodzakelijk de veranderingen in chemische samenstelling en temperatuur van het te analyseren gasmonster correct te ondervangen door de resonantiefrequentie van de meetcel instantaan te meten en electronisch bij te regelen.
Gy.Z.Angeli, Z.Bozóki, A.Miklós, A.Lörincz, A.Thöny and M.Sigrist, Rev.Sci.Instrum., 62, 810-813, (1991).

[6]

Voor het meten van de absolute waarde van de warmtegeleidingscoefficient met behulp van de niet-stationaire naaldmethode dienen de meetnaaldkarakteristieken voor verschillende ijkstoffen bepaald te worden.

W.van Loon, Heat and Mass Transfer in Frozen Porous Media, 123-131, proefschrift Landbouwuniversiteit Wageningen (1991).

[7]

Opschaling van plantprocessen naar gebiedsprocessen in berekeningen van meteorologische parameters (verdamping, fotosynthese) staat gelijk aan het zoeken van een naald in een hooiberg. Derhalve kunnen dit soort technieken beter achterwege gelaten worden. M.Rapach, Canopy Transport Processes, in: "Forward Transport in the Natural Environment" Springer Verlag (1988).

[8]

In meteorologische energiebalans berekeningen nabij het aardoppervlak worden de warmtecapaciteit van bodem en vegetatie maar ook de fotosynthese onterecht verwaarloosd. A.F.J.Jacobs en A.van Pul, Conference Agricultural Forrest Meteorology (1991).

[9]

Een goed abstract is niet abstract.

[10]

In het LU-regelement is een equivalent genomen van "omstreeks 5000 studie belastingsuren als norm voor het promotieonderzoek en de afronding daarvan". Dit equivalent is i.h.a. een onderschatting van de hoeveelheid werk en een overschatting van de capaciteiten van de promovendus.

[11]

Het dragen van een walkman kan een teken van sociale armoede zijn.

[12]

Het verdwijnen van de overtreffende trap in het Nederlands is een teken van de invloed van de Engelse taal.

Was wir besiegen, ist das Kleine,
und der Erfolg selbst macht uns klein.
Das Ewige und Ungemeine,
will nicht von uns gebogen sein.

    R.M. Rilke

jeschreëve vuur der Pap enn de Mam

Voorwoord

Hoewel dit proefschrift de naam van slechts één persoon draagt, zijn de resultaten weergegeven in dit boekje totstand gekomen door het werk en de inzet van velen. Dank verschuldigd ben ik aan:

mijn begeleider Dane Bićanić: Cijenjeni co-promotor, dragi Dane. Četiri godine, od dec.'87 do dec.'91 si me ti vodio. Na sljedećim stranicama možeš pročitati rezultat svojih napora. Sada, dok ovo pišem, nije mi lako točno opisati svoje osjećaje gledajući ovu doktorsku radnju. Jednu stvar znam sigurno, Dane. Ovo nisam mogao ostvariti bez tebe. Tok istraživanja kroz ove četiri godine je često bio promjenljiv kao godišnja doba: bilo je sunca, ali isto i kiše. Posebno za kišnih razdoblja stajao si ne nad menom, nego uz mene. Dane, ako sam te u ove četiri godine ikada razočarao, žao mi je iskreno. Sada kada sam gotov i gledam unatrag, znam sigurno da sa naučnom obukom, koju sam od tebe dobio, mogu sa punim povjerenjem početi rad u Kingston-u. Bude li poteškoća u tom istraživanju, misliti ću na tebe, prijatelju, jer to si za mene postao, počevši kao Dr.Dane Bićanić, a završivši kao Dane, prijatelj. Hvala ti na svemu, Dane, a takoder bi se želio zahvaliti tvojoj ženi Vesni i djeci Ivi i Timiju da su mi dozvolili uzeti toliko tvog vremena za sebe. Nadam se da ću jednom imati šansu voditi svog promovendusa na isti način kao što si ti to radio samnom.

Professor Jörg Reuss voor de betoogde steun en de klare, "to the point" begeleiding tijdens de vier Wageningse jaren. Geachte promotor, beste Jörg, door jouw hulp heb ik dit laatste, voor mij spannende, jaar meerdere hindernissen tegelijk kunnen nemen en overwinnen. De inzet en hulp van Professor Antoni Dymanus, Professor Dave Parker, Hans Ter Meulen, Leo Meerts, Frans Harren, Frans Bijnen, Frans van Rijn, John Holtkamp, Cor Sikkens, Eugène van Leeuwen, Leo Hendriks, Annette van der Heijden, John van Bladel, Henk Neijenhuizen en Gerrit van der Sanden, allen verbonden aan de Katholieke Universiteit Nijmegen, heb ik zeer gewaardeerd.

Professor Eep Adema die zich van de lastige taak gekweten heeft als promotor namens de Landbouwuniversiteit op te treden. Zijn kritische opmerkingen en aantekeningen betreffende het luchtverontreinigingsgedeelte hebben hun plaats in het proefschrift gevonden.

Henk Jalink die aan de basis gestaan heeft voor ontwikkeling en technische vervolmaking van de Stark cel en de nieuwe CO_2 laser. Beste Henk, de drie jaren waarin we samengewerkt hebben zijn voor mij de vruchtbaarste geweest. Dane's alles verzengende energie gekoppeld aan jouw technisch-fysisch inzicht vormden de ideale basis voor het beslechten van de legio schier onoverwinbare problemen waarmee ik geconfronteerd werd.

András Miklós for technical and theoretical support on many subjects concerning the intermodulated photoacoustic detection of ammonia. Dear András, to me, your scientific knowledge has not been surpassed. Although being intellectually my superior, you have always tried to explain physical facts in a simple and modest way. The help and support of your wife Judit Angster and your collegues, Zoltán Bozóki, Györgi Angeli and Anikó Sólyom, all associated with the Institute of Isotopes, Budapest, Hungary, has lead to the major breaktrough in July 1990 when "IMPASS" was born.

the godfather of Intermodulated Photoacoustic Stark Spectroscopy, the late Professor Eugène Strauss of Georgia Tech University in Athens, Georgia. Your abrupt passing away was a shock to all of us. Without your help "IMPASS" detection of ammonia would simply not have existed today.

Anton Jansen, Willy "Maradonna" Hillen, Hennie "The Dressman" Boshoven, Teun Jansen, Dik Welgraven en Peter Lam voor de technisch-mechanische ondersteuning tijdens

la femme dans ma vie. Chère Marie-Claude, je te remercie pour ton soutien et ta confiance qui, tout au long de ces deux dernières années, m'ont permis d'achever cette thèse.

mijn ouders en broer Jos. Hun bijdrage tot het slagen van mijn promotieonderzoek overschrijdt de marge van dit boekje. Leeve Pap, Mam en Jos, ohne uunge isatz, vertroowe en heulup heij iech ut werrik nit kenne doë. Iech dank uuch vuur alles.

Contents

Preface

This study is concerned with the development, construction and testing in the practice of a prototype CO_2 laser photoacoustic monitor for interference-free and 'on-line' detection of ammonia trace gas concentration levels in the ambient air.

The motivation for conducting research towards the development and testing of a novel field type ammonia detector was a two-fold one. It was proposed to employ optical methods and in particular CO_2 laser photoacoustic spectroscopy, as a possible candidate technique to overcome the problems of spectral interferences (met with conventional photoacoustic ammonia monitors). Secondly, there is a demand for an ammonia point sensor capable of trace level detection and fast signal response times (10 sec or less). This last requirement is important in atmospheric chemistry and in research studies concerned with gas flux measurements revealing the net upward or downward ammonia transport rates from the atmosphere to the ground level and vice-versa (deposition and uptake by vegetation).

At the time of writing this thesis (1991), optical detection of ambient ammonia is mainly performed by long-path spectroscopic absorption measurements. The systems most commonly encountered in the practice of air-pollution monitoring are tunable diode laser absorption spectroscopy (TDLAS) and differential absorption spectroscopy (DOAS). Both are based on the proportionality existing between the attenuation of a light beam due to molecular absorption and the (average) gas concentration along its optical path (Lambert-Beer's law). As the concentration of air-pollutants is normally very low, long pathlengths (hundreds to thousands of meters) are required in order to achieve detection sensitivity at ppbv-level ($1:10^9$ in units of volume). A distinctive drawback common to DOAS and TDLAS is the poor spatial resolution as the absorption measurements only reveal the averaged gas concentration along the optical path. As a consequence, these systems are of little use in gas flux measurements. However, by incorporating sophisticated techniques a reasonable degree of spatial resolution has been reported in the literature[1].

Attempts towards detecting ambient ammonia using CO_2 laser photoacoustics as a point sensor have lately received attention within the scientific community. The utilization of a CO_2 laser in trace detection of ammonia is advantageous for different reasons. To start with ammonia exhibits several strong absorption lines in the CO_2 laser wavelength region. The availability of high laser output powers (few Watts) is of benefit in photoacoustic detection as the generated acoustic signal is proportional to the laser power and the concentration of the gas absorbing the laser radiation. Secondly, the wavelength tunability of the CO_2 laser enables the experimentalist (to some extent) to deal with the problem of spectral interference that is frequently encountered when working with gas samples consisting of more than one absorbing constituent.

The photoacoustic experiments on ambient ammonia detection reported in the literature, utilize the 'classical' photoacoustic arrangement in which the gas sample is flown through a chamber (either acoustically resonant or non-resonant). Employing a radiation beam from a chopped CO_2 waveguide laser, the modulated radiation absorbed by the gas confined in the cell generates pressure fluctuations that are detected by a suitable transducer (normally a microphone). The resulting electric microphone signal is processed by phase sensitive detection techniques. The physical factors limiting the sensitivity of 'classical' photoacoustic ammonia detection in the practice are molecular spectral interferences, the

kinetic cooling effect and the cell window noise. Additionally, all photoacoustic experiments performed so far reported the annoying effect of ammonia adsorption to the photoacoustic cell walls.

The prototype ammonia monitoring system described in this thesis is based on the combined use of a traditional beam chopped $^{12}C^{16}O_2$ laser photoacoustic spectroscopy (frequency f_{chop}), Stark modulation (frequency f_{Stark}) and intermodulation spectroscopy respectively. The photoacoustic signal generated at either the sum $(f_{chop}+f_{Stark})$ or the difference $(f_{Stark}-f_{chop})$ sidebands of the modulated laser and Stark electric fields (heterodyne frequency mixing) is detected at $f_{det}=f_{Stark}\pm f_{chop}$, using lock-in technique and a photoacoustic cell the resonant frequency of which equals f_{det}.

Employing such hyphenated technique, the kinetic cooling effect, the spectral interferences (due to the absorption of water vapor and carbon dioxide at the 10R(6) and 10R(8) $^{12}C^{16}O_2$ laser lines used) as well as the window noise, were all effectively suppressed. At present the achieved (2-3 ppbv NH_3) detection sensitivity is limited by the system's overall noise (lock-in amplifier, signal preamplifiers and gas flow noise), the restricted range of Stark electric field strengths ($E_{Stark} \leq 6$ kV/cm) and the moderate laser output power ($P_{laser} \leq 2.5$ Watts) respectively. In addition, the adsorption of ammonia to the walls of the photoacoustic cell shows to be dependent on the amount of water vapor present in the gas sample: the chemical gas phase equilibrium between ammonia and water vapor changes as a result of variation in water vapor content thereby affecting the magnitude of the recorded photoacoustic signal and the response time of the system.

Outline of this thesis

This thesis is divided into 5 chapters. In Chapter 1 (Introduction) the need for a fast and accurate NH_3-sensor and the importance of gaseous ammonia in atmospheric chemistry and air-pollution science are discussed. The problems frequently encountered in the practice when employing the 'classical' CO_2 laser photoacoustic detection mode are described too. InterModulated Photoacoustic Stark Spectroscopy (IMPASS) is proposed as a technique to surmount difficulties of the classical photoacoustic detection mode previously described and the mathematics of its operational principles given.

Chapter 2 (Spectroscopy of Ammonia) is devoted to absorption features of ammonia in the 9-11 μm region and other molecules largely abundant in the atmosphere. This chapter is completed by a short theoretical description of the Stark effect induced in ammonia and the narrowing of molecular linewidths at reduced working pressure ($P_{gas}=200$ mbar).

Chapter 3 (Constructional Details) deals with an improved design of the CO_2 waveguide laser constructed in this laboratory and used during the course of all IMPASS ammonia experiments. The results of experimental studies performed on the adsorption of ammonia to various surfaces, the material choice and the constructional details of the photoacoustic Stark cell are discussed in three published articles (3.3, 3.4, and 3.5).
The optical and the electronic components of the IMPASS detection scheme are presented.

The chapter is closed by a novel method used for the calibration of microphones at reduced gas pressures without making use of an actual calibrated gas mixture (section 3.6).

Ammonia measurements performed in the IMPASS mode using a simulated atmosphere as well as realistic air samples are discussed in Chapter 4.

Closing remarks concerning the outlook and suggestions that might lead to an improved performance are summarized in Chapter 5 at the end of the thesis.

Chapter 1   Introduction

Atmospheric deposition (tons*km^{-2}*y^{-1}) of ammonia (NH$_3$) in The Netherlands is found to be the highest among the northern and western European countries. The high deposition of NH$_3$ originates almost entirely from emission sources in The Netherlands itself. Table I shows the total anthropogenic NH$_3$ emissions in Europe around 1980[2].

Emissions 1980 (tons per km^2)	
Albania	0.73
Belgium	2.46
Bulgaria	0.67
Denmark	1.98
Finland	0.11
France	0.97
F.R.G.	1.43
G.D.R.	1.37
Greece	0.33
Hungary	0.75
Ireland	2.14
Italy	0.73
The Netherlands	3.10
Norway	0.08
Poland	0.99
U.K.	1.49

Table I. Total anthropogenic ammonia emissions in Europe around 1980

The dominant agricultural NH$_3$ emission sources are livestock wastes. Maximum monthly-mean NH$_3$ concentrations of 55 ppbv have been measured in areas with concentrated livestock breeding[3]. Hourly-mean NH$_3$ concentrations as high as 90 ppbv have been found after manure deposition on agricultural fields. However, these figures largely exceed the NH$_3$ concentration levels measured in other parts of the country (< 10 ppbv). Numerous reports concerning the ecological conditions of Dutch forests indicate leaching of potassium (K), magnesium (Mg) and Calcium (Ca) from the soil and leaves due to high atmospheric NH$_3$ concentrations (> 100 ppbv). Ecophysiological experiments proved that increased ammonium to potassium ratios inhibit the growth of symbiotic fungi and the uptake of potassium and

4

magnesium by the root system. This again can lead to a deficiency of both elements, severe nitrogen stress and as a consequence, premature shedding of leaves or needles[4]. Deposition of ammonia can also cause nitrification in soil, surface and ground waters according to the following chemical reactions:

$$NH_3 + H_2O \leftrightarrow NH_4^+ + OH^-$$

$$NH_4^+ + 2O_2 \rightarrow 2H^+ + NO_3^- + H_2O$$
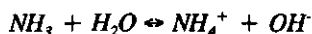
Under steady state conditions the NH_3 deposition is determined from measuring gas concentrations at different sample points i (point source measurements revealing the concentrations $C_{NH3,i}$) along a vertical line[5], i.e.

$$F_{NH3} = -K_z (dC_{NH3,i}/dz)$$

where K_z is the average eddy diffusity, z is the height measured with respect to the ground level and F_{NH3} is the ammonia flux. In order to calculate gas fluxes and to correlate different concentrations $C_{NH3,i}$ the ammonia monitor used in such flux experiments must be fast and sensitive in the 1-100 ppbv concentration range.

The commonly used NH_3 gas point sensor is the one based on the catalytic conversion of NH_3 to NO_x in a high temperature oven and subsequent detection of the reaction product. Besides its intrinsically slow response time, interference effects due to other atmospheric molecules (peroxyacetylnitrate (PAN), NH_4^+, nitrogen oxides) that, after catalytic conversion have the same end products as NH_3, do affect the measurement.

The problems of ammonia gas flux measurements met in the practice have stimulated the development of physical techniques based on infrared optical detection like laser photoacoustic spectroscopy. The resurgence of interest in photoacoustics is mainly due to its reasonably high sensitivity (sub-ppbv concentration detection levels have been reported in the scientific literature), moderate selectivity, a large dynamic range (linearity in signal response over more than 5 orders of magnitude; the detected microphone signal $S(V)$ is directly proportional to the incident laser power $P(W)$ and the gas concentration C), operational simplicity, capability of performing multicomponent analysis, and reasonable cost. Competing techniques including gas chromatography, mass spectrometric analysis, and the already mentioned long path absorption techniques all fail in one or more of the above mentioned criteria.

Optical air pollution monitors are based on the interaction between electromagnetic radiation and matter. The radiation emitted by a properly chosen light source is absorbed by the trace analyte molecule(s) of interest (absorption spectroscopy). As far as air pollution is concerned, the infrared region between 2 and 15 μm is especially suitable for monitoring purposes. At first, many atmospheric gaseous species (for example, different hydrocarbons (e.g. C_2H_2, C_2H_4, C_6H_6), CCl_4, NO, NO_2, CO, CO_2, H_2O, H_2O_2, HNO_3, NH_3, SO_2, peroxyacetylnitrate (PAN), O_3, freons, ClO, H_2S and H_2CO) known to play a crucial role in atmospheric chemistry exhibit multiplicity of moderate to strong absorption lines in this

5

spectral region. Secondly, a wide variety of high power molecular gas laser systems operating on a large number of discretely tunable frequencies are found in this region. For example, the HF and DF lasers[6] provide emission in the 2.8- to 3.4 μm spectral region; the CO laser[7] lases in the 4.7- to 7.5 μm range with output wavelengths separated by ≈ 4 cm^{-1}; the N_2O laser[8] operates on lines spaced by ≈ 1 cm^{-1} in the 9.5- to 11.2 μm region and the CS_2 laser[9] covers the 11- to 11.5 μm region on lines separated by ≈ 0.2 cm^{-1}. In addition, isotopic substitution further increases the number of discrete laser lines in the above molecules and extends the effective wavelength range.

The CO_2 waveguide laser[10-14] is especially suited for photoacoustic studies on ammonia; this molecule exhibits several large absorption cross-sections, the strongest of which coincide with laser lines at 9R(30) ($\alpha = 56$ atm^{-1}cm^{-1}) around 9.217 μm, 10R(6) ($\alpha = 26$ atm^{-1}cm^{-1}) near 10.346 μm and 10R(8) ($\alpha = 20.6$ atm^{-1}cm^{-1}) at 10.331 μm respectively. Furthermore, its high stability, compactness and several Watts of output power at most lines make the CO_2 laser waveguide laser a valuable instrument for field measurements.

The first 'in situ' photoacoustic ammonia measurements were reported by McClenney and Bennet[15]. The system they utilized involved short term integrative sampling onto teflon beads with subsequent analysis of the desorbed ammonia by CO_2 laser photoacoustic detection. Photoacoustic measurements by ammonia preconcentration employing selective NH_3-adsorbers were performed by Copeland et al.[16] and Gelbwachs et al.[17] Although these measurements can be regarded as the first actual 'in situ' monitoring attempts of ambient ammonia levels, the determination of concentration levels by such methods reveal only information about the average concentration during the period of sampling rather then providing the 'on-line' values.

1.1.Basic principles of photoacoustic soundwave generation in gases

Consider a beam of electromagnetic radiation with power P impinging on a gaseous column (cylindrical symmetry) of length L. The power transmitted P_{trans} through the column is given by Lambert-Beer's law:

$$P_{trans} = Pexp(-\beta L) \qquad (1.1.1)$$

with the coefficient β (cm^{-1}) being the absorbance of the sample per unit length. The power absorbed by the sample is then:

$$P_{abs} = P - P_{trans} = P - Pexp(-\beta L) \qquad (1.1.2)$$

In case of weak absorption, β is small, and taking the first order term in the expansion of the exponential function yields:

$$P_{abs} = P\beta L \qquad (1.1.3)$$

The coefficient β can also be expressed in terms of the absorption coefficient α (atm^{-1}cm^{-1}) or the absorption cross-section σ (cm^2/mole):

$$P_{abs} = P\sigma N_a L \qquad (1.1.4)$$

where N_a is the number of absorbing molecules per unit volume. If C is the fractional concentration (defined according to $N_a = CN^0$ where N^0 is the total gas density) of the absorbing species then α and σ are related through: $N_a\sigma = C\alpha$.
For the power P_{abs} absorbed by the sample, the following relationship is obtained:

$$P_{abs} = P\sigma N^0 CL \qquad (1.1.5)$$

Using a modulated infrared radiation beam (frequency f_{mod}) gas molecules are excited from the ground vibrational state into a rotational level of a higher vibrational state. In the infrared region the probability for radiative decay is small (proportional to the third power of the absorption frequency); therefore the relaxation takes place by collisions with surrounding bulk gas molecules along the non-radiative channel. For the majority of the molecules, collisional deactivation is fast (some μsec) causing subsequently a periodic increase in kinetic energy of the gas molecules and hence of the gas temperature (δT). The molecules confined within a vessel of constant volume V experience the periodic rise in temperature which leads to a modulated gas pressure δP at a frequency f_{mod}. Choosing the inverse of the modulation frequency f_{mod} longer than the molecular collisional relaxation time, the pressure variation generated in the gas sample can be detected by a transducer. In photoacoustic studies involving the absorption of radiation of a single constituent, the electric signal $S(V)$ in the transducer can be expressed as:

$$S(V) = P(W)\alpha CR(Vcm/W) \qquad (1.1.6)$$

The factor R is called the responsivity of the photoacoustic system and depends, just like the absorption coefficient α, on the pressure. Inspection of eq.(1.1.6) suggests that the measured microphone signal $S(V)$ solely depends on the power incident on the gaseous medium if the remaining parameters α, C and R are kept constant.

A little more than 50 years after its discovery (in 1881 by A.G.Bell[18], J.Tyndall[19] and W.C.Röntgen[20]) the photoacoustic effect found its first application when E.Lehrer and F.K.Luft[21] two German scientists from the laboratory of Control Engineering of the I.G.Farben Industries utilized an infrared absorption recorder (URAS or Ultrarotabsorptionsschreiber) for detection of carbon monoxide (CO). The original URAS consisted of a double-beam transmission spectrometer that accommodated two cells. As only

one of the cells contained the sampled CO gas, the CO concentration was determined by subtracting the magnitude of the photoacoustic signals (recorded with a membrane microphone) generated in both cells. With a limited available output power (150 mWatts) the achieved CO detection limit was not better than 10 ppmv.

It was not any earlier than 1968 that photoacoustic spectroscopy, following the advent of powerful and wavelength tunable lasers, was recognized as a strong analytical tool for monitoring the concentration of atmospheric trace gases. In that year E.L.Kerr and J.G.Atwood[22] performed a classical experiment in which they utilized a CO_2 laser for photoacoustic (PA) detection of carbon dioxide (CO_2). A few years later L.B.Kreuzer and C.K.N.Patel developed a spin flip Raman laser PA monitor[23] to measure nitric oxide (NO) in car parking lots. The availability of collimated and monochromatic light sources has upsurged a worldwide interest for photoacoustic quantization of ultra-weak absorptions of atmospheric and industrial pollutants ever since.

At the end of the 80's several attempts were made using the 'classical' (or conventional) CO_2 laser photoacoustic spectroscopy for monitoring ambient ammonia. The term 'classical' refers here to photoacoustic detection systems by which the ammonia concentration levels were deduced from successive measurements with the laser tuned into coincidence with different gas absorption lines. The total number of laser lines taken for analysis is generally equal to or larger than the amount of absorbing constituents present in the gas sample. Only quite recently the CO_2 laser photoacoustics was combined with different spectroscopic techniques (e.g. photoacoustic Stark spectroscopy[24]) in order to enhance spectral discrimination without a need for sequential tuning of the laser.

1.2. Photoacoustic instrumentation

A typical experimental arrangement for gas phase photoacoustic studies is shown in Fig.1.2.1
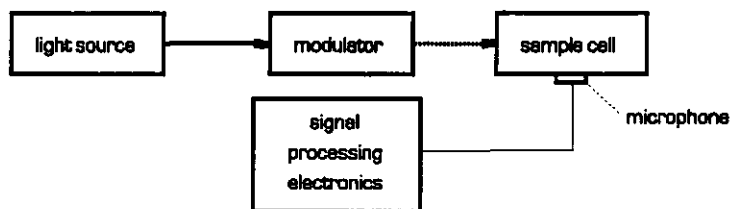
Fig.1.2.1 Schematic diagram of a photoacoustic set-up used for gas-phase studies

Not more than a brief outline of the classical beam chopped CO_2 laser photoacoustic method is given here; details are available in many of the books and articles listed in the scientific literature. The traditional experimental set-up for beam chopped CO_2 laser

8

photoacoustic monitoring of air pollution constitutes the radiation source and modulator (mechanical chopper), a chamber (cell) that accommodates the gaseous specimen and incorporates a microphone to detect the generated acoustic wave, a detector to measure the intensity of the radiation source, and electronic equipment for processing the signal.

1) The light source (CO_2 laser)

The $^{12}C^{16}O_2$ laser[25] provides radiation in the infrared region (at about 70 discrete lines) between the 9.2 and 11 μm of the electromagnetic spectrum. The CO_2 (waveguide) laser emits on a gas mixture consisting of carbon dioxide, nitrogen and helium. Nitrogen molecules are excited into the first vibrational level, about 2360 cm^{-1} above the ground state by a discharge. As this level is close to the $\nu_3(\Sigma_u^+)$ CO_2 asymmetric stretching vibration at 2350 cm^{-1}, the CO_2 molecules are excited to many of the rotational levels of the $\nu_3(\Sigma_u^+)$ vibration through collisional energy transfer with the excited N_2 molecules. Rotational levels up to 200 cm^{-1} above the lowest state of the ν_3 are effectively populated in this way.
Stimulated emission is possible to many rotational levels of the $\nu_1(\pi_u^+)$ CO_2 symmetric stretching mode at about 1390 cm^{-1}. Transitions $\Delta J = \pm 1$ between the rotational states in the $\nu_3(\Sigma_u^+)$ and $\nu_1(\pi_u^+)$ vibration modes result in a large number of discrete laser emission lines conveniently grouped into four (10P, 10R, 9P and 9R) bands[26].

2) The photoacoustic cell

Depending on their operational principles, photoacoustic cells are usually divided into two categories: the non-resonant and the resonant type. As the theory and the operation of photoacoustic cells have extensively been covered in the literature[27-30] only a brief description of the most important features of photoacoustic cells will be given. The non-resonant type is designed in such a way that acoustical amplification does not affect the cell's signal response. Most commonly used in the practice are the resonant cells. Although different types have been proposed, designed and tested, the most frequently encountered resonant photoacoustic cell is the one exhibiting cylindrical geometry. In most designs the radius R of this cylindrical sample chamber is substantially larger than the diameter of the excitation laser beam. Periodic heating of the gas caused by absorption of the modulated laser radiation and subsequent relaxation generates a local pressure increase which propagates radially outward (i.e. perpendicular to the direction of the exciting light beam). Successive periodic laser pulses result in a generation of a standing acoustic wave inside the chamber. The acoustic amplification of the resonant acoustic cell can conveniently be expressed by the quality factor (Q-factor) defined in terms of the resonant acoustic frequency ω_n and the change in frequency $\Delta\omega$ (full width at half maximum) required for the amplification to drop to half its value at the resonance frequency, i.e. $Q = \omega_n/\Delta\omega$ (at $\omega = \omega_n \pm \frac{1}{2}\Delta\omega$ the amplitude of the microphone signal is $\frac{1}{2}\sqrt{2}$ times the maximum at $\omega = \omega_n$).
The pressure distribution $P_{k,m,n}$ within a cylinder of length L and radius R is given by[31]:

9

$$P_{k,m,n}(r,\phi,x,t) = cos(m\phi)cos(k\pi x/L)J_m(\alpha_{m,n}\pi r/R)exp(-i\omega t) \quad (1.2.1)$$

where J_m is a mth order Bessel function of the first kind and the integers k, m, and n refer to the longitudinal, azimuthal, and radial acoustic modes, respectively. Since each mode is discrete, an integer is normally ascribed to indicate the mode excitation in the cell (k,m,n, respectively with k,m,n=0,1,2,..). The acoustic resonances in the photoacoustic cell, found by solving the wave equation in cylindrical coordinates, occur at frequencies f_{res}:

$$2\pi f_{res} = \omega = \pi c_0 \sqrt{[(k/L)^2 + (\alpha_{m,n}/R)^2]} \quad (1.2.2)$$

where c_0 is the sound velocity in the sample and $\alpha_{m,n}$ is the nth root of the equation $dJ_m/dr \mid_{r=0}$. The sound velocity can be calculated from $c_0 = \sqrt{(\gamma R_g T/M)}$ with R_g the gas constant, T the absolute temperature of the sample, M the molecular weight of the gas and $\gamma = C_p/C_v$, its ratios of specific heats. For a mixture of chemically non-interacting gases the speed of sound is given by[32]:

$$c_0' = \sqrt{(\chi R_g T/\underline{M})} \quad (1.2.3)$$

where χ and $\underline{M}$ are the effective ratio of specific heats and the average molecular weight respectively expressed by:

$$\chi = \sum_i r_i C_p / \sum_i r_i C_v \quad \text{and} \quad \underline{M} = \sum_i r_i M_i \quad (1.2.4)$$

with r_i being the fractional concentration of gas i, and M_i the molecular weight of species i. Photoacoustic cells with low Q-factors (20-50) are less susceptible to drifts in laser modulation frequency f_{mod} and temperature T. Since both, the sound velocity in the sample and the physical dimensions of the cell are temperature dependent, active frequency locking is required when working with cells exhibiting a high Q-factor (>100).

The noise sources[31] present in photoacoustic systems can be divided into two categories, i.e., electrical noise N_{elec} and optical noise N_{opt}.

Electrical noise N_{elec} originates mainly from the microphone and the electronic detection equipment (signal preamplifiers). As these noise sources usually exhibit a $1/f_{mod}$ noise power dependence, the system sensitivity (defined as the system response for a signal to noise ratio of unity) favours operation at audio frequencies. Employing high quality FET amplifiers and a small electronic frequency bandwidth (1 Hz) upon integrating the periodic signal detected by the microphone, under practical conditions the system overall noise can be reduced typically to some 50 nV.

The minimal theoretical noise present in a photoacoustic system results from random density fluctuations (Brownian motion) in the sample gas. In the practice the incoherent and random thermal noise presents the lowest achievable noise level of the photoacoustic system. The main optical noise source N_{opt} and therefore the largest contribution to the signal amplitude arises due to absorption or scattering of the modulated laser radiation in the windows terminating the photoacoustic cell. The periodic window heating, generated at the

laser modulation frequency f_{mod}, is transferred to the gas sample and generates a photoacoustic signal that fluctuates and impedes detection of weak acoustic signals. In the 'classical' photoacoustic detection mode this background signal is one of the sources determining the ultimate detection limit.

3) Laser beam modulation techniques

In CO_2 laser photoacoustic spectroscopy either the amplitude or the frequency of the light source radiation must be modulated in order to generate acoustic signals.

With a mechanical chopper, inexpensive and efficient, a modulation depth of 100% is easily achieved. Phase-locked, low vibration choppers are commercially available. Focusing the CO_2 laser beam (typical diameter 1-2 mm) onto the chopping slit reduces the chopper-induced sound vibration in the air that can be transmitted to the microphone as noise interference.

In electro-optic modulation the plane of polarization of an incoming laser beam alters in a non-linear crystal through the application of a modulated electric field. Employing a polarizer the laser output power can be varied by adjusting the crystal voltage. Although the noise levels are lower than in the case of mechanical modulation, the limited amount of power the crystal can handle, the cost and the wavelength specificity, are the reasons for the fact that mechanical modulation is preferred in the practice.

4) Electronic detection

As the concentration of trace molecules in the ambient air is normally very low (ppbv), the sound pressure $P_{k,m,n}$ of the standing wave generated in the photoacoustic cell and hence, the microphone signal $S(V)$ is small. In order to detect low periodic signal levels, generally obscured by noise sources, phase-sensitive techniques are used. Figure 1.2 depicts schematically the basic operational principle of the lock-in amplifier.
A periodic reference signal f_r tuned to the frequency f_s of the signal of interest is, together with the sample signal, fed into the lock-in amplifier. The sample signal is amplified by a high-gain AC coupled differential amplifier and its output multiplied subsequently by a phase-locked loop (PLL) output (proportional to $cos(f_s t + \phi)$ in the phase-sensitive detector (PSD)). This multiplication shifts each frequency component of the output signal f, by the reference frequency f_s, which results at the PSD-output in:

$$V_{psd} = cos(f_s t + \phi)cos(ft) = \tfrac{1}{2}cos[(f_s + f)t + \phi] + \tfrac{1}{2}cos[(f_s - f)t + \phi] \qquad (1.2.5)$$

The sum-frequency component is attenuated by the low-pass filter and only difference frequency components within the low-pass filter's narrow bandwidth will pass through the DC amplifier. The periodic signal (frequency f_s) will be detected by the lock-in as a DC-signal.
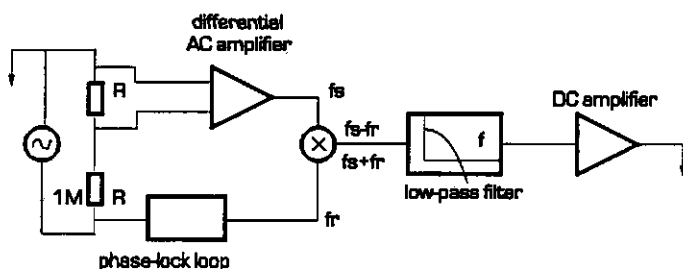
Fig.1.2.2 Lock-in amplifier scheme

1.3.Multi-component photoacoustic analysis of gas mixtures

The photoacoustic detection of ammonia in realistic air-samples in the 9-11 μm region is impeded by the absorption of the CO_2 laser radiation due to other atmospheric constituents, in particular water vapor (H_2O) and carbon dioxide (CO_2). Before proceeding with the real time monitoring of ambient ammonia, the concept of multi-components photoacoustic studies is discussed.

The relationship $S(V) = P\alpha RC$ describing the linearity between the signal strength $S(V)$, the incident radiation power P_{laser}(Watts) and the concentration C is valid only when dealing with a single absorbing constituent. In a first approximation, when investigating multi-component specimen, the above equation can be replaced by the more general expression $S_i = \Sigma \alpha_{ij} C_j$ (where S_i are the measured photoacoustic signals at the different laser lines i, α_{ij} is the absorption coefficient of the jth pollutant at wavelength i, and C_j are the unknown concentration levels of the gases present in the mixture). However, the expression is only valid under the condition that the phases of the recorded photoacoustic signals S_i obtained at the different laser lines i remain constant during the entire course of the experiment.

Perlmutter et al.[34] performed CO_2 laser photoacoustic studies using a 'classical' set-up, on a four-constituents gas mixture (C_2H_4, H_2O, CO_2 and a mixture of atmospheric constituents producing a 'white' photoacoustic signature) dispersed in nitrogen (N_2). The photoacoustic analysis involved four laser transitions, two of which coincided with sharp peaks of the C_2H_4 (at the 10P(14) line) and H_2O (at the 10R(20) line) in the infrared spectrum. Sequential tuning of the laser to four different wavelengths resulted in the measured photoacoustic signals S_i and a set of four linear equations, containing the unknown concentration levels C_i. Introducing three different noise sources, the intrinsic noise of the photoacoustic set-up i.e. the microphone's electrical noise, the instabilities of various components (e.g. laser power, window absorption) in the analyzing photoacoustic system, and incorporating the inaccuracy of reported gaseous absorption coefficients α_i, the practical limitation of each noise source on the minimal detectable C_2H_4 concentration was investigated. Quantifying the different noise sources in terms of photoacoustic signal strengths S_i, the concentration C_i of each gaseous species was calculated using a matrix scheme. Due

12

to the uncertainty in value of the CO_2 absorption coefficient α_i at the laser lines used, the minimal detectable C_2H_4 concentration decreased from 1.6 ppbv measured with a CO_2 concentration of 300 ppmv, to 53 ppbv C_2H_4 in the presence of 1% CO_2 (10^4 ppmv). A remarkable fact reported in their measurement of ethylene using a realistic atmosphere, was the evidence for a "negative" carbon dioxide concentration calculated from the obtained signal strengths S_i. The minus sign was attributed to the kinetic cooling effect which experimentally manifested itself (in their resonant photoacoustic cell) by a 180°-phase reversal of the photoacoustic signal relative to the C_2H_4-phase. In addition, it was found that use of a NaOH-scrubber eliminated effectively both, the CO_2 and the H_2O interference without changing the ethylene concentration (or introducing new interfering gases as a result of chemical reactions originating at the surface of the scrubber). The use of an isotopic $^{13}C^{16}O_2$ laser was proposed as an alternative to surmount the problems of H_2O and CO_2 spectral interferences.

At the University of Arizona Tilden and Denton[35] performed 'classical' high concentration (10 ppmv or more) multi-component $^{12}C^{16}O_2$ laser photoacoustic studies on a mixture of absorbing gases involving ammonia, ethylene, furan, freon-12 and methanol. Upon applying a least square multivariant analysis (including absorption coefficient weighting factors) the signal strengths S_i at 10 respectively 20 laser lines were recorded. Using mixtures containing high furan and freon-12 concentrations the calculated concentration levels C_i compared within 10% of the certified gaseous concentration levels admitted to the photoacoustic cell. However, in case of high ammonia concentrations (300 ppmv NH_3) admitted together with low furan (20 ppmv) and freon-12 (14 ppmv) concentrations, the multivariant analysis failed to provide the correct concentration levels. This fact was explained by invoking the methanol and ammonia spectral overlap at the freon-12 and furan CO_2 laser absorption wavelengths, which impeded the determination of minor components in the presence of major interfering components.

Multi-component photoacoustic analysis of trace pollutant becomes often even more difficult when working with realistic air samples.

The most abundant components in the ambient atmosphere are nitrogen ($N_2 \approx 79\%$), oxygen ($O_2 \approx 19\%$), water vapor ($H_2O \approx 1\%$), carbon dioxide ($CO_2 \approx 350$ ppmv) and the noble gases (He, Ar, Xe, Ra, etc.). In the CO_2 laser emission frequency region the 8 to 14 μm wavelength region is characterized by continuum absorption spectra of both water vapor and carbon dioxide. Although characterized by small absorption coefficients α, their large abundance in the atmosphere is relevant when attempting real-time detection of atmospheric trace pollutants. When dealing with multi-component photoacoustic studies involving a mixture of absorbing gases the photoacoustic signal is a linear superposition of the signals originating as a consequence of the absorption of each specific component. When interpreting the results, the phases of the photoacoustic signals have to be considered in addition to the photoacoustic amplitudes as well[36,37], i.e.

$$S_i cos\Phi_i = \Sigma C_j S_{ij}^{\;0} cos\Phi_{ij}^{\;0} \qquad (1.3.1)$$

In eq.(1.3.1) S_i and Φ_i represent the normalized signal amplitude and phase at the given laser transition i, C_j is the concentration of the mixture component j giving rise to a normalized and calibrated amplitude $S_{ij}^{\;0}$ and phase $\Phi_{ij}^{\;0}$.

Sigrist and co-workers from the ETH (Zürich) utilized a CO_2 laser photoacoustic

system for in-situ measurements of trace pollutants in industrial and rural areas (car exhaust gases). Since air exhaust represents a complex mixture of numerous components (the concentration levels of which vary in time), the continuous monitoring of the main constituents is of great importance. In order to perform multi-component analysis a computer program has been developed for concentration calculations using the mathematical scheme discussed above.

'Classical' CO_2 laser photoacoustic studies involving real time detection of ambient ammonia have recently been reported in the scientific literature. Olafsson et al.[38,39] used a single mode, 500 MHz line tunable CO_2 waveguide laser in conjunction with a 10 cm long non-resonant flow-through photoacoustic cell for detection of NH_3 in power plant emission. To solve the problem of spectral interference of CO_2 and H_2O, the pressure inside the cell was reduced to 12 mbar. At this sub-atmospheric pressure the molecular absorption lines approach the Doppler limit (about 70 MHz), but the linewidths are still considerably below the 500 MHz tuning range of the laser. For detection of NH_3 the sR(5,0) line, (located 190 MHz below the 9R(30) CO_2 laser line center), was chosen, while carbon dioxide absorbs at the laser line center. Fitting the recorded spectrum to a sum of two Voigt profiles and a constant N_2 background the NH_3 concentration is calculated from the amplitude of the NH_3 signal. Including the phase reversal in the photoacoustic signal (resulting from the kinetic cooling effect) it was possible to uniquely resolve the NH_3 concentration levels down to 1 ppmv in the presence of 15% CO_2.

At the KEMA-Institute in Arnhem (The Netherlands), R.Rooth and A.Verhage[40] utilized a CO_2 laser photoacoustic system (incorporating a resonant flow-through cell (f_{res}=560 Hz)) for low level (detection limit 1 ppbv NH_3) ammonia monitoring. A mathematical model describing the molecular dynamics of ammonia and the main atmospheric constituents was derived from photoacoustic experiments performed in the laboratory using a simulated atmosphere. Such a model, which includes the effect of kinetic cooling on the photoacoustic signal, is necessary whenever using a resonant photoacoustic cell of which the operating frequency f_{res} is much larger than the inverse of the relaxation time dominating the molecular deactivation processes.

As the recorded photoacoustic signal includes the absorption of ambient ammonia, water vapor and carbon dioxide, the 'real-time' ammonia concentration is derived by proper interpretation of the magnitudes and phases of the photoacoustic vector signals $\bar{S}$. In order to do so the water vapor concentration is monitored at the 10R(20) CO_2 laser line, at which it exhibits maximum absorption. Accordingly the laser is tuned to the strongest ammonia absorption line located at 9.217 μm (9R(30)) and the CO_2 concentration is than calculated from the measured photoacoustic signals recorded at the 9R(28) and 9R(18) laser lines. This method of consecutive laser tuning offers a means to account for both the water vapor and carbon dioxide spectral interferences as well as the kinetic cooling effect.

However, the time needed (2 min.) for successive tuning and recording of the measured signal is a disadvantage when employing CO_2 laser photoacoustics as a point gas sensor in ammonia gas flux measurements. The time necessary to tune the CO_2 laser to the different gaseous absorption can be substantially shortened when instead only one laser line is used for monitoring purposes. A prerequisite for this is a drastic suppression of the spectral interferences that mask the sensing of accurate gaseous ammonia at trace levels.

Due to the notoriously adhesive properties of ammonia, the reduction of interfering water vapor and carbon dioxide using chemical scrubbers is precluded, since their effect is very likely to affect (chemical reactions occurring at the scrubber's surface) the ammonia concentration in the gas sample. Therefore, real-time trace level photoacoustic monitoring

of ambient ammonia using a single laser absorption line requires the use of an additional physical phenomenon that can be used to discriminate ammonia against other spectral interfering gaseous components.

The heteronuclear structure of ammonia gives rise to a large dipole moment (1.48 Debye) in the ground state. This forms the base for tuning the ammonia molecule into near coincidence with the CO_2 laser through the application of an electric (Stark) field. Since carbon dioxide exhibits infrared absorptions only at 667.3 cm^{-1} ($\nu_2(\pi_u^+)$ bending mode) and at 2349.3 cm^{-1} ($\nu_3(\Sigma_u^+)$) antisymmetric stretch mode), and doesn't possess a permanent dipole moment in the 10 μm CO_2 laser wavelength region, the application of an electric field doesn't perturb its energy levels and therefore it cannot be shifted into resonance with the CO_2 laser: carbon dioxide is said to be Stark-inactive.

Although H_2O, (an asymmetric top molecule), possesses a permanent dipole moment, the application of an electric Stark field does not result in a substantial change of absorption strength. Therefore, Stark modulation (at a frequency f_{Stark}) of the ammonia absorption coefficient α offers a means to detect NH_3 in a matrix of absorbing gases. The kinetic cooling effect can be avoided by chopping the laser at a frequency f_{chop} which is much lower than the inverse of the relaxation time governing the molecular de-excitation of the sampled air. Using the photoacoustic cell as a audio-frequency heterodyne mixer and phase-sensitive processing (detection frequency of the lock-in amplifier f_{det}), photoacoustic signals due to the absorption of ammonia can be detected at the sum ($f_{chop}+f_{Stark}$) or difference frequency ($f_{Stark}-f_{chop}$) sidebands of the modulated laser and Stark electric fields, i.e. $f_{det}=f_{Stark}\pm f_{chop}$. Besides the already mentioned kinetic cooling effect, the window absorption signal (modulated at frequency f_{chop}) as well as the absorption of the modulated laser radiation (laser is chopped at frequency f_{chop}) due to water vapor and carbon dioxide is effectively suppressed using this detection scheme.

In mathematical terms detection of a photoacoustic signal, composed of the convolution of the Fourier transform $\mathscr{F}$ of two block-waves with frequencies ω_1 and ω_2, is performed at the sum ($\omega_1+\omega_2$) or difference ($\omega_1-\omega_2$) frequency of the carrier waves ω_1 and ω_2. Let $L(t)$ and $S(t)$ represent the periodic laser and the Stark electric fields respectively, with

$S(t)=E_1 \quad 0<t<T_1 \quad$ and $S(t)=0 \quad T_1<t<2T_1 \quad \omega_1T_1=2\pi$
$L(t)=E_2 \quad 0<t<T_2 \quad$ and $L(t)=0 \quad T_2<t<2T_2 \quad \omega_2T_2=2\pi$

The interaction of both the modulated laser and Stark electric fields with the ammonia molecule is described as:

$$\mathscr{F}=\mathscr{F}(L(t))\mathscr{F}(S(t)) = \{cos(\omega_1t)+cos(3\omega_1t)+....\}\{cos(\omega_2t)+cos(3\omega_2t)+....\} \quad (1.3.2)$$

Neglecting the harmonics $n\omega$ ($n>1$) in the Fourier expansion, gives:

$$\mathscr{F}=\mathscr{F}(L(t))*\mathscr{F}(S(t))=cos\omega_1t cos\omega_2t=cos(\omega_1-\omega_2)t+cos(\omega_1+\omega_2)t \quad (1.3.3)$$

Using narrow-bandwidth ($\omega=1$ Hz, $\omega \ll \omega_1,\omega_2$) phase-sensitive detection at either the sum ($\omega_1+\omega_2$) or the difference ($\omega_1-\omega_2$) frequency sidebands, complete suppression of photoacoustic signals generated at the fundamental frequencies ω_1 and ω_2 is obtained.

References

1. D.C.Wolfe Jr., and R.L.Byer, Appl.Opt., **21**, 1165, (1982).
2. W.A.H.Asman Ph.D.thesis Wageningen Agricultural University (1987).
3. A.W.M. Vermetten, W.A.H.Asman, E.Buijsman, W.Mulder, J.Slanina and A.Waijers-Ipelaan, Concentration of NH_3 and NH_4^+ over The Netherlands, VDI Berichte, Vol.560, 241-251 (1985).
4. J.G.M.Roelofs, A.W.Boxman and H.F.G.van Dijk, Effects of Airborne Ammonium on Natural Vegetation and Forests, in "Ammonia and acidification", Eds. W.Asman and H.Diederen, Proceedings EURASAP Symposium 13-15 April 1987, National Institute of Public Health and Environmental Hygiene, Bilthoven, The Netherlands.
5. A.van Pul, Ph.D.thesis, Wageningen Agricultural University (1991) in press.
6. T.F.Deutsch, Appl.Phys.Lett., **10**, 234, (1967).
7. C.K.N.Patel and R.J.Kerl, Appl.Phys.Lett., **5**, 81, (1964).
8. C.K.N.Patel, Appl.Phys.Lett., **6**, 12, (1965).
9. C.K.N.Patel, Appl.Phys.Lett., **7**, 273, (1965).
10. C.K.N.Patel, Phys.Rev.Lett., **12**, 588, (1964).
11. C.K.N.Patel, P.K.Tien, and J.H.McFee, Appl.Phys.Lett., **7**, 290, (1965).
12. A.J.DeMaria, Proc.IEEE, **61**, 731, (1973).
13. O.R.Wood, Proc.IEEE, **62**, 355, (1974).
14. Compilation of laser wavelengths, in "Tables of Laser Lines in Gases and Vapors", Eds. R.Beck, W.Englisch, K.Gurs, Springer-Verlag, New York, (1978).
15. W.A.McClenney and C.A.Bennet Jr., Atmospheric Environment **14**, 641, (1980).
16. G.E.Copeland, M.D.Aldridge, and C.N.Harvard, Final Report, December 1981, under NASA contract, NASA-15468-63, Old Dominion University, Norfolk, Virginia, USA.
17. J.Gelbachs, G.E.Loper, S.M.Beck, R.S.Kell, FY Report, Progress Towards the Development of a CO_2 Laser PA Toxic Vapor Monitor (1984).
18. A.G.Bell, Proc.Am.Assoc.Adv.Sci. **29**, 115 (1880).
19. J.Tyndall, Proc.R.Soc. **31**, 307, (1881).
20. W.C.Röntgen, Philos.Mag. **11**, 308, (1881).
21. E.Lehrer and K.F.Luft, Z.Techn.Phys, **24**, 97, (1943).
22. E.L.Kerr and J.G.Atwood, Appl.Opt., **7**, 915 (1968).
23. L.B.Kreuzer and C.K.N.Patel, Science, **173**, 45 (1971).
24. H.Sauren, D.Bićanić and K.van Asselt, Infrared Phys. **31**, 475-484, (1991).
25. C.K.N.Patel, Science, **202**, 157, (1978).
26. A.J.Witteman, The CO_2 laser, Springer Series in Optical Sciences, Volume 53.
27. L.G.Rosengren, Appl.Opt. **14**, 1960, (1975).
28. C.F.Dewey Jr., R.D.Kamm and C.E.Hackett, Appl.Phys.Lett., **23**, 633, (1973).
29. C.F.Dewey Jr., Opt.Eng. **13**, 483, (1974).
30. A.G.Bell, Philos.Mag. **11**, 510, (1881).
31. G.A.West, J.J.Barrett, D.R.Siebert and K.Virupaksha Reddy, Rev.Sci.Instrum. **54**, 797, (1983).
32. P.J.K.Kay, Ph.D.thesis, Department of Physics, Harriot-Watt University, Edinburgh, Scotland (1982).
32. L.B.Kreuzer, J.Appl.Phys. **42**, 2934, (1971).
34. P.Perlmutter, S.Shtrikman and M.Slatkine, Appl.Opt. **18**, 2267, (1979).

35. S.B.Tilden, Ph.D.thesis,. The University of Arizona (1983).
36. S.Bernegger and M.W.Sigrist Appl.Phys.B, **44**, 125, (1987).
37. S.Bernegger, P.L.Meyer, C.Widmar and M.W.Sigrist in "Photoacoustic and Photothermal Phenomena", Eds.P.Hess and J.Pelzl, Springer Verlag, Heidelberg (1988).
38. A.Olafsson, Ph.D.thesis, Oersted Institute, Danemark, (1990).
39. J.Henningsen, A.Olafsson and M.Hammerich, Trace Gas Detection with Infrared Gas Lasers, in "Applied Laser Spectroscopy", Eds. Inguscio and Demtröder, Plenum ASI 1990.
40. R.A.Rooth, A.J.L.Verhage and L.W.Wouters, 6th Int. Topical Meeting on Photoacoustic and Photothermal Phenomena, Baltimore (1989).

Chapter 2   Spectroscopy of Ammonia

2.1. Introduction

Next to nitrogen (N_2) and oxygen (O_2), water vapor (H_2O) and carbon dioxide (CO_2) are the most abundant components in the atmosphere. Contrary to nitrogen and oxygen, the latter ones are known to absorb in the 2-20 μm (5000 cm^{-1}-500 cm^{-1}; 10μm=1000 cm^{-1}) infrared region. As seen from the low-resolution spectrum depicted in Fig.2.1.1, their absorbance is considerable over a large part of the spectrum, with exception of the 9-11 μm (1110 cm^{-1}-990 cm^{-1}) region.
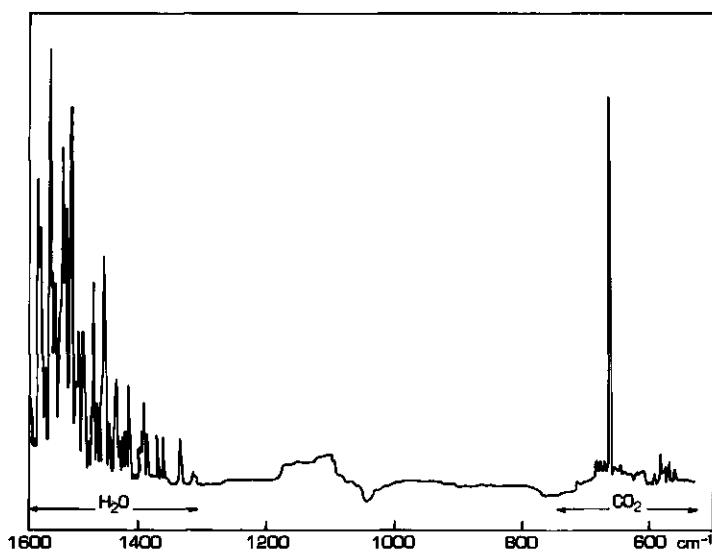
Fig.2.1.1 The infrared spectrum of atmospheric water vapor and carbon dioxide (taken from C.N.Banwell, Fundamentals of Molecular Spectroscopy[1])

Water, an asymmetric top molecule, belongs to the C_{2v} point group. This implies that the molecule has a 2-fold axis C_2, and two symmetry planes σ_v symmetrically oriented at angles π/2 through the molecular symmetry axis. The observed low-resolution infrared absorption bands in Fig.2.1.1 are due to three fundamental vibrations: the ν_1 symmetric

18

stretch vibration around 3651.7 cm^{-1}, the ν_2 symmetric bending vibration around 1595.0 cm^{-1} and the ν_3 asymmetric stretch vibration around 3755.8 cm^{-1} (the vibrations are labelled in the order of decreasing frequency within their symmetry type).

In the CO_2 laser wavelength region (Fig.2.1.2) the H_2O spectrum is characterized by a few weak (typical absorption coefficients $\alpha \approx 10^{-5}$ atm^{-1}cm^{-1}) purely rotational absorption lines superimposed on a weak continuum, that has been the subject of numerous experimental and theoretical investigations.
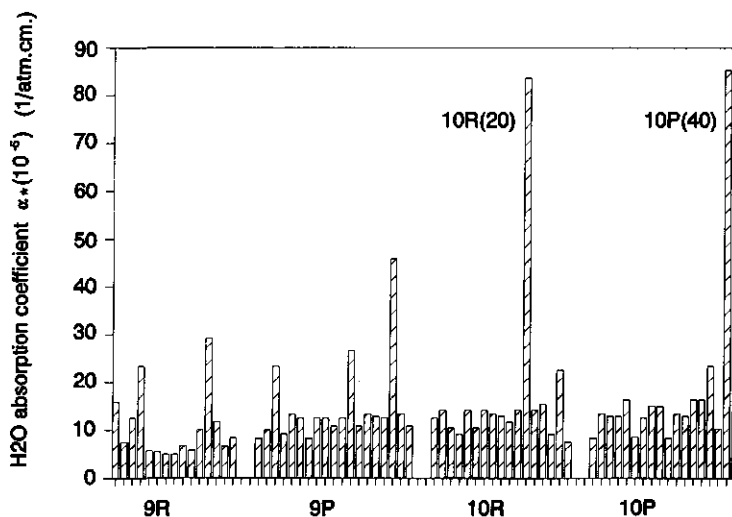
Fig.2.1.2 Absorption coefficients of H_2O vapor at $^{12}C^{16}O_2$ laser wavelengths taken from Bernegger et al.[2]

For example, Wood et al.[3] assume that the collision broadened wings of the rotation band extending from the far infrared give rise to absorption features near 10.6 μm. Lately, it was tried to account for the continuum in terms of far-wing absorptions, water dimers and clusters of water vapor[2]; a satisfactory theoretical model however has not been developed so far. The strongest ($\alpha = 8.36*10^{-4}$atm^{-1}cm^{-1}) water vapor absorption line is that at the frequency coinciding with the 10R(20) emission frequency of the CO_2 laser (967.276 cm^{-1}).

The CO_2 molecule belongs to the C_∞ point group having an ∞-fold axis. An infinite number of rotations around the molecular symmetry axis transform the molecular configuration into an equivalent one. As only the ν_2 bending mode and the ν_3 asymmetric stretch vibration cause a change in dipole moment, two infrared absorption bands are found around 2349.3 cm^{-1} and 667.3 cm^{-1} respectively. Similar to the case of water vapor, the CO_2 absorption spectrum in the 9-11 μm region is characterized by a broad band continuum with a few weak lines atop (Fig.2.1.3); the strongest absorption ($\alpha = 3.8*10^{-3}$ atm^{-1}cm^{-1}) is located at the 9R(18) laser line.
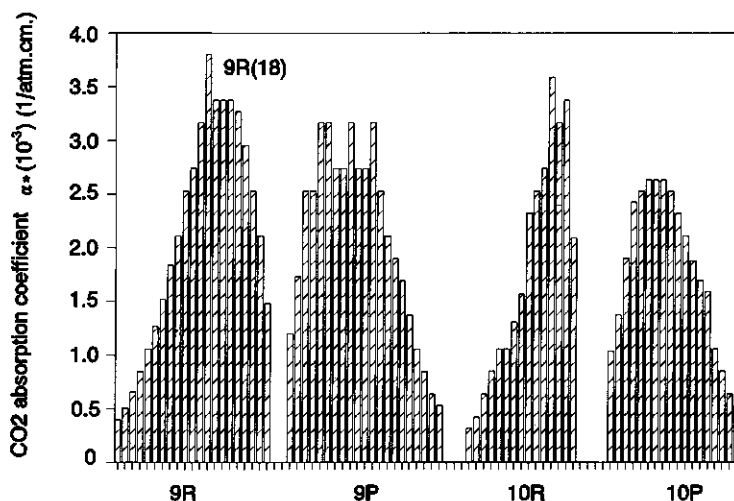
Fig.2.1.3 Absorption coefficients of CO_2 at $^{12}C^{16}O_2$ laser wavelengths after Bernegger *et al.*[2] and Rothman *et al.*[4]

Investigations of the rotational Raman and infrared spectra have established that the NH_3 molecule is a symmetrical top molecule possessing a permanent dipole moment. From the recorded spectra, a symmetrical pyramidal structure of the ammonia molecule (symmetry group D_{3h}) is deduced[5]. From four fundamental vibrations the ν_1 (centered around 3335.9 cm^{-1} and 3337.5 cm^{-1}) and the ν_2 (centered around 931.58 cm^{-1} and 968.08 cm^{-1}) are symmetric, while the ν_3 and the ν_4, centered around 3450 cm^{-1} and 1627 cm^{-1}, are doubly degenerate. A peculiar feature of the ammonia symmetric fundamentals ν_1 and ν_2 is the evidence of double lines in the vibration spectrum. Such a doubling is due to the fact that there are two equilibrium positions for the N atom at either side of the H_3 plane which leads to a splitting of all vibrational levels into two sublevels (inversion doubling). Subtracting the splitting in the vibrational ground state (0.79 cm^{-1})[6] from those in the infrared, it follows that the ν_1 (ν_1, ν_2, ν_3, ν_4 = 1,0,0,0) and the ν_2 (0,1,0,0) upper states are split by 0.9 cm^{-1} and 35.69 cm^{-1} respectively. The NH_3 (ν_2) fundamental vibration band overlaps with the 9-11 μm wavelength region of the $^{12}C^{16}O_2$ laser emission. In this region fourteen $\Delta J=0,\pm1$ lines corresponding to (0,0,0,0)$\rightarrow$(0,1,0,0) transitions, (all exhibiting an absorption coefficient α larger than 1.0 atm^{-1}cm^{-1}), are found[7]. The strongest NH_3 absorption ($\alpha=56$ atm^{-1}cm^{-1}) line is the one coinciding with the 9R(30) (9.217 μm or 1084.95 cm^{-1}) $^{12}C^{16}O_2$ laser line, followed by the 10R(6) ($\alpha=26.0$ atm^{-1}cm^{-1}) and 10R(8) ($\alpha=20.6$ atm^{-1}cm^{-1}) coincidences, located at 10.346 μm (966.56 cm^{-1}) and 10.331 μm (967.96 cm^{-1}). The $NH_3(\nu_2)$ rotational-vibrational (rovibronic) absorption spectrum in the $^{12}C^{16}O_2$ laser emission region is depicted in Fig.2.1.4.

20
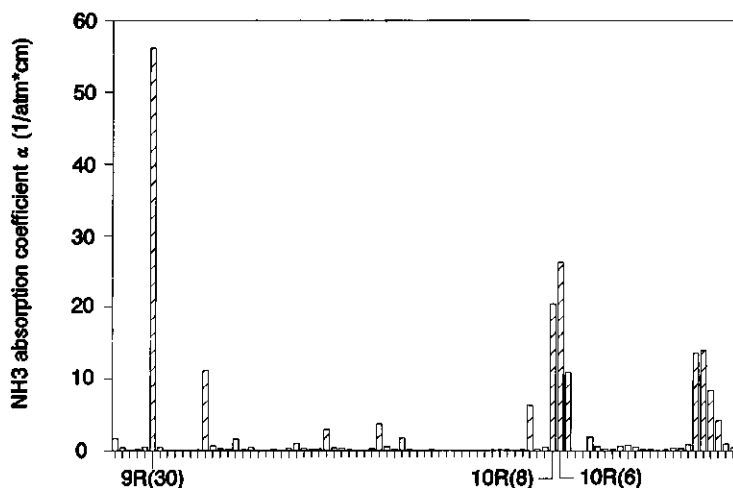
Fig.2.1.4 Absorption coefficients of $^{14}NH_3$ at $^{12}C^{16}O_2$ laser wavelengths measured by Brewer and Bruce[7].

The fractional absorption of these gases can be estimated by calculating the magnitude of the expected photoacoustic signal strength $S(V) \propto C\alpha$ (C is the fractional concentration of the species in air and α is the molecular absorption coefficient). For H_2O, CO_2 and NH_3 the mean ambient concentration C is about 10^7 ppbv, $35*10^4$ ppbv, and 10 ppbv respectively. At the 10R(6) line the NH_3 photoacoustic signal strength S is about $26*10^{-8}$ atm^{-1}cm^{-1}, while for H_2O and CO_2 at this line the signal strength is about $10*10^{-8}$ atm^{-1}cm^{-1} and $35*10^{-8}$ atm^{-1}cm^{-1}. The effect of atmospheric water vapor and carbon dioxide hence produces the absorption that is comparable to that of ammonia. This interference effect together with the kinetic cooling process (section 2.7) imposes serious problems when the unambiguous photoacoustic detection of ambient ammonia is considered.

As the IMPASS approach in detecting ambient ammonia relies on the use of the Stark effect, it is necessary to discuss the infrared (rovibronic) spectrum of this molecule in the unperturbed case (zero E-field), as well as its Stark effect.

2.2. Rotation of molecules

In this section only the pure rotation of polyatomic molecules is considered neglecting their vibration and, in case of NH_3, the electronic motion. The selection rule for dipole

21

transition requires that a state function ψ^+ (i.e. rotational states ψ^+ which are symmetric in their coordinates under the inversion operation) combines only with state functions ψ^- (i.e. state functions which are asymmetric under the inversion operation). Further the $\Delta J = \pm 1$ selection rule holds true for linear molecules (e.g. CO_2), while for the symmetric top molecule NH_3 $\Delta K = 0$ and $\Delta J = 0, \pm 1$ are obeyed.

The three dimensional rotation of a body[1,5,8] is described about three mutually perpendicular directions (called the principal axes of rotation) through the centre of gravity. A rigid body exhibits three (one about each axis) principal moments of inertia usually denoted by I_{xx}, I_{yy}, and I_{zz}. The moment of inertia of a rigid body about a single axis is defined by

$$I = \Sigma m_i \rho^2_i \qquad (2.2.1)$$

where ρ_i is the perpendicular distance of the mass element m_i from this axis.
Classically the kinetic energy of a rotating body with a moment of inertia I_{jj} and angular velocity ω_j about an axis j yields

$$T = \Sigma \tfrac{1}{2} I_{jj} \omega^2_j \qquad (2.2.2)$$

or

$$T = \tfrac{1}{2} I_{xx} \omega^2_x + \tfrac{1}{2} I_{yy} \omega^2_y + \tfrac{1}{2} I_{zz} \omega^2_z \qquad (2.2.3)$$

Introducing the classical expression for the components of angular momentum $J_j = I_{jj}\omega_j$, gives

$$T = J^2_x/2I_{xx} + J^2_y/2I_{yy} + J^2_z/2I_{zz} \qquad (2.2.4)$$

Molecules are classified according to the relative values of their three moments of inertia; molecules with three different principal moments of inertia are called asymmetric tops (or asymmetric rotators). If however two of the three principal moments of inertia are equal, one deals with a symmetric top (symmetric rotator). It is possible that one of the principal moments of inertia is zero or very small, while the other two are equal; this is the case for all linear polyatomic molecules. Finally, the term spherical top applies to a molecule with three equal moments of inertia. Consider now a symmetric top molecule such as NH_3. The Hamiltonian describing the energy of the molecular system is written as

$$H = \tfrac{1}{2} J^2/(I_B) + \tfrac{1}{2} J^2_z/(I_A - I_B) \qquad (2.2.5)$$

with $I_B = I_{xx} = I_{yy}$, $I_A = I_{zz}$ and $J^2 = J^2_x + J^2_y + J^2_z$ and J^2 is the magnitude of the total angular

momentum.

The energy eigenvalues $\dot{E}$ of the Hamiltonian H, $H|\psi> = E|\psi>$ are related to the eigenvalues of the angular momentum operators:

$$J^2|\psi> = J(J+1)\hbar^2|\psi>, \quad J=0,1,2,.... \quad (2.2.6)$$

$$J_z|\psi> = K\hbar|\psi>, \quad K=J,J-1,....,-J \quad (2.2.7)$$

in which K is the projection of J on the molecular symmetry axis. When $K=0$ there is no rotation around the figure axis, and the angular momentum gives rise only to an end-over-end rotation. A third component of the angular momentum (about the space or laboratory axis Z) J_Z must also be specified in order to present a full description of the molecule. The operator J_z^- commutes with J_z and J^2 and its eigenvalues are written: $M\hbar$, $M=J,J-1,.....,-J$. In the absence of any external field, for a given J,K quantum pair, different M-values represent the same rotational energy. Hence, for a symmetric top molecule the state $|J,K,M>$ is completely specified by:

$$|JKM>, \quad J=0,1,2,....; \quad (2.2.8)$$

$$K=J,J-1,...,-J; \quad M=J,...,-J$$

(neglecting centrifugal distortion)

It is convenient to introduce the rotation constants A and B: $(A=\hbar/4\pi cI_A$ and $B=\hbar/4\pi cI_B)$ and to write the rotational energy levels (neglecting centrifugal distortion) as

$$E_{rot} = BJ(J+1) + (A-B)K^2 \quad (2.2.9)$$

The states $|\psi> = |JKM>$ with the same J and $|K|$-value, have the same energy. Consequently, all states with $K>0$ are doubly degenerate, i.e. their total degeneracy is $2(2J+1)$. Two important cases have to be considered now: if the rotation constants A and B are equal the molecule is called a spherical top (examples are CH_4 and SF_6; these molecules belong to the cubic groups). Spherical top molecules exhibit an additional degeneracy due to the independence of the energy levels of K. The spherical top molecules are characterized by

State vector: $|JKM>, \quad J=0,1,..; \quad K=J,...-J; \quad M=J,...,-J \quad (2.2.10)$

Energy levels: $E_{JKM}/hc = BJ(J+1) \quad (2.2.11)$

23

For a given J-value the energy levels are $(2J+1)^2$-fold degenerated.

On the other hand linear molecules such as CO_2 cannot rotate about the figure axis. In such case the angular momentum vector must be perpendicular to the symmetry axis, i.e. $K \equiv 0$, and the corresponding state vector is

$$\text{State vector: } \mid JM >, \; J=0,1,2,\ldots \quad (2.2.12)$$

$$M=J,J-1,\ldots,-J;$$

The energy levels of the linear rotator are $(2J+1)$-fold degenerate for a given J-value.

The case of asymmetric top molecules (e.g. H_2O) is not treated here as one is mainly concerned with the symmetric top molecule NH_3. However, a general treatment can be found in Herzberg's classical work "Infrared and Raman Spectra"[5].

2.3 Vibrations of symmetric top molecules and vibrational selection rules

For the scope of this thesis it suffices to consider the vibrations of polyatomic molecules as a collection of independent harmonic oscillators. A quantum mechanical treatment using the overknown harmonic oscillator eigenfunctions and eigenvalues yields for the vibrational energy

$$E_{vib} = (\nu + \tfrac{1}{2})\varpi_e \quad (2.3.1)$$

in which ϖ_e is called the band origin.

In order to derive the vibrational (infrared) selection rules the reasoning of Herzberg is adopted[5].
The dipole moment of a molecule is defined by the integrals

$$[M]^{nm} = \int \Psi_n \Psi_m^* M d\tau \quad (2.3.2)$$

in which M is a vector having components (M_x, M_y, M_z), with $M_j = \sum e_i j_i$, in which j has been used as a short notation for the (x,y,z) coordinates respectively; e_i denotes the charge of particle i having coordinates (x_i, y_i, z_i). Ψ_n and Ψ_m are the (time dependent) eigenfunctions of the system in the states n and m, while the asterisk denotes the complex conjugate wavefunction. The permanent dipole moment of the molecule in the eigenstate n is calculated by choosing the index $m=n$ while the so called off-diagonal elements $(n \neq m)$ are responsible for dipole transitions from the n-state to the m-state.
Consider now vibrational transitions between the upper and lower vibrational levels v' and v''. The probability of an infrared transition is proportional to the square[5] of $[M]^{nm}$.
Using the Born-Oppenheimer approximation the total eigenfunction ψ can be written as a

24

product of an electronic, a vibrational and a rotational eigenfunction $\Psi = \psi_e \psi_v \psi_r$. Taking into account that for the pure vibration spectrum the contribution ψ_e and ψ_r to the transition probability $[M]^{nm}$ is constant, it follows that transition moment is proportional to the square of[10]

$$[M]^{v'v''} = \int \psi_{v'} \psi_{v''} \cdot M d\tau \qquad (2.3.3)$$

The off-diagonal matrix elements $[M]^{v'v''}$ are only different from zero if the molecular symmetry operations do not change one of the vector components of the integrand $\psi_{v'} \psi_{v''} M$, i.e. a transition $v' \leftrightarrow v''$ is allowed only when there is at least one component of the dipole moment M exhibiting the same symmetry properties as the product $\psi_{v'} \psi_{v''}$. This means for NH_3 that in the infrared region only vibrational transitions between states n and m of opposite parity (with respect to the center of symmetry) are allowed ($+ \leftrightarrow -$).

The vibration spectrum of NH_3 is affected by the so-called inversion doubling. Inversion results from the pyramidal structure of ammonia in which the nitrogen atom is considered to move through the plane of the hydrogen molecules, i.e. $NH_3 \leftrightarrow H_3N$ (tunnelling effect). If the potential energy for this type of motion (umbrella motion inversion) is drawn as a function of the distance of the N atom from the H_3-plane, a potential well with a barrier of height V positioned at the center of the well is found. The probability for the N atom to tunnel through the plane of the H atoms (the symmetry plane) depends on the height of the barrier, which in the case of ammonia is around 2072 cm^{-1}. The inversion motion results in a doubling of the vibrational energy levels, and the splitting between the symmetric and anti-symmetric energy levels increases rapidly with increasing vibrational energy: in the vibrational ground state (0,0,0,0) the splitting is small (0.79 cm^{-1}); for the (0,1,0,0) ($\nu_2 = 1$) state the splitting is 35.69 cm^{-1}, for the $(0,2,0,0)$[11] it is 284.71 cm^{-1}.

For the $\nu_1 = 1$, ν_3, and ν_4 the splittings are 1 cm^{-1} or less.

2.4. Rotational-vibrational spectra

Using the Born-Oppenheimer approximation the rotational-vibrational energy levels for symmetric top molecules are found by the summation of rotational and vibrational energy levels,

$$E_{J,v} = E_{vib} + E_{rot} = (v + \tfrac{1}{2}) \omega_e + BJ(J+1) + (A-B)K^2 \quad cm^{-1} \qquad (2.4.1)$$

In the calculation of the NH_3 rotational-vibrational levels for the $(0,0^+,0,0) \rightarrow (0,1^-,0,0)$ transition (ν_2), the centrifugal distortion and the Coriolis interaction will be neglected. The superscripts $+$ and $-$ are used to denote the symmetric and anti-symmetric wavefunctions respectively.

The molecular constants of the ammonia are found in numerous articles published in the

25

literature. The constants given below are taken from Urban *et al.*[11]

<div style="border:1px solid">

Ground state molecular parameters of $^{14}NH_3$

	s (0^+)	a (0^-)
B_0	9.9466529 ± 0.0000004 cm^{-1}	9.9416356 ± 0.0000004 cm^{-1}
$[^aA_0-^aB_0]-[^aA_0-^aB^0]$		$(6.9989 \pm 0.0001)*10^{-3}$ cm^{-1}

Ground state dipole moment[12] ($0^+ \leftrightarrow 0^-$) 1.4673 ± 0.0028 Debye

</div>

The subscripts 0 refer to the ground state, while s (or 0^+) and a (or 0^-) refer to the symmetric and anti-symmetric wavefunction respectively. It should be noted that the symmetric wavefunction 0^+ is associated with the lowest energy level in the vibrational ground state and further $0^- - 0^+ = 0.79$ cm^{-1} is the experimentally found inversion frequency in the ground state.

<div style="border:1px solid">

Molecular parameters in the ν_2 Band of $^{14}NH_3$ (in cm^{-1})

Band origin $\nu(0^+ \rightarrow 1^-)$	968.12224 ± 0.00006
^aB	10.21521 ± 0.00007
$[^aA-^aB]-[^aA_0-^aB_0]$	-0.33864 ± 0.00007
Band origin $\nu(0^- \rightarrow 1^+)$	931.64155 ± 0.00007
^aB	10.50682 ± 0.00003
$[^aA-^aB]-[^aA_0-^aB_0]$	-0.65066 ± 0.00003

Inversion splitting in the J=0, K=0 ν_2=1 state: 35.68728 ± 0.00020

ν_2=1 ($1^+ \leftrightarrow 1^-$) dipole moment[12] 1.2474 ± 0.0027 Debye

</div>

2.4.1 Infrared rotational-vibrational selection rules

As stated before, the umbrella (ν_2) vibration of ammonia changes the dipole moment parallel to the molecular top axis. The selection rules for this $\parallel$ -band are:
$\Delta K=0$, $\Delta J=0$, ± 1 ($K \neq 0$). In addition to the above selection rules for the rotational quantum numbers, the selection rules describing the symmetry properties of the rotational levels have to be obeyed, too. In the absence of any external field, in all symmetric top molecules only transitions between levels of opposite parity are allowed i.e. $\psi_s \leftrightarrow \psi_a$.
Knowing the selection rules, the rotational-vibrational transitions for parallel vibrations can be calculated according to (neglecting centrifugal distortion effects)

1) $\Delta J=+1$, $\Delta K=0$ (R-branch lines)

$$\nu=E_{J+1,v+1}-E_{J,v}=\varpi_o+(J+1)[(J+2)B'-JB'')]+K^2(A'-A''-B'+B'') \ cm^{-1}$$

2) $\Delta J=-1$, $\Delta K=0$ (P-branch lines)

$$\nu=E_{J+1,v+1}-E_{J,v}=\varpi_o+J[(J-1)B'-(J+1)B'')]+K^2(A'-A''-B'+B'') \ cm^{-1}$$

3) $\Delta J=0$, $\Delta K=0$ (Q-branch lines)

$$\nu=E_{J+1,v+1}-E_{J,v}=\varpi_o+J(J+1)(B'-B'')+K^2(A'-A''-B'+B'') \ cm^{-1}$$

ϖ_o denotes the band origin, further (J',K') and (J'',K'') are the upper and lower states respectively
The band origin of the NH_3 ν_2 $((0,0^+,0,0)\rightarrow(0,1^-,0,0))$[9] 968.12224 ± 0.00006 cm^{-1}, the Q-branch in the ν_2 umbrella vibration) is found within the 10R band of the $^{12}C^{16}O_2$ laser. The 10R(6) CO_2 laser line at 966.2504 cm^{-1} presumably excites the ammonia molecule from the ground state into the $\mid J,K> =saQ \mid 5,4>$ ν_2 (obeying the selection rules $\Delta J=0$, $\Delta K=0$) in which s indicates the symmetric wavefunction of the ground state, and Q denotes the $\Delta J=0$-branch.

2.5 The Stark effect induced in ammonia

The effect of an electric field on optical spectra was first described by Johannes Stark[13] in 1913 and is now known as the Stark effect. The Stark effect has been an important tool in the investigation of atomic and molecular spectra ever since[14-17]: the application of an external electric field E to a polar gas results in a splitting of the rotational levels, due to the interaction between the electric field E and the electric dipole moment μ (Debye; 1 Debye$=10^{-18}$ electrostatic units cm (e.s.u cm)) of the molecule.
In the molecular Stark effect the relative direction of the dipole moment μ and the angular

momentum vector J determines the occurrence of a first (in symmetric top molecules without inversion doubling) or second order Stark effect (in linear molecules, asymmetric top molecules and molecules exhibiting inversion doubling like NH_3).

In the Stark effect of rotational spectra, the electric field E is assumed to be constant in magnitude and to have a fixed direction Z with respect to the laboratory frame.

The perturbing potential is written as $H_{Stark} = \mu Er = \mu Ez$ in which E is the applied electric field and μ is the molecular dipole moment.

In the presence of an electric field the Schrödinger equation becomes[20]:

$$H\Psi_n \equiv (H_o + \lambda H_{Stark})\Psi_n = W_n\Psi_n \qquad (2.5.1)$$

in which the energy eigenvalues now have become W_n and the new eigenfunction describing the perturbed NH_3 molecule is denoted by Ψ_n. The problem now is to determine the new eigenfunctions Ψ_n. Since the eigenfunctions ψ_n of H_o form a complete set, the Ψ_n eigenfunction are expressed as power series in λ involving all the eigenfunctions ψ_n of the unperturbed Hamiltonian H_o i.e.

$$H_o\psi_n = W_n^{\ 0}\psi_n$$

and
$$\Psi_n = \{\psi_n + \Sigma C_{nk}(\lambda)\psi_k\} \qquad (2.5.2)$$

in which the summation is taken over all indices $k \neq n$. In the limit $\lambda \to 0$, it is assumed that $W_n \to W_n^{\ 0}$ and $\Psi_n \to \psi_n$, and furthermore

$$C_{nk}(\lambda) = \lambda C^1_{nk} + \lambda^2 C^2_{nk} + \ldots\ldots$$

and
$$W_n = W^0_{\ n} + \lambda W^1_{\ n} + \lambda^2 W^2_{\ n} + \ldots\ldots \qquad (2.5.3)$$

The Schrödinger equation then becomes

$$(H_o + \lambda H_{Stark})\{\psi_n + \Sigma\lambda C^1_{nk}\psi_k + \Sigma\lambda^2 C^2_{nk}\psi_k + \ldots.\} = \qquad (2.5.4)$$

$$= (W^0_{\ n} + \lambda W^1_{\ n} + \lambda^2 W^2_{\ n} + \ldots.)\{\psi_n + \Sigma\lambda C^1_{nk}\psi_k + \Sigma\lambda^2 C^2_{nk}\psi_k + \ldots.\}$$

Identifying powers of λ yields a series of equations. The first one is

$$H_o\Sigma C^1_{nk}\psi_k + H_{Stark}\psi_n = W^0_{\ n}\Sigma C^1_{nk}\psi_k + W^1_{\ n}\psi_n \qquad (2.5.5)$$

with
$$H_o\psi_k = W^0_{\ k}\psi_k$$

it results

$$W^i_n\psi_n = H_{Stark}\psi_n + \Sigma(W^0_k - W^0_n)C^i_{nk}\psi_k \qquad (2.5.6)$$

taking the scalar product with ψ_n ($k \neq n$) and making use of the orthonormality condition $<\psi_n \mid \psi_k> = \delta_{nk}$, it follows

$$W^i_n = <\psi_n \mid H_{Stark} \mid \psi_n> \qquad (2.5.7)$$

or

$$W^i_n = -\int \psi_n \mu(\underline{n}.\underline{E})\psi_n^* d^3r \qquad (2.5.8)$$

This expression equals E times the z-component of the dipole moment matrix element which, for a symmetric top molecule, can be split into several factors:

$$W^i_n = -\mu E\phi_{JJ'}\phi_{JKJ'K'}(\phi_z)_{JMJ'M'} \qquad (2.5.9)$$

The ϕ's are called factors of the direction cosine matrix[19] given below

Matrix element   J'-value

factor	J+1	J	J-1
$\phi_{JJ'}$	$[4(J+1)\sqrt{(2J+1)(2J+3)}]^{-1}$	$[4J(J+1)]^{-1}$	$[4J\sqrt{(4J^2-1)}]^{-1}$
$\phi_{JKJ'K'}$	$2\sqrt{((J+1)^2-K^2)}$	$2K$	$2\sqrt{(J^2-K^2)}$
$(\phi_z)_{JMJ'M'}$	$2\sqrt{((J+1)^2-M^2)}$	$2M$	$2\sqrt{(J^2-M^2)}$

For symmetric top-molecules the first order Stark effect can be written as:

$$W^i_n = -[\mu EMK]/[J(J+1)] \qquad (2.5.10)$$

If μ is measured in Debyes and E in kV/cm, the application of the appropriate conversion factors yields[18]:

$$W^i_n = -503.48\mu EMK/J(J+1) \text{ (in MHz per Debye per kV/cm)}$$

29

The second order Stark effect is found by identifying terms proportional to λ^2, i.e.

$$H_o\Sigma C^2_{nk}\psi_k + H_{Stark}\Sigma C^1_{nk}\psi_k = W^0_n\Sigma C^2_{nk}\psi_k + \Sigma W^1_n C^1_{nk}\psi_k + W^2_n\psi_n \qquad (2.5.11)$$

Taking the scalar product in eq.2.5.11 with ψ_n ($k \neq n$) yields

$$W^2_n = \Sigma <\psi_n \mid H_{Stark} \mid \psi_k> C^1_{nk} \qquad (2.5.12)$$

The coefficient C^1_{nk} is found by taking the scalar product in eq.2.5.9 with ψ_m, for $m \neq n$

$$<\psi_m \mid H_{Stark} \mid \psi_n> + (W^0_m - W^0_n)C^1_{nm} = 0 \qquad (2.5.13)$$

thus $\qquad C^1_{nk} = <\psi_k \mid H_{Stark} \mid \psi_n> [(W^0_n - W^0_k)^{-1}] \qquad (2.5.14)$

The second order Stark effect is then

$$W^2_n = \Sigma <\psi_n \mid H_{Stark} \mid \psi_k> <\psi_k \mid H_{Stark} \mid \psi_n> [(W^0_n - W^0_k)^{-1}] \qquad (2.5.15)$$

and using the hermiticity of H_{Stark}

$$<\psi_n \mid H_{Stark} \mid \psi_k> = <\psi_k \mid H_{Stark} \mid \psi_n>^* \qquad (2.5.16)$$

$$W^2_n = \Sigma \mid <\psi_k \mid H_{Stark} \mid \psi_n> \mid^2 [(W^0_n - W^0_k)^{-1}] \qquad (2.5.17)$$

It is of interest to examine the influence of the applied electric field on the parity of some operators used in the above calculation[21]. The parity operator $\mathcal{P}$ inverts the coordinates of all particles of the system, but not the fixed external electric field E. For example $\mathcal{P}r = -r$, $\mathcal{P}p = -p$, $\mathcal{P}\mu = -\mu$ and $\mathcal{P}H_o = H_o$ due to the commutation of $\mathcal{P}$ and H_o i.e.

$$\mathcal{P}H_o - H_o\mathcal{P} = 0 \qquad (2.5.18)$$

since H_o is determined by p^2 and $\mid R-R_e \mid$,

$$H_o = p^2/2m + V(\mid R-R_e \mid) \qquad (2.5.19)$$

This means that H_o is unaffected by inversion of all coordinates. Thus the eigenfunctions $\psi_{a,s}$ of H_o are also eigenfunctions of $\mathcal{P}$ and therefore of even or odd parity. Since μ is of odd parity

$$<\psi_{a,s} \mid \mu \mid \psi_{a,s}> = 0 \quad (2.5.20)$$

Hence first-order Stark effect occurs only if there exist degenerate or nearly degenerate levels of opposite parity.

The Hamiltonian $H = H_o - \mu E$ does not commute with $\mathcal{P}$, since E is not changed by the operation of inversion. This means that through the application of an external electric field parity is destroyed, and if Ψ_n is an eigenfunction of H

$$<\Psi_n \mid \mu \mid \Psi_n> \neq 0 \quad (2.5.21)$$

This leads to the very important breaking of parity, meaning that due to the presence of the Stark field, infrared transitions between states of equal parity are now also possible, i.e. $+\rightarrow+$, $-\rightarrow-$ next to $+\rightarrow-$ and $-\rightarrow+$.

As shown in section 2.1, symmetric top molecules exhibit degenerated energy levels ($K \neq 0$). In the case of ammonia this degeneracy is removed due to the inversion doubling. It was shown in section 2.3 the potential energy barrier gives rise to a symmetric ψ_s and an anti-symmetric ψ_a wavefunction describing different energy levels, i.e. $W(\psi_a)-W(\psi_s)=0.79$ cm^{-1}. Therefore, the unperturbed state (E=0 kV/cm) of the ammonia molecule is described by the two wavefunctions ψ_a and ψ_s.

The Stark effect induced in the NH$_3$ molecule can be calculated using the above developed results of the time-independent perturbation theory. In the following it is assumed that the Hamiltonian H_o describing the unperturbed NH$_3$ molecule (i.e. in the absence of any external field) has a complete set of symmetric rotator state orthonormal eigenfunctions ψ_a and ψ_s with eigenvalues W^0_a and W^0_s respectively, i.e.

$$H_o\psi_a = W^0_a\psi_a$$
$$\text{and} \qquad\qquad\qquad\qquad (2.5.22)$$
$$H_o\psi_s = W^0_s\psi_s$$

Due to the inversion doubling NH$_3 \leftrightarrow$ H$_3$N occurring in NH$_3$, the ammonia wavefunction Ψ is a linear combination of the symmetric ψ_s and anti-symmetric ψ_a wavefunctions

$$\Psi = a\psi_a + b\psi_s \quad (2.5.23)$$

and therefore the Stark effect induced in NH$_3$ can be calculated using non-degenerated perturbation theory. Shimizu[22-24] has pointed out that the Stark effect induced in ammonia can

31

be expressed as the sum of the Stark shifts in the vibrational ground state and the $\nu_2=1$ excited state: $\Delta\nu = \Delta\nu_{gr.st.} + \Delta\nu_{ex.st.}$. For the range of applied electric field strengths in the experiments described later on in this thesis ($E \leq 6$ kV/cm), it suffices to calculate the first order perturbation term in the determination of the Stark shifts induced in the ground and excited states respectively

$$(H_o + H_{Stark})\Psi = W\Psi \quad \text{or}$$

$$(H_o + H_{Stark})(a\psi_a + b\psi_s) = W(a\psi_a + b\psi_s) \quad (2.5.24)$$

Taking the scalar products in the above expression with ψ_a and ψ_s and bearing in mind the orthonormality properties of ψ_a and ψ_s, yields the following eigenvalue problem

$$[W^0_a - <\psi_a \mid H_{Stark} \mid \psi_a>]a + [<\psi_a \mid H_{Stark} \mid \psi_s>]b = aW \quad (2.5.25)$$

$$[<\psi_s \mid H_{Stark} \mid \psi_a>]a + [W^0_s - <\psi_s \mid H_{Stark} \mid \psi_s>]b = bW \quad (2.5.26)$$

The scalar products $<\psi_a \mid H_{Stark} \mid \psi_a>$ and $<\psi_s \mid H_{Stark} \mid \psi_s>$ are equal to zero on account of parity considerations.
The non-trivial energy eigenvalues are found by solving the discriminant

$$\begin{vmatrix} W^0_a - W & -\mu EMK/J(J+1) \\ -\mu EMK/J(J+1) & W^0_s - W \end{vmatrix} = 0$$

After some algebra the eigenvalues are found to be

$$W = \tfrac{1}{2}(W^0_a + W^0_s) \pm \surd[\tfrac{1}{4}(W^0_a - W^0_s)^2 + (\mu EMK/J(J+1))^2] \quad (2.5.27)$$

In the vibrational ground state $W^0_a - W^0_s = 0.79$ cm^{-1}, while in the $\nu_2 = 1$ state $W^0_a - W^0_s = 35.69$ cm^{-1}.
The largest induced Stark shift with $E = 6$ kV/cm $\mu_{gr.st.} = 1.47$ Debye, is found in the vibrational ground state $\Delta\nu_{Stark} = 4.44$ GHz or 0.148 cm^{-1}. As $\mu EKM/J(J+1) < \tfrac{1}{2}(W^0_a - W^0_s)$ a Taylor expansion of the energy eigenvalue expression can be given

$$W = \tfrac{1}{2}(W^0_a + W^0_s) \pm \{\tfrac{1}{2}(W^0_a - W^0_s) + [(\mu EMK/J(J+1))^2]/(W^0_a - W^0_s)\} \text{ cm}^{-1} \quad (2.5.28)$$

The splitting between the upper anti-symmetric and lower symmetric inversion level amounts to

$$2[(\mu E M K / J(J+1))^2] / (W^o_a - W^o_s) \text{ cm}^{-1} \qquad (2.5.29)$$

As can be seen at the low electric field strengths used in the experiments the Stark effect induced in ammonia depends quadratically on E.

The contribution from the second order term (in λ^2) of the Stark perturbation for the symmetric top molecule takes into account the interaction between the $| J,K \rangle$ and the $| J+1,K \rangle$ and $| J-1,K \rangle$ levels[25] and can be calculated using the direction cosine matrix elements and the energy differences

$$W_{J,K} - W_{J+1,K} = 2B(J+1) \text{ cm}^{-1}$$

$$W_{J,K} - W_{J-1,K} = 2BJ \text{ cm}^{-1}$$

it then results

$$W = \mu^2 E^2 / 2B \{ [(J^2 - K^2)(J^2 - M^2)] / [J^3(2J-1)(2J+1)] -$$

$$- [[(J+1)^2 - K^2][(J+1)^2 - M^2]] / [(J+1)^3(2J+1)(2J+3)] \}$$

since for NH_3 the rotational constant B is of the order of 10 cm^{-1} the contribution from the second order Stark perturbation in the range of the applied electric field strengths is negligible. Therefore when using field strengths not exceeding 6 kV/cm, the Stark effect is mainly induced in the ammonia ground state.

2.6 Molecular linewidths at reduced gas pressures

The enhancement of spectral coincidence between the 10R(6) and 10R(8) emission frequencies of the CO_2 waveguide laser and the Stark absorption wavelengths of ammonia can be achieved by reducing the gas pressure in the photoacoustic cell, which results in a narrowing of the molecular absorption lines. Another advantage of working at sub-atmospheric pressure is the increased microphone sensitivity S_m. Experimentally it was proved that both phenomena produced an optimum in signal to noise ratio of the recorded photoacoustic signal at 200 mbar. For pressure broadened lines the absorption profile is a Lorentzian[26]:

33

$$\alpha(\nu) = [\sigma n / \pi \Delta \nu_L] \Delta \nu_L^2 / [\Delta \nu_L^2 + (\nu - \nu_0)^2] \qquad (2.6.1)$$

where σ is the molecular absorption cross-section (cm^2/mole), n the density of absorbing molecules per unit volume (mole/cm^3) and $\Delta \nu_L$ the homogeneous width (half width at half maximum in cm^{-1}). The linewidth $\Delta \nu_L$ can be expressed as the sum of a self broadening and a buffer gas broadening term, i.e.:

$$\Delta \nu_L = c_s p_n + c_b p_b \equiv cp \qquad (2.6.2)$$

The coefficients c_s and c_b refer to the self and buffer broadening, whilst p_n and p_b indicate the partial pressure of the absorbing and buffer molecules respectively. For realistic air samples containing NH_3 at trace levels, the self broadening coefficient c_s is negligible. According to Baldacchini et al.[27] and Young[28,29], the buffer gas broadening coefficient for NH_3 in nitrogen is 4.2 MHz/Torr (760 Torr ≡ 1013.25 mbar). Kinetic theory predicts the absorption halfwidth of a Lorentzian shaped line to vary as:

$$\Delta \nu_L(p,T) = \Delta \nu_L(p_0, T_0)(p/p_0) \sqrt{(T_0/T)} \qquad (2.6.3)$$

where $\Delta \nu_L(p_0, T_0) = 0.11$ cm^{-1} for NH_3 buffered in N_2 at 760 Torr and 296 K. Thus, the absorption halfwidth of an ammonia | J,K> line at a pressure of 200 mbar and at room temperature is about 700 MHz (0.022 cm^{-1}).

The ammonia lines in the $\nu_2 = 1$ mode have been accurately determined in various experiments and published in the literature[11]. Taking into account the pressure broadening at a gas pressure of 200 mbar, in the absence of any external field the 10R(6) $^{12}C^{16}O_2$ laser (966.2504 cm^{-1})line excites the $\nu_2 = 1$ umbrella vibration via the | J,K,M> = saQ | 5,4,M> transition (966.2691 ± -0.0002 cm^{-1}), while the 10R(8) line (967.707 cm^{-1}) excites the | J,K> = saQ | 2,2,M> transition (967.7386 cm^{-1}).

Using the above derived Stark shifts for the applied field strength E of 6 kV/cm, it can be calculated that for the 10R(6) line the NH_3 molecule is excited into the $\nu_2 = 1$ vibration via the aaQ | 4,1,M>, and the aaQ | 4,2,M> transitions. The transitions are tuned into resonance with the CO_2 laser, while the saQ | 5,4,M> transition is gradually tuned out of resonance. At the 10R(8) line the saQ | 2,2,M> is slightly detuned. The positions of different rotational lines of the ν_2 ammonia vibration mode have been measured very accurately[11,30,31]. The rotational lines of the sQ(5,K) NH_3 multiplet are:

sQ | 5,K,M >[11]	frequency (cm⁻¹)
sQ | 5,2,M >	966.4735
sQ | 5,3,M >	966.3821
sQ | 5,4,M >	966.2691
sQ | 5,5,M >	966.1512

and the lines of the sQ(2,K) NH_3 multiplet are calculated to be at:

sQ(2,K)	frequency (cm⁻¹)
sQ(2,1)	967.7748
sQ(2,2)	967.7386

2.7 Kinetic cooling effect

Apart from the interference effect of H_2O and CO_2 absorption the N_2-O_2 collisions affect the magnitude and phase of photoacoustic signals (kinetic cooling effect). The molecular dynamics involved in the process of kinetic cooling following the absorption of laser radiation can best be understood by studying the main collisions occurring in a mixture of gases consisting of water vapor, carbon dioxide and nitrogen. In the text the reasoning of Wood et al.[3]., Olafsson[26], and Rooth et al.[32] is adopted. The main energy transfer reactions involved in the kinetic cooling effect are given below

$H_2O^* + M \leftrightarrow H_2O + M$ (1) $\tau_1 = 6.3*10^{-7}$ sec

$CO_2(100) + h\nu \leftrightarrow CO_2(001)$ (2) $\tau_2 = 2.2*10^{-4}$ sec

$CO_2^*(010) + M \leftrightarrow CO_2 + M$ (3) $\tau_3 = 7.5*10^{-7}$ sec

$CO_2^*(001) + N_2 \leftrightarrow CO_2 + N_2^*$ (4) $\tau_4 = 1.0*10^{-7}$ sec

35

$$N_2^* + H_2O \leftrightarrow N_2 + H_2O^*(010) \qquad (5) \qquad \tau_5 = 1.2*10^{-2} \text{ sec}$$

$$N_2^* + O_2 \leftrightarrow N_2 + O_2^* \qquad (6) \qquad \tau_6 = 3.2*10^{-2} \text{ sec}$$

$$CO_2^*(001) + M \leftrightarrow CO_2^*(030) + M \qquad (7) \qquad \tau_7 = 1.4*10^{-2} \text{ sec}$$

$$O_2^* + H_2O \leftrightarrow O_2 + H_2O^*(010) \qquad (8) \qquad \tau_8 = 2.9*10^{-7} \text{ sec}$$
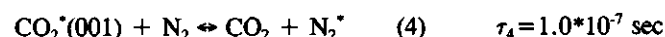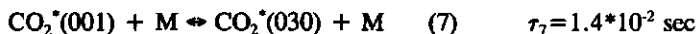
with the relaxation times τ taken from Wood et al.[3].

In the above reactions the notation (000) stands for (ν_1, ν_2, ν_3)-vibrational modes, while the asterisks is used to denote an excited state. Contrary to carbon dioxide, the water vapor molecules release directly the absorbed laser radiation via molecular collisions described by the reaction (1). In view of the typical CO_2 concentration in the atmosphere (350 ppmv), the collisional partners of primary importance are N_2, O_2 and H_2O (denoted by M). In a mixture containing the CO_2 and N_2, carbon dioxide is excited from the (100) hot band level into the (001) level (2). Due to the proximity of the latter and the first excited N_2 vibration, energy from the CO_2(001) level is rapidly transferred to N_2 (4). As the concentration of nitrogen is much higher than that of carbon dioxide, almost all the vibrational energy is transferred to the former species.

The excited N_2 molecules release their energy via three reaction channels. One involves collisions with H_2O via (1) and (5), other channels involve (6), (8) and (1). The final path contains (4), (7) and (3). Energy release through (1) and (8) is sufficiently fast, in contrast to the depletion of N_2^* via (5) and (6). The net effect of the three deactivation channels is the transfer of vibrational energy into translation motion, leading to an increase in kinetic energy, and subsequently a heating of the gas. However, a delay in energy transfer results from the relatively slow deactivation processes (5), (6) and (7). This again, leads to a cooling of the gas via the fast reaction (3) and the equilibrium condition existing between $CO_2^*(100)$ and $CO_2^*(010)$. In the traditional chopper mode photoacoustics the kinetic cooling effect manifests itself when the laser exposure time (or pulse time) is either comparable or less than the relaxation time dominating the deactivation reactions (5), (6) and (7).

The kinetic cooling effect affects the phase but also the magnitude of the recorded photoacoustic signal. The total phase measured in a photoacoustic experiment depends on the phases of the individual gaseous constituents. The time lag existing between the molecular deactivation rates results in a out-of-phase signal between the gas of interest and gaseous CO_2 lowering the magnitude of the photoacoustic signal. However, it will be shown that the molecular relaxation processes accelerate at increasing water vapor concentration. To do so, it suffices to determine the effect of vibrational energy change on the gas temperature. The total rate of energy absorbed by a gas is:

$$dH/dt = (C_p/R)dT/dt + dE_{vib}/dt \qquad (2.7.1)$$

in which H denotes the enthalpy, C_p is specific heat at constant gas pressure, and R is the universal gas constant.

The total energy absorbed in the gas mixture is the sum of the energies absorbed by CO_2 and H_2O, and is equal to the change in enthalpy:

$$dH/dt = A(T,\phi,P)(\alpha_{CO2}+\alpha_{H2O}) \qquad (2.7.2)$$

in which A is a function depending on the temperature of the gas (T), the laser intensity (ϕ), and the gas pressure (P), while α denotes the absorption coefficient of carbon dioxide and water respectively.

It can be shown that the time rate change (with respect to time) of the total vibrational energy E_{vib} of the gas mixture is:

$$dE_{vib}/dt = B(T,\nu,P,\phi)\alpha_{CO2}exp(-t/\tau_n) \qquad (2.7.3)$$

in which τ_n is the net relaxation time (for the reactions (5), (6) and (7)) and ν denotes the spacing between the CO_2 (100) and (001) vibrational levels. Substituting equations (2.7.2) and (2.7.3) into equation (2.7.1) leads to:

$$dT/dt = C(1 + \alpha_{H2O}/\alpha_{CO2} - \nu exp(-t/\tau_n)) \qquad (2.7.4)$$

A cooling of the gas occurs when the term within brackets is negative. For t=0, such a condition exists if:

$$\alpha_{H2O}/\alpha_{CO2} < 1-\nu = 1.444 \qquad (2.7.5)$$

i.e. the duration t of the laser illumination (chopper period) is shorter than the relaxation dominating the deactivation processes. From eq.(2.7.5) it is clear that the effect of the kinetic cooling depends on the amount of water vapor in the gas mixture.

Consequently, kinetic cooling and the concentration of water vapor present in realistic air samples is of particular interest when employing a resonant photoacoustic cell. A maximum acoustic amplification of the generated signal occurs at the resonance frequency. A typical photoacoustic cell exhibits resonance frequencies above 500 Hz, and therefore the kinetic cooling effect manifests itself when working with 'dry' air samples. In fact, the effect of variable amounts of water vapor on the dominating relaxation process in mixtures involving CO_2 and N_2 is known and can be calculated:

$$1/\tau_4 = (x_1/\tau_{31}+x_4/\tau_{34}+x_5/\tau_{35})x_3/x_4+x_1/\tau_{41}+x_5/\tau_{45} \qquad (2.7.6)$$

in which the indices 1 to 5 refer to gases ($1 \equiv H_2O$, $2 \equiv NH_3$, $3 \equiv CO_2$, $4 \equiv N_2$, $5 \equiv O_2$) and x_i are the respective fractional concentrations ($0 < x_i < 1$). The time constants τ_{ij} are the

37

relaxation times for vibrational to translational energy transfer due to collisions between molecules i and j (i,j=1,...,5). According to Rooth et al.[32]. $1/\tau_4$ is 48 Hz for 0% H_2O and 1410 Hz for 1% H_2O (x_i=0.01). For chopping frequencies exceeding 1410 Hz (C_{H2O}=1% i.e. the normal ambient concentration level in the Netherlands) kinetic cooling effect occurs. To avoid cooling of the gas, regardless of the amount of water vapor present in the gas sample, the optimum laser beam chopping frequency must be maintained below 48 Hz.

References

1. C.N.Banwell, Fundamentals of Molecular Spectroscopy, third edition, McGraw-Hill Publishing Company (1983).
2. P.L.Meyer, Ph.D.thesis, 8651 ETH, Zürich, Switzerland (1988).
3. A.D.Wood, M.Camac, and E.T.Gerry, Appl.Opt., 10, 1877, (1971).
4. L.S.Rothman et al., Appl.Opt., 26, 4058, (1986).
5. G.Herzberg, Infrared and Raman Spectra of Polyatomic Molecules, Van Nostrand-Reinhold Company (1945).
6. P.R.Bunker, W.P.Kraemer, and V.Špirko, Can.J.Phys., 62, 1801, (1984).
7. R.J.Brewer and C.W.Bruce, Appl.Opt., 17, 3746, (1978).
8. P.W.Atkins, Molecular Quantum Mechanics, second edition, Oxford University Press, (1983).
9. D.M.Dennison, Rev.Mod.Phys, 12, 175, (1940).
10.A.Dymanus, Lectures on Molecular Spectroscopy, Volume II, Notebook Catholic University Nijmegen.
11.Š.Urban, V.Špirko, D.Papoušek, R.S.McDowell, N.G.Nereson, S.P.Belov, L.I.Gershstein, A.V.Maslovskij, A.F.Krupnov, J.Curtis, and K.N.Rao, J.Mol.Spectrosc., 79, 455, (1979).
12.V.Špirko, J.Mol.Spectrosc., 74, 456, (1979).
13.J.Stark, Sitz. Akad. Wiss. Berlin, 47, 932, (1913).
14.G.Duxbury, Int.Rev.Phys.Chem., 4, 237, (1985).
15.J.H.Shirley, J.Chem.Phys., 38, 2896, (1963).
16.D.K.Coles, W.E.Good, J.K.Bragg, and A.H.Sharbaugh, Phys.Rev., 82, 877, (1951).
17.J.M.Jauch, Phys.Rev., 72, 715, (1947).
18.T.M.Sugden and N.C.Kenney, Microwave Spectroscopy of Gases, Van Nostrand (1965).
19.C.H.Townes and A.L.Schalow, Microwave Spectroscopy, McGraw-Hill (1955).
20.S.Gasiorowicz, Quantum Physics, Wiley & Sons (1974).
21.A.D.Buckingham, The Stark Effect, 3, MTP Int.Rev.Sci., Phys.Chem., Series One, Eds.A.D.Buckingham and D.A.Ramsey, Butterworths Univ. Park Press (1972).
22.F.Shimizu, J.Chem.Phys., 51, 2754, (1969).
23.F.Shimizu, J.Chem.Phys., 52, 3572, (1970).
24.F.Shimizu, J.Chem.Phys., 53, 1149, (1970).
25.W.Gordy and A.L.Cook, Microwave Molecular Spectra, Wiley, New York, (1970).
26.A.Olafsson, Ph.D.thesis, Ørsted Inst., Univ.Copenhagen (1990).
27.G.Baldacchini, G.Buffa, and O.Tarrini, in "Monitoring of Gaseous Pollutants by Tunable Diode Lasers", Eds. R.Grisar, G.Schmidtke, M.Tacke, Kluwer Acad. Publ., Dordrecht (1988).

28. U.Persson, B.Marthinsson, J.Johansson, and S.T.Eng, Appl.Opt., **19**, 1711, (1980).
29. L.G.Young, "Compilation of stratospheric trace gas spectral parameters", AFCRL-TR-76-0033, Air Force Cambridge Research Laboratories, Hanscom AFB, Mass. (1976).
30. K.Shimoda, Y.Ueda, J.Iwahori, Appl.Phys., **21**, 181, (1980).
31. H.Sasada, Y.Hasegawa, T.Amano, and T.Shimizu, J.Mol.Spectrosc., **96**, 106, (1982).
32. R.Rooth, A.Verhage, and L.J.Wouters, Appl.Opt., **29**, 3643, (1990).

Chapter 3   Constructional Details

3.1 The three frequency phase-locked loop

Intermodulated photoacoustic spectroscopy makes use of a home-made three frequency phase locked loop (PLL) to simultaneously drive the chopper (frequency f_{chop}), the Stark modulation unit (frequency f_{Stark}) and to provide the reference (or detection) frequency (frequency f_{ref}) for the two phase lock-in amplifier. In addition the phases ϕ_{chop}, ϕ_{Stark} and ϕ_{ref} of the driving signals must be mutually stable and phase-locked. These requirements were met by using a home-made device (PLL), the scheme of which is shown in Fig.3.1.1.

The PLL consists of four electronic circuits A, B, C and D. The circuits A, B, and C are identical and provide the reference frequency f_{ref} (numerically equal to K) for the lock-in amplifier, the driving frequency f_{Stark} (numerically equal to L) for the Stark high voltage unit, and the driving frequency f_{chop} (numerically equal to N) for the chopper motor, respectively. As A, B and C are mutually identical, it suffices to describe the operational principles of circuit A.

A TCXO (Temperature Compensated Crystal Oscillator) with a fixed output frequency of 2.4576 MHz is used as a reference frequency clock for the entire PLL. The clock frequency is divided down to 128 Hz (reference frequency for the PLL) and fed into one (1) of the two inputs ((1) and (2)) of a phase comparing unit (PCU (I)). The output of the PCU (I) generates pulses proportional to the phase difference of inputs (1) and (2), which in turn are fed into an integrator. Its output signal is used as a control voltage for a voltage controlled oscillator (VCO). The output frequency of the VCO is in turn, divided by an integer K in a 4 decade divider ($3 \leq K \leq 9999$) and its output signal fed into the second input (2) of the PCU (I). PCU (I) compares the 128 Hz reference to this signal, until a stable output frequency of 128*N Hz is obtained. This stable frequency is then divided by 128 to obtain a frequency (numerically equal to N) previously selected by the 4 decade divider.

As far as the chopper motor is concerned an additional circuit D was developed. The selected output signal (a frequency numerically equal to N) is fed into input (1) of PCU (II), the output signal of which was fed into an integrator and passed to a transistor. It is the output voltage of the transistor that was used to drive the chopper motor (M). After selecting a chopper blade with the proper amount of slits, the chopping frequency is accordingly measured by a light emitting diode (LED) and its output is fed into the input (2) of the PCU (II).
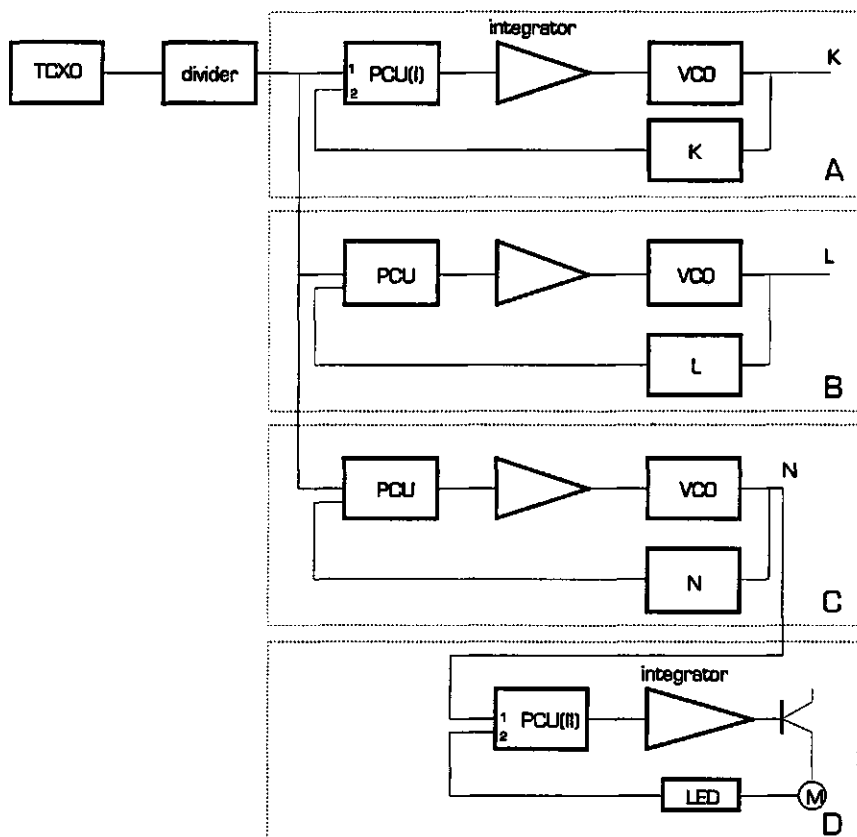
40

Fig.3.1.1 Phase-locked loop (PLL)

41

3.2 The photoacoustic Stark cell

    In this section a detailed description of the resonant photoacoustic Stark cell is presented. Alpase-Aluplus aluminum provided by B.V. IMCO HOLLAND Rotterdam was selected as a material. This kind of aluminum is tension-free and exhibits a fairly high tensile strength. The material was tooled on a milling-machine to leave a solid aluminum block forming the body frame. Out of this frame (length*width*height:240.0*140.0*66.0 mm^3) a rectangular hole (dimensions l*w*h=200.0*60.5*46.0 mm^3) was made to accommodate the photoacoustic Stark cell. Another rectangular hole (dimensions 220.0*50.0*40.0 mm^3) was milled alongside the body frame to hold the compartment containing the electronic preprocessing equipment (1) shown in Fig.3.2.1.
    Four holes (each 3 mm in diameter and 3 mm deep), were drilled in the floor of the photoacoustic Stark cell. A PTFE-teflon block (2), U-shaped in transverse cross-section (outer dimensions 100.0*60.5*35.0 mm^3 and inner dimensions 100.0*19.0*25.0 mm^3) was fitted centrally into the Stark cell. (its width and dimension match that of the photoacoustic Stark cell). With the teflon block (2) in position (fixed by four teflon pins (length 6 mm, diameter 3 mm)) two buffers (3) of equal volume (50.0*60.50*46 mm^3) are formed at either end of the photoacoustic Stark cell. Two identical Stark plates (100.0*19.0*10.0 mm^3) (4,5) were made from Alpase-Aluplus aluminum (the width and the length of the Stark plates equal the inner dimensions of (2)). In the upperside of one (4) of the Stark plates three identical slots were milled.
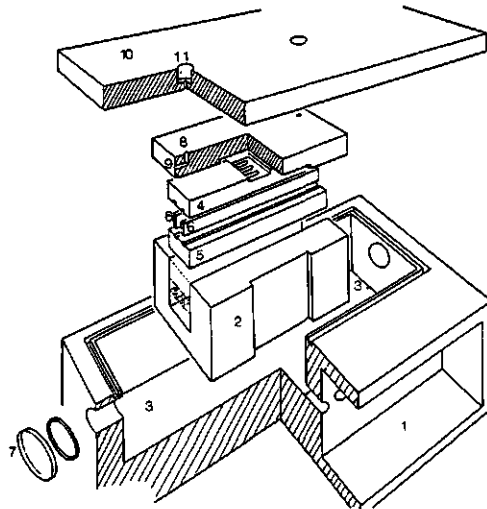
Fig.3.2.1 Exploded view of the Stark cell showing the photoacoustic section and the electronic preprocessing compartment

42

Each slot accommodates a single electret M37 microphone (12) manufactured by Microtel Amsterdam; this latter fits exactly into the slot to prevent undesired pressure leakage. The M37 microphone's operating voltage is 9 V_{DC}; its typical sensitivity specified at STP is 10 mV/Pa. The frequency characteristic for this type of microphone is shown in Fig.3.2.2.

Typical response curve

Fig.3.2.2 Frequency characteristic of the Microtel M37 microphone

Fig.3.2.3 Photoacoustic Stark cell; Stark plate (4) removed

43

Fig.3.2.4 Stark plate (4) in position. Photograph shows the M37 Microtel Microphone (12)

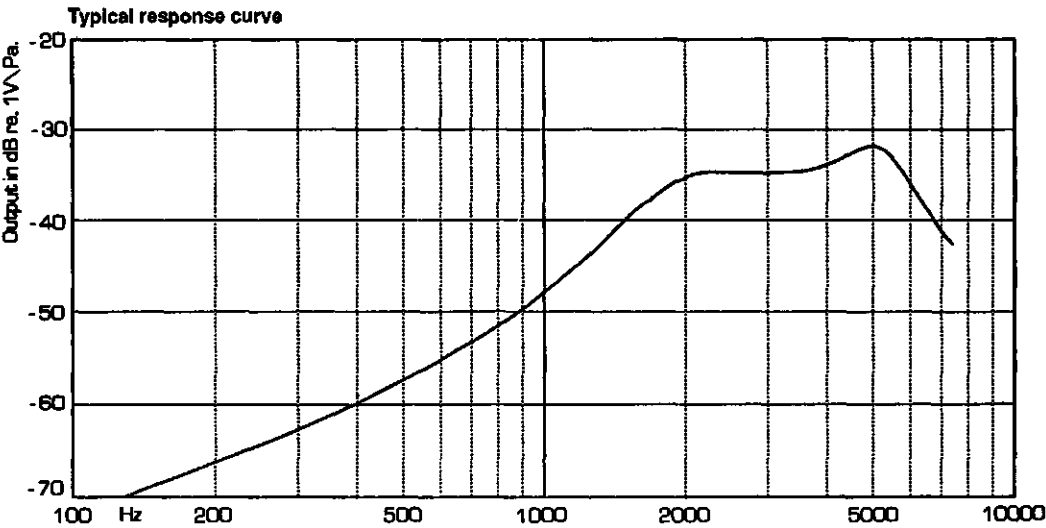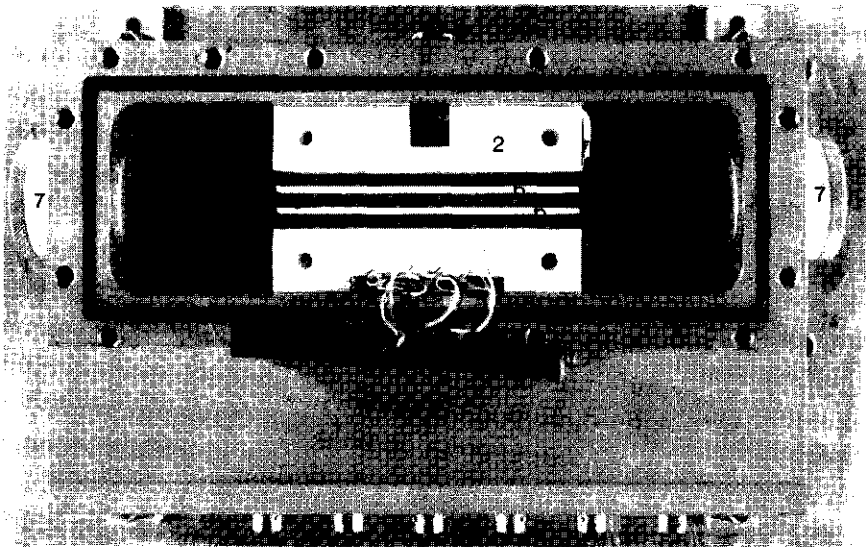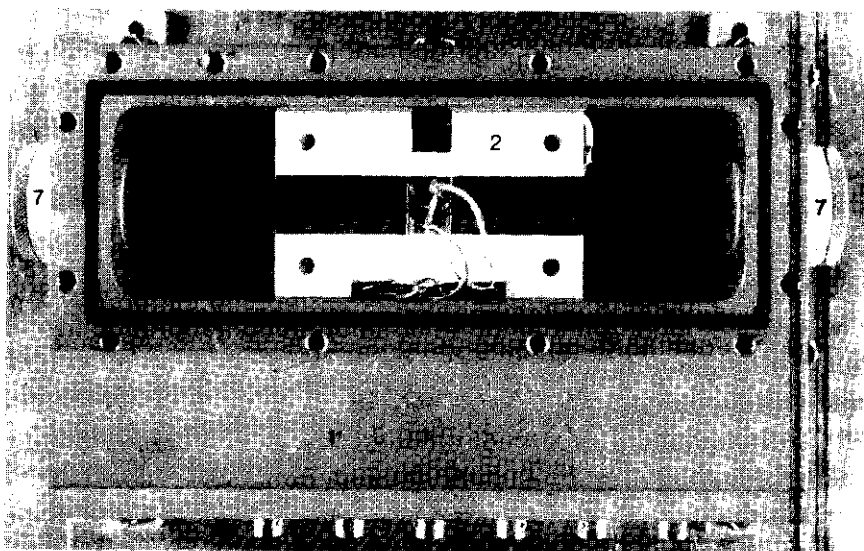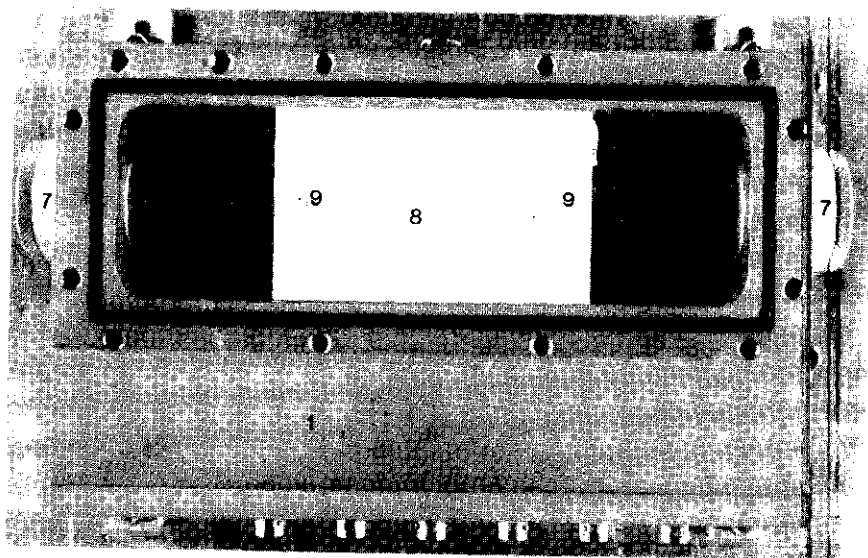**Fig.3.2.5** Cover plate (8) in position

Two narrow, longitudinal grooves were made in the underside of the upper Stark plate (4) and the upperside of the lower Stark plate (5). Two PTFE-teflon spacers (6) were slotted into these two grooves (Fig.3.2.3). In such a way three identical, rectangular, longitudinal channels (100.0 mm long with a cross-section (5.0 * 5.0 mm^2) are formed.

The teflon block (2) (accommodating the Stark plates (4 and 5) shown in Fig.3.2.4) was closed by a teflon cover plate (8) (Fig.3.2.5). The teflon cover plate runs flush with the frame. In each short end of the teflon cover plate an "elbow-shaped" channel (9) (1 mm in diameter) was drilled, serving as gas in- and outlets (Fig.3.2.5).

At either end of the Stark cell compartment a flat ZnSe AR/AR window (25.4 mm (1") in diameter; Janos Technology, Vermont, USA) was mounted in an aluminum cap (7). In a side wall of the Stark cell a "LEMO" (size 1) plug (13) was mounted to pass the high voltage modulation to the Stark plate (5) (the Stark plate (4) was grounded). The maximum tolerable DC voltage for this plug is 7 kV, with maximum peak voltages not exceeding 15 kV.

In the wall opposite to that carrying the LEMO high voltage connector, four "LEMO" (size 0) connectors were mounted. The microphones were connected to three of the "LEMO 0" plugs; a Motorola MX-1000 temperature compensated pressure sensor (14) was connected to a fourth plug. The four plugs were fixed into the walls using an air-tight fast-drying glue.

A round-edged rectangular groove was cut into the top section of the body frame, and provided with an O-ring (15) to assure sealing. The cell was closed from above by an aluminum cover plate (10) bolted to the frame. Two swagelock ¼" fittings (11) mounted on top of the cover plate serve as gas in- and outlet ports (Fig.3.2.6).

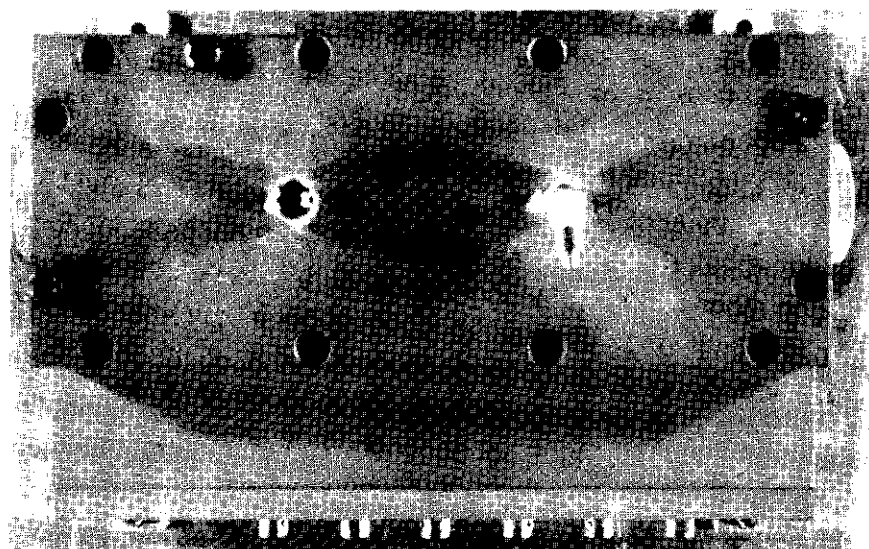**Fig.3.2.6** Photoacoustic Stark cell closed by the aluminum cover plate (10)

The $^{12}C^{16}O_2$ waveguide laser

The home-made $^{12}C^{16}O_2$ laser used here was an improved version (H.Jalink) of the early model designed by C.Sikkens and used by Harren *et al.*[1] This previous design featured a plasma tube and a cooling jacket consisting of two equal but separate sections joined together by means of a silicon glue. Further, the laser was susceptible to a substantial degree of contamination (cathode sputtering, dirt, material disintegration and deposition of hot gas on the optical components etc.). This resulted in a relatively short life time of the plasma tube and a frequent need for dismantling of the laser.

The present laser consists of a single, one-piece quartz plasma tube and cooling jacket (both equal in size) fused together. The plasma tube (500 mm long, inner diameter 1.8 mm) is filled with the flowing active gas mixture consisting of 65% He, 22% N_2 and 13% $^{12}C^{16}O_2$. The optical components mounted in teflon cylinders are continuously flushed by the active gas mixture. In this way degradation by deposition is substantially reduced.

The laser tube rests on three aluminum guard brackets, each provided with three adjustable pins terminated by teflon heads in order to facilitate lateral and vertical centring of the tube. This type of mounting is more sturdy and less prone to bending; in addition it enables an easy and rapid alignment.

References

1. F.Harren, P.D.thesis, Catholic University Nijmegen (1988).

3.3 ON THE ADSORPTION PROPERTIES OF AMMONIA TO VARIOUS SURFACES

Hans Sauren[1], Bert van Hove[2], Wim Tonk[2], Henk Jalink[1] and Dane Bićanić[1]

[1] Department of Physics and Meteorology,
  Agricultural University,
  Duivendaal 1,
  6701 AP Wageningen
  The Netherlands.

[2] Department of Plant Physiology,
  Agricultural University
  Wageningen
  The Netherlands

INTRODUCTION

Ammonia resulting from intensive agricultural livestock and fertilizing activities is nowadays considered to be one of the main causes of soil acidification. To set up an active program to attack the acid rain issue, "on-line" monitoring with sufficient sensitivity (down to 1 ppbv) of the ambient ammonia (NH_3) concentration is an impetus. However, due to the polar nature and electronegative character of NH_3, overlap of the nitrogen lone pair electrons with the surface atoms of the detector occurs, resulting in strong bonds at the detector's cell walls; this phenomena is called adsorption. Laser photoacoustic spectroscopy (PAS) provides a sensitive and general technique tor trace level vapors[1,2]. We have used the photoacoustic (PAS) arrangement consisting of a tunable CO_2 laser, a mechanical chopper and a cell in which the photoacoustic signal is generated by excitation and deactivation of the gas of interest (here NH_3). In this setup the confined gas adsorbs on the cell walls, thereby producing an error in real time low concentration measurements. The problem is to find the material, for construction of the PA cell, that shows lowest adsorption affinity for ammonia. In recent years experiments have been carried out to determine photoacoustically the uptake of ammonia by materials such as PTFE-teflon, paraffin, gold and different kinds of teflon tubing[3,4]. However, these data contain the relative values only. In this paper ammonia rise times for aluminium, silicon coated aluminium, brass and teflon have been determined by using a novel method. With this basically different method, using a 'leaf chamber', it is possible, at least theoretically, to derive the absolute amount of adsorbed ammonia.

47

EXPERIMENTAL

Detailed studies of the uptake and response by plants to pollutant gases require precisely controlled environmental conditions. Therefore a device called leaf chamber has been designed and used by plantphysiologists. Some problems have been encountered with the early models; one of the main problems being the intrinsic interaction between the pollutant gas and the leaf chamber walls. At the Agricultural University in Wageningen, W. Tonk and B. van Hove[5] designed a new chamber by which most of the drawbacks could be overcome. This new device has been extensively used by van Hove for his adsorption experiments with biological material (leaves).

Measuring NH_3 adsorption on non-biological samples (such as metals etc.) requires less strict conditions than when dealing with biological material; therefore the Tonk-van Hove leaf chamber is certainly suited for such studies with materials. The leaf chamber meets the following requirements:

1. glass and teflon (PTFE) have been used for all internal parts. These materials show a low adsorption affinity for pollutant gases like SO_2, O_3, NO_2 and to a lesser extent NH_3.
2. precise control of air temperatures in the chamber enables one to study the effect of different temperatures on adsorption. It is necessary to avoid large fluctuations in the concentrations of pollutant gases and in relative air humidity. In addition, condensation of water vapour on internal surfaces, in which the pollutant gases may dissolve, should be prevented.
3. the internal volume of the cell amounts to 2.6 l. Differences between inlet and outlet concentrations are only detectable if flow rates of air passing the leaf chamber are small (5 to 6 l/min). As a consequence mechanical mixing within the leaf chamber is part of a gas exchange fumigation system described in a previous paper by van Hove[6].

The uptake of ammonia is determined by measuring the difference between inlet and outlet concentration of the leaf chamber. At the outlet port NH_3 is detected with a NO_x-analyzer equipped with a catalytic converter to oxidize NH_3 to NO. A more extended description of this Tonk-van Hove leaf chamber is given by van Hove[7]. In this study ammonia rise times have been measured for aluminium, silicon coated aluminium, brass, and PTFE-teflon. These materials, frequently used as construction materials for photoacoustic cells, were cut into plates of 15x15x0.1 cm., resulting in a total area of 456 cm^2. Before entering the chamber, the plates (samples) were cleaned with pure alcohol.

Because mixing of the leaf chamber air is uniform, the accumulation of the internal concentration of NH_3 following gas injection can be determined by measuring the outlet concentration of the leaf chamber (C_{out}). Then C_{out} is given by an exponential function:

$$C_{out} = C_{in}[1 - exp(-t/\tau)]$$

The curve is characterized by the time constant τ (relaxation time). In absence of adsorption on the internal surfaces, τ is numerically equal to the residence time, i.e. the ratio between leaf chamber volume and the flow rate: V/f. First the response of the empty chamber is measured (chamber without a sample). After this reference measurement the response of the chamber with specimen is determined. The output concentration, for both, the empty

chamber and the chamber with a sample, is expected to reach the NH_3 input concentration after a certain time (for f = 6 l/min. and V = 2.6 l τ is expected to be 0.43 min^{-1}, so C_{out} will reach 68% of its final value after 2.30 minutes when no adsorption of ammonia on the internal surface occurs). Out of the experiments two functions can be generally derived:

$$C_{out \cdot e.c.} = C_{in}[1 - exp(-t/\tau_{e.c.})] \qquad e.c. = \text{empty chamber}$$

$$C_{out \cdot c.s.} = C_{in}[1 - exp(-t/\tau_{c.s.}] \qquad c.s. = \text{chamber} + \text{sample}$$

The difference between $\tau_{e.c.}$ and $\tau_{c.s.}$ is a specific measure for the amount of adsorbed molecules on the sample.
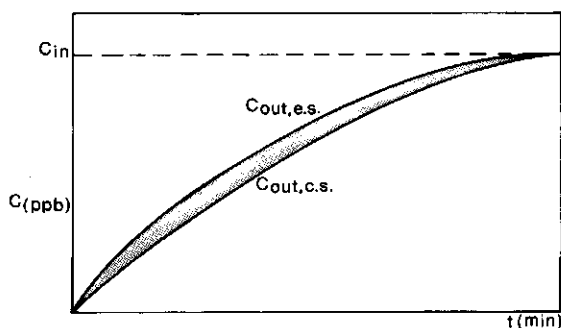

Fig.3.3.1 Theoretical adsorption curves for the empty leaf chamber ($C_{out,e,s}$) and the leaf chamber + sample ($C_{out,c,s}$)

The area can be calculated exactly by integrating the substraction of both functions. Because flow rate and the are of the sample are know, the amount of adsorbed molecules per square angstrom can be worked out. This peculiar feature makes this method so special.

After the whole system had been equilibrated at relative air humidity (RH) of 15%, 50 ppbv NH_3 was injected into the flow of conditioned air passing the leaf chamber. The outlet concentration was then recorded until a steady state for the system was attained. The whole experiment was repeated for the system without leaf chamber in order to correct for a contribution of the in- and outlet tubing of the leaf chamber.

During the experiments the temperature in the chamber was kept constant at 25^{0}C. Relative humidity of 15% could be reduced further only by flushing the chamber using a very large flow rate of N_2. Rise time curves for the empty chamber and the chamber with sample (Fig.3.3.2) show significantly different behaviour than was predicted (Fig.3.3.1). In contrast to the theoretical curves all the measured signals rise more rapidly than was expected. Only the tail section of the measured curves agrees well with the theoretically predicted values. Another striking fact is that even after 6 hours the response of the empty chamber and the chamber with sample approach asymptotically different steady state values: that is to say the output concentrations don't approach the input concentration C_{in} (C_{in} = 50

49

ppbv). It appears as if ammonia continuously lost in the chamber. Furthermore, the rise time of all signals is slower than expected.
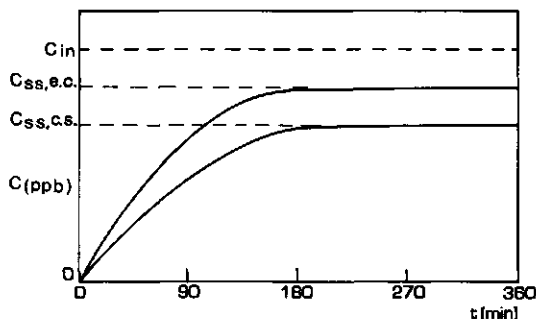

Fig.3.3.2 Experimentally found adsorption curves ($C_{ss,c.s.}$ steady state concentration chamber + sample; $C_{ss,e.c.}$ steady state concentration empty chamber; C_{in} input concentration)

DISCUSSION

Although the data gathered on the adsorption experiments at first glance don't look very promising, most of the unpredicted facts can be explained.

To start with, the function $C_{ss}[1 - \exp(-k_1\tau_1 - k_2(\tau_2)^2]$ fits the measured curves better than the one predicted by theory, because the former function rises faster. Work on this matter is still in progress. At present substraction of both measured steady state functions results in an infinite area, i.e. no absolute adsorption values can be calculated out of the data. Instead, only relative values (i.e. one curve, corresponding to a specific material, approaches the reference signal - chamber without a sample - more closely than another one. Therefore a meaningful conclusion about the adsorption properties can be derived by comparing the relative positions of the curves to each other, and comparing those to the reference measurement). In our measurements PTFE-teflon showed the lowest adsorption affinity for NH_3 followed by aluminium, brass and silicon coated aluminium (the adsorption affinity increases from teflon to coated aluminium). This conclusion is in agreement with results of Beck *et al*[5] who measured adsorption photoacoustically. Teflon was shown to have the least affinity for NH_3 followed by paraffin and gold. Because of the apparent adsorptive capacity of the teflon chamber, C_{out} approaches asymptotically to C_{ss} instead of the input concentration C_{in}. This would imply that layers of NH_3 are formed continuously on the chamber walls. In fact this accumulation rate can be calculated[8]. However, this process can't continue indefinitely. A better explanation lies perhaps in the fact that NH_3 is soluble in water. This suggests that the adsorption of NH_3 is a result of a reaction with water, rather than a direct

50

reaction with teflon or glass. It is assumed that water is present as a thin water layer or waterfilm on the internal surfaces of the chamber although relatively "dry" air has been used (RH of 15%)[10]. A new leaf chamber, which overcomes the water film problem, is being developed by W. Tonk. Materials described here provided with new, different coatings, will be tested using this novel chamber in the near future. A photoacoustic Stark cell based on the knowledge attained by the adsorption experiment mentioned above has been constructed by Sauren *et al*[9]. It is this new photoacoustic cell that will be used soon for measuring low NH_3 concentrations in air.

ACKNOWLEDGEMENT

REFERENCES

1. E.L. Kerr and J.G. Atwood, "The laser Illuminated Absorptivity Spectrophone: a Method for Measurements of weak Absorptivity in Gases at Laser Wavelengths", Appl. Opt. **7**, 915 (1968); L.B. Kreuzer, N.D. Kenyon and C.K.N. Patel, "air Pollution:Sensitive Detection of Ten Pollutant Gases by Carbon Monoxide and Carbon Dioxide Lasers", Science **177**, 347 (1972); L.B. Kreuzer "Laser Optoacoustic Spectroscopy - A new Technique of Gas Analysis", Anal. Chem. **46**, 239A (1974).
2. R.J. Brewer and C.W. Bruce, "Photoacoustic Spectroscopy of NH_3 at the 9-micro. and 10-micro. $^{12}C^{16}O_2$ Laser Wavelengths", Appl. Opt. **17**, 3746 (1978).
3. S.M. Beck, "Cell coatings to minimize sample (NH_3 and N_2H_4) adsorption for low level photoacoustic detection", Appl. Opt. **24**, 1761 (1985).
4. G. Cooper, G. Gelbwachs, S. Beck, "Progress Report FY 1985/86"' Aerospace Corp., El Segundo, California, USA.
5. B. van Hove, Internal Report, RIVM, Bilthoven, The Netherlands.
6. B. van Hove, Atm. Environment, **8**, 1759-1763 (1987).
7. B. van Hove, Atm. Environment, in press.
8. H.H. Rogers, H.E. Jeffries, E.P. Stahel, W.W. Heck, L.A. Ripperton and A.M. Witherspoon, "Measuring Air Pollutant Uptake by Plants: A Direct Kinetic Technique"' Journal of the Air Pollution Control Association **27**, 1192 (1977).
9. H. Sauren, H. Jalink, D. Bićanić and J.Reuss, J.Appl.Phys, **66**, 5085, (1989).
10. B. van Hove, Atm. Environment, in press.

3.4 Resonant Stark spectrophone as an enhanced trace level ammonia concentration detector: design and performance at CO_2 laser frequencies

Hans Sauren, Dane Bicanic, Willy Hillen, Henk Jalink, Kees van Asselt, Jaco Quist, and Jörg Reuss

A design of a Stark photoacoustic cell capable of detecting ammonia in ambient air at trace levels is discussed.
Key words: Photoacoustic spectroscopy, CO_2 laser, Resonant cell, Ammonia trace detection, Stark spectroscopy, Infrared spectroscopy, Atmospheric pollution.

I. Introduction

Ammonia emission due to intensive agriculture (livestock breeding and fertilizing activities) is nowadays considered to be one of the main causes of soil acidification. The control of ammonia (NH_3) production rates by monitoring its concentration levels has become a necessity. Throughout the past years various types of ammonia monitors have been constructed. However, these monitors are known to have only moderately fast response times (10 min or longer) and are unreliable for detecting concentrations <10 ppb. Conventional photoacoustic spectroscopy (PAS) when combined with a CO_2 laser, has proved to be a sensitive technique, for monitoring toxic vapors and a variety of pollutant gases at trace levels.[1,2] Due to the presence of large amounts of both water vapor (few percent) and carbon dioxide (~350 ppm) in ambient air, and the additive character of the PA signal, interference free detection of ammonia at either of the three strong ammonia absorption lines coinciding with $9R(30)$, $10R(8)$, and $10R(6)$ CO_2 laser transitions is not possible without correcting the measured signals for phase reversal due to the kinetic cooling effect.[3] An interesting methodology for dealing with problems of this kind has been developed and tested in practice.[4] Essentially it implies quasisimultaneous (CO_2 laser is tuned successively) measurements of the magnitude and the phase of the PA signals recorded at the $9R(30)$, $9P(18)$ (corresponding to the wavelength of maximum absorp-

tion strength for ammonia and of carbon dioxide respectively), and the $9R(28)$ laser transitions. The concentration of ammonia in a matrix of the other two gases is then obtained by solving a set of linear equations.

A more elegant approach to selectively detecting ammonia in a matrix of various absorbing gaseous pollutants is based on the Stark effect.[5] Due to its large dipole moment (1.48 debye in the ground state) NH_3 shows an appreciable Stark splitting in an external electrical field: i.e., the application of an electric field shifts the molecular absorption line into resonance with a properly chosen CO_2 laser line. Stark tuning of ammonia, using CO_2 laser PAS (thereby greatly enhancing the sensitivity) has been demonstrated in the laboratory by numerous authors.[6-10]

In this paper a design and use of a Stark tuned cell developed for fast (response time <2 min) and interference free PA detection of ambient ammonia is described.

II. Experimental

Figure 1 shows the exploded view of the Stark cell used here. The cell housing was fabricated on a milling machine out of an aluminum (alpase–aluplus) working piece. Upon removing the metal, a 200.0 × 60.5 × 40.00-mm cavity (leaving the overall wall thickness of 20.0 mm) used to accommodate the cell's constituent parts is formed. The compartment (1) used to accommodate components for electronic processing was machined in one side of the cell. A poly tetra fluor ethylene (PTFE) teflon block (2) (its width closely fitting that of the cavity) placed symmetrically in the middle of the available cell volume and carrying the three microphones forms the heart of the PA cell. The remaining volumes (3) on either side of the block serve as baffles (expansion chambers). The length (one-quarter of the resonant wavelength) of each baffle is precisely equal to one-half of the block length, so that

Jörg Reuss is with Catholic University, Department of Laser & Molecular Physics, Toernooiveld, 6525 DE Nijmegen, The Netherlands; the other authors are with Agricultural University, Department of Agricultural Engineering & Physics, Laser Photoacoustic Laboratory, 1 Duivendaal, 6701 AP Wageningen, The Netherlands.
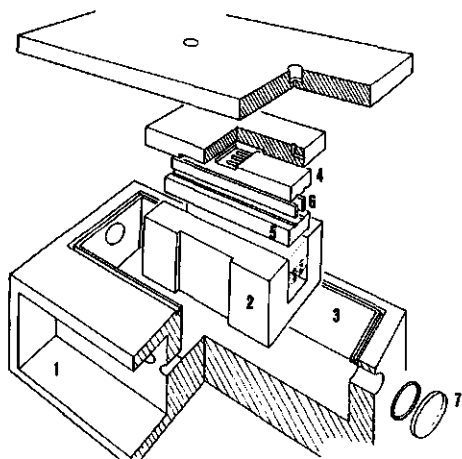
52

Fig. 1. Stark tuned photoacoustic cell.

the background signal due to window absorption will not couple efficiently to the resonant cavity of block (2).[11] The block is composed of three small channels and two flat polished aluminum plates (4,5). Uniform separation of the Stark plates over the entire length is provided by two teflon spacers (6). The cross section of each channel is 5.0×5.0 mm, and its length is 100 mm. The PTFE teflon was chosen as a material for constructing the block (2) because of its favorable insulation (Stark plates are insulated from the cell housing) and adsorption (low affinity for ammonia) properties. The upper Stark plate is grounded and accomodates three miniature electret microphones (M37 Microtel, Amsterdam) mounted flush with the plate, while the Stark voltage is applied to the bottom plate. Microphones in the side channels average the background signals prior to subtraction from the signal recorded in the main channel. An ultralow noise amplifier (30 nV at the input) is used before feeding the signals into the Ithaco 3961 A two phase lock-in amplifier. The cell is terminated on both ends by AR coated ZnSe windows (7).

III. Performance

The Stark cell was first used in the chopped radiation mode to test its operation and to determine its responsivity at room temperature and atmospheric pressure with the certified ethylene mixture (101.6 ppm C_2H_4 in N_2) used as a test gas. Published values of the absorption coefficient α for C_2H_4 at the $10P(14)$ line show considerable scatter.[12] In this study the absorption coefficient $\alpha = 30$ atm^{-1} cm^{-1} $\pm$ 10% was taken for ethylene (based on an average of published data[13,14]). The calibration was repeated several times during the course of the measurements to check system repeatability. The cell was operated at its first longitudinal resonance (1608 Hz). A Q-factor (FWHM) of

(24.0 $\pm$ 0.4) for this cell was found experimentally. The mean responsivity R obtained was 13.0 V cm/W and the variation among several calibration runs was ~5%.

The R value (R is directly proportional to the microphone sensitivity M) specified above refers only to atmospheric pressure. Both, the absorption coefficient α and the microphone sensitivity M are pressure dependent,[15] a fact often overlooked by other investigators. This is of particular interest when PA measurements are carried out in a flow regime and at a reduced pressure. Since the product of the absorption coefficient α and the microphone sensitivity M appears in the equation for the magnitude of the normalized photoacoustic signal, $[S = PR\alpha C$, (P = power in Watts and C = concentration as partial pressure)] it is necessary to perform the cell calibration in two distinct steps. A novel, absolute method to calibrate the photoacoustic cell has recently been suggested.[16] Briefly, after filling the cell (containing the metal strip that simulates the absorbing gas and which is heated periodically at the cell resonant frequency) with the flowing nonabsorbing gas (i.e., nitrogen) to any of the values of pressure within $10^{-2} \leq p \leq 760$ Torr, range, the corresponding microphone signal is measured. Having established the microphone sensitivity's-pressure dependence, the experiment is repeated using the calibrating gas mixture.

For the cell described here, the background signal (due to sources other than C_2H_4 absorption) was measured using the $10P(14)$ line and at atmospheric pressure by filling the cell with 99.9995% pure N_2. This signal (3 μV per Watt laser power) was vectorially subtracted from the ethylene signal to calculate the responsivity R.

To narrow the linewidth, the Stark modulated detection with moderate electric field strengths (2 kV/cm–5 kV/cm) is performed at reduced pressures (50–500 mbar).

The efficiency of the Stark cell for detecting ambient ammonia was tested by drawing real air samples into the cell using a suction pump. With the laser operating in the chopped radiation mode and the modulation frequency of the chopper tuned to that of the cell resonance, a 5 kV/cm Stark field (provided by a high voltage power supply FUG 7E-12500) was made to alternate at 0.1 Hz with a square waveform. This was done to eliminate the appearance of transient signals normally occurring at high (>300 Hz) modulation frequencies. Figure 2 displays the Stark tuned signal due to ambient ammonia measured in the flow through mode (0.5 l/min). This particular measurement was taken at the $10R(6)$ laser line with an electrical field strength of ~5 kV/cm. The polarization direction of the laser radiation was chosen parallel to the electrical field ($\Delta M = 0$ transitions). The $Q(J = 5, K = 5, M = 5)$ ammonia line was Stark tuned at 50 mbar and room temperature. Under these conditions 0.5 W of the unfocused laser power produced a PA signal of 0.30 μV while the magnitude of the field-free signal was 0.15 μV.[17]

53

signal

E = 0 kV/cm
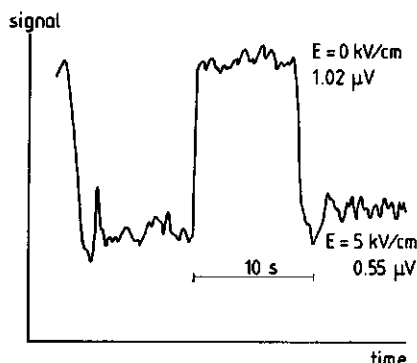1.02 µV

E = 5 kV/cm
0.55 µV

10 s

time

Fig. 2. Zero-field and field on (5 kV/cm) photoacoustic signal due to ambient ammonia at 10R (6) laser line recorded at 50 mbar and a flow rate of 0.5 l/min.

To test the identity of the measured signals several control tests have been run. The increase of the signal magnitude was observed when a small vessel containing few droplets of 32% aqueous solution of ammonia was placed in the vicinity of the cell feed line tubing. As a final test very pure nitrogen (class 5.0) was flown through a bubbler, which contained only distilled water at 293 K. When the mixture of saturated water vapor (10^4 ppmv) and nitrogen at the reduced pressures was drawn into the cell, no Stark shift at $10R(6)$ was observed.

IV. Conclusion

Selective detection of ammonia present in urban air has been demonstrated. Detection sensitivity of the given experimental setup was derived by ratioing the magnitude of the PA signal to the noise voltage of this signal.

An ultimate ammonia concentration limit of 0.4 ppbv (corresponding to a SNR of unity) is obtained under the following experimental conditions: integration time of the lock-in amplifier 1 s, Stark field modulation 0.1 Hz, flow 0.5 l/min, cell pressure 50 mbar, electric field strength 5 kV/cm, and the $10R(6)$ laser line with 0.5 watts of unfocused laser power.

Despite good long term power stability of the CO_2 laser the measurement is, at present, impaired to some extent by the nonavailability of the piezo laser cavity tuning option and the limited range of the electric field strength (maximum 5 kV/cm). Elimination of these restrictions might improve detection sensitivity substantially.

The cell is potentially susceptible to further optimization such as volume minimization and the application of a Stark field modulation at the cell's true resonant frequency (1608 Hz). As far as the latter is concerned the preliminary measurements indicate strong pickup of spurious signals by the electret microphones at high modulation frequencies. To be able to

fully exploit the potential of the Stark modulated detection mode to find the solution to the above problem is an impetus. Work on this matter is already in progress.

References

1. E. L. Kerr and J. G. Atwood, "The Laser Illuminated Absorptivity Spectrophone: A Method for Measurements of Weak Absorptivity in Gases at Laser Wavelengths," Appl. Opt. 7, 915–921 (1968).
2. R. J. Brewer and C. W. Bruce, "Photoacoustic Spectroscopy of NH_3 at the Wavelengths of Carbon Dioxide Laser," Appl. Opt. 17, 3746 (1978).
3. J. Henningsen, A. Olafsson, and M. Hammerich, "Trace Detection with Infrared Lasers," Applied Laser Spectroscopy, M. Inguscio and K. Demtröder, Eds. (Plenum ASI 1990 (to be published).
4. R. Rooth and A. Verhage, "On the Photoacoustic Measurement of Ammonia in the Atmosphere," in Proceedings Fourth CIRP Zurich, 1988.
5. G. Duxbury, "Laser Stark Spectroscopy," International Review in Physical Chemistry 4, 237–278 (1985).
6. P. Angus, Ph.D. Thesis, Herriot-Watt University, Edinburgh (1976).
7. R. A. Crane, Ultra Lasertech Inc., Mississauga, Ontario, Canada. Priv. comm. (1988).
8. P. J. A. Kay, "Photoacoustic Measurements in Reacting Gas Mixtures," Ph.D. Thesis, Herriot-Watt U., Edinburgh (1982).
9. M. J. Kavaya, J. S. Margolis, and M. S. Shumate, "Optoacoustic Detection Using Stark Modulation," Appl. Opt. 18, 2602–2606 (1979).
10. P. Minguzzi, M. Tonelli, A. Carrozzi, and A. Di Lieto, "Optoacoustic Laser Spectroscopy in the ν_2 Band of Ammonia," J. Mol. Spectrosc. 96, 294–305 (1982).
11. F. Harren, "The Photoacoustic Effect, Refined and Applied to Biological Problems," Ph.D. Thesis, Catholic U., Nijmegen, The Netherlands (1988).
12. R. R. Patty, G. M. Russworm, W. A. McClenny, and D. R. Morgan, "CO_2 Laser Absorption Coefficients for Determining Ambient Levels of O_3, NH_3, and C_2H_4," Appl. Opt. 13, 2850–2854 (1974).
13. U. Persson, B. Marthinsson, J. Johansson, and S. T. Eng, "Temperature and Pressure Dependence of NH_3 and C_2H_4 Absorption Cross Sections at CO_2 Laser Wavelengths," Appl. Opt. 19, 1711–1715 (1980).
14. L. G. Rosengren, E. Max, and S. T. Eng, "A Study of Laser-Acoustic Air Pollution Monitors," J. Sci. Instrum. 7, 125–133 (1974).
15. J. Angster and E. Arato, Akusztika (Akademiai Kiado, Budapest 1986, in Hungarian).
16. A. Miklós, H. Sauren, and D. Bicanic, "On the Calibration Procedure of Photoacoustic Cell Using a Vibrating Metal Strip," to be submitted.
17. H. Sauren, D. Bicanic, H. Jalink, and J. Reuss, "High Sensitivity Interference-Free Stark Photoacoustic Detection of Urban Ammonia," J. Appl. Phys. 66, 5805–5807 (1989).

54

3.5 High-sensitivity, interference-free, Stark-tuned CO_2 laser photoacoustic sensing of urban ammonia

Hans Sauren, Dane Bicanic, and Henk Jalink
Laser Photoacoustic Laboratory, Department of Agricultural Engineering and Physics, Agricultural University, Duivendaal 1, 6701 AP Wageningen, The Netherlands

Jörg Reuss
Department of Laser and Molecular Physics, Faculty of Sciences, Catholic University, Toernooiveld, 6525 ED Nijmegen, The Netherlands

Low-concentration (few ppbv), interference-free, on-line photoacoustic detection of ambient ammonia (NH_3) is reported by Stark tuning the $Q(J=5, K=5, M=5)$ NH_3 absorption line into resonance with the CO_2 laser. Measurements were made over a range of total pressure between 600 and 50 mbar.

Photoacoustic spectroscopy (PAS), in particular when combined with strong lasers as radiation sources, has been recognized for its capacity to measure weak absorptions in gases, liquids, and solids.[1] Since the majority of pollutants absorb in the infrared between the 2- and 20-μm region, also characterized by the availability of several strong lasers, there have been considerable amounts of laboratory and field work performed towards a practical instrument for on-line analysis of atmospheric gases in the low-concentration range (several ppbv).[2]

Among those, ammonia, due to its role in the soil acidification, has received ample attention from worldwide scientific communities, and its control through the concentration of measurements has become a necessity. Fortunately there is a good degree of spectral overlap between ammonia absorption frequencies and the frequencies of the CO_2 laser, the strongest one being that coinciding with the $9R(30)$ laser transition.

In situ, conventional chopped radiation mode photoacoustic studies of ammonia carried out so far, encompass

both low- and high-concentration ranges. Examples involve trace detection in ambient air by preconcentrating the sample on the selective absorber[3] and flux measurement of NH_3 emitted from the fertilized fields.[4] Gandurin *et al.* constructed a modular (three lasers) laboratory setup for photoacoustic analysis of mixtures containing NO, NO_2, NH_3, C_2H_4, and saturated hydrocarbons, by making use of a two-channel differential scheme and a wavelength-modulation technique.[5] Above ppmv level, ammonia emission rate measurements in a power plant using a CO_2 laser[6] and diode laser studies of ammonia concentration, diurnal variation[7] have been reported.

Due to the additive character of the photoacoustic signal under normal atmospheric conditions, the presence of a large amount of water vapor and carbon dioxide impedes NH_3 detection in the low-concentration range (ppbv). Consequently, some means of selective spectral discrimination is required if ammonia is to be detected interference free in the matrix of absorbing gases.

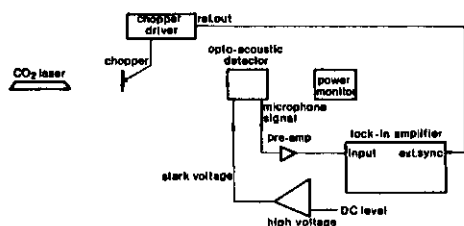An interesting methodology that enables the experi-

55

FIG. 1. Experimental setup used in this study.

FIG. 2. Stark signal of NH_3 obtained at $10R(6)$ CO_2 laser line at the total pressure of 50 mbar and the electric field strength of 3. 5 kV/cm.

mentalist to deduce the NH_3 concentration through the proper interpretation of phases and signal strengths obtained by measurements at selected CO_2 laser wavelengths has recently been suggested.[8] The effectiveness of ammonia, present in a mixture of four gases, on the photoacoustic signal has been studied in the laboratory.[9] Tuning the NH_3 absorption into resonance with a proper CO_2 laser line by means of the Stark effect, thereby greatly enhancing the specificity, has been demonstrated in laboratory studies.[10-13] In this communication we report on the design and use of a Stark-tuned spectrometer (see Fig. 1) that has permitted, what is believed, the first PA measurements of ammonia ever conducted in the outside air.

A home-made, stable CO_2 line-tunable waveguide laser was used in this experiment. The resonant photoacoustic cell made of high-quality polytetrafluoroethylene (PTFE) Teflon was designed for the operation in the flow-through mode and can be driven either in the conventional chopper mode or the Stark-tuned mode. It is equipped with carefully designed baffle volume[14]: its resonance frequency corresponded to the first longitudinal mode is 1608 Hz (293 K). The cell incorporates three identical rectangular channels of 5.0×5.0 mm^2 cross section and of 100 mm length. Only the middle channel is illuminated by the unfocused laser radiation. Each channel is equipped with a miniature Microtel M37 microphone (10 mV/Pa at 1608 Hz); those in the side channels serve for averaging of the background signals prior to the subtraction from the signal recorded in the main channel. An ultralow noise amplifier used before feeding the signals into the Ithaco 3961-A two-phase lock-in amplifier. A detailed description of cell construction and accompanying electronics will be given elsewhere.[15] Two identical rectangular, polished aluminum plates, forming a 5-mm gap, are separated by two PTFE-Teflon spacers. High dc voltage generated by power supply (FUG HCN 7E-12500) is applied to the bottom plate; the upper plate carrying the three microphones is grounded.

Figure 2 displays results of the measurement taken at $10R(6)$ laser line in the flowing regime (0.4 ℓ/min). The outside air was drawn through tetrafluoroethylene-perfluorpropylene (FEP)-Teflon tubing by a vacuum pump. With an electric field strength of 5 kV/cm, without causing electric breakdown, $Q(J = 5, K = 5, M = 5)$ of the multiplet transitions with $\Delta M = 0$ was Stark tuned at 50 mbar and room temperature. The cell with the laser beam mechanically chopped at 1608 Hz is 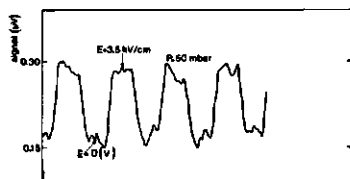operated in the first longitudinal mode. The Stark field which is modulated by a square wave at 0.1 Hz is provided by the FUG HV power supply driven by a Wavetek generator. Measurements performed at different pressures, while maintaining the experimental conditions unaltered, show the same trend as illustrated in Fig. 2 above. With increasing pressure the modulation depth decreases. No Stark shift is observed at pressures exceeding 600 mbar, with a field strength of 5 kV/cm. In order to check the identity of the measured signals, several control tests have been run. At first, a small vessel containing a few droplets of 32% aqueous solution of ammonia (Merck) was placed in the immediate vicinity of the feed-line tubing. Accordingly, a rapid and large increase of the photoacoustic signal (lock-in signal 10 mV) at $10R(6)$ laser line was observed under normal operating conditions.

As a final test, the cell was coupled to a bubbler containing only distilled water at 293 K, through which very pure (class 5.0) nitrogen is flowed. No Stark shift was observed when the mixture of saturated water vapor $\approx 10^4$ ppmv and nitrogen at pressures between 50 and 600 mbar in the cell.

With the CO_2 laser mechanically chopped and tuned to the $10P(14)$ transition, the cell was calibrated using a certified precision mixture of 101.6 ppm C_2H_4 [absorption cross section[16] of ethylene is about 35 atm^{-1} cm^{-1} at $10P(14)$] at the first longitudinal resonance mode (1608 Hz, 293 K), yielding a cell constant of $(3.9 \pm 0.1) \times 10^3$ Pa cm/W for one microphone. Using this value, the observed signal (Fig. 2) is found to correspond to 7.5 pppbv of ammonia. The ultimate (S/N = 1) detection limit of 0.4 ppbv for a given set is derived by considering the noise atop the signal shown in Fig. 2.

In conclusion, on-stream and interference-free detection of ammonia present in the urban air has been demonstrated. The cell is potentially susceptible to further optimization, such as the reduction of baffle volume dimensions and modulation of the Stark field at resonant frequency.

[1] H. Vargas and L. C. M. Miranda, Phys. Rep. 161, 43 (1988).
[2] P. Hess, Ed., *Photoacoustic, Photothermal and Photochemical Processes in*

56

Gases (Springer Series Topics in Current Physics, Springer, Heidelberg, 1989), Vol. 46.

[3]G. E. Copeland, M. D. Aldridge, and C. N. Harvard, Final report, December, 1981, under NASA contract NASA-15468-63, Old Dominion University, Norfolk, Virginia.

[4]V. M. Artemov, E. M. Artemov, V. P. Zharov, I. M. Nazarov, S. D. Friedman, and V. P. Biriolin, in *Trudi Ordena Trudovogo Krasnogo Znameni Institute Prikladnoi Geofizika* (Gidrometeoizdat, Moscow, 1986), Vol. 67, pp. 106–114 (in Russian).

[5]A. L. Gandurin, S. B. Gerasimov, A. A. Zheltukhin, I. P. Konovalov, S. T. Kornilov, G. F. Melnik, Yu. Yu. Mikhalevich, D. D. Ogurok, V. A. Petrischev, and S. N. Chirikov, Appl. Spectrosc. **45**, 886 (1986).

[6]A. Olafsson, M. Hammerich, J. Bülow, and J. Henningsen (to be published).

[7]T. Y. Chang, Ph. D. thesis, Chemistry Department, Iowa University, Ames, 1981.

[8]R. Rooth and A. Verhage, *Proceedings of the 4th ICRP Conference* (Pergamon, London 1986), pp. 593–595.

[9]S. B. Tilden and M. B. Denton, Appl. Spectrosc. **39**, 1018 (1985).

[10]R. A. Crane Ultra Lasertech Inc., Mississauga, Ontario, Canada (private communication, 1988).

[11]P. J. A. Kay, Ph. D. thesis, Department of Physics, Herriot–Watt University, Edinburgh, Scotland, 1982.

[12]M. J. Kavaya, J. S. Margolis, and M. S. Shumate, Appl. Opt. **18**, 2602(1979).

[13]P. Minguzzi, M. Tonelli, A. Carrozzi, and A. Di Lieto, Mol. Spectrosc. **96**, 294 (1982).

[14]F. Harren, Ph. D. thesis, Department of Physics, Catholic University, Nijmegen, The Netherlands, 1988.

[15]H. Sauren, W. Hillen, H. Jalink, D. Bicanic, K. van Asselt, and J. Reuss (unpublished).

[16]P. Perlmutter, S. Strikman, and M. Slatkine, Appl. Opt. **18**, 2267 (1979).

57

3.6

An experimental methodology for characterizing the responsivity of the photoacoustic cell for gases at reduced pressure by means of the vibrating strip as the calibrating sound source

András Miklóst, Hans Saurent and Dane Bićanić‡

†Institute of Isotopes of the Hungarian Academy of Sciences, Budapest, Hungary
‡Photoacoustic Laser Laboratory, Department of Agricultural Engineering and
Physics, Agricultural University, Dulvendaal 1, 6701 AP Wageningen, The
Netherlands

Abstract. Real time, high-sensitivity and interference-free Stark-tuned photoacoustic concentration detection of atmospheric pollutants at CO_2 laser wavelengths requires subatmospheric pressures in the cell containing the gaseous sample of interest. The detected photoacoustic signal is in general directly proportional to the cell responsivity, a definition which implies, among the other parameters, the product of the microphone sensitivity and the absorption cross section of the measured species. For correct interpretation of the results it is necessary to determine the dependence of both of these quantities on pressure. A novel effective methodology is proposed, making no use of a test gas and based on a vibrating strip as the calibrating source. Once the cell responsivity has been determined the method described can be used to study the pressure dependence of the absorption cross section of an arbitrary gas.

1. Introduction

Laser photoacoustic spectroscopy (LPAS) has proven to be a powerful and sensitive technique for spectroscopic studies in gas, liquid and solid phases (Vargas and Miranda 1988). One of the most widely encountered practical uses of LPAS is the concentration monitoring of primary pollutant gases (Miklós and Lörincz 1989, Olafsson 1990, Meyer and Sigrist 1990, Angeli *et al* 1991).

Atmospheric ammonia (NH_3), considered a primary pollutant in the soil acidification, has received much public attention over the past few years. Knowledge about the deposition of ammonia is of crucial importance when considering the initialization of an environmental programme aimed to combat this problem. For on-line detection of NH_3 deposition rates laser photoacoustics combined with Stark-modulation spectroscopy has recently been suggested (Sauren *et al* 1989a) as a new method with the potential to overcome problems such as selectivity and sensitivity, normally met with conventional techniques.

The method makes use of a stable, line-tunable CO_2 laser in conjunction with a carefully designed photoacoustic Stark cell. The knowhow gathered in the studies of ammonia adsorption to different metals and cell polymer coatings (Sauren *et al* 1989b) as well as improvements in cell design (Harren 1988, Harren *et al* 1990) was utilized when constructing this instrument (Sauren *et al* 1990). However, in order to achieve a good signal-to-noise ratio (SN ≈ 50–100) with this technique, it was necessary to operate the Stark cell at reduced (50 to 100 mbar) pressure (Sauren *et al* 1989a).

Generally, in a photoacoustic experiment performed in the gas phase and at atmospheric pressure, the photoacoustic signal $S(V)$, detected either by electret or condenser microphones (the performance characteristics of which usually refer to atmospheric pressure), depends on the incident laser power P (in watts), the sample's absorption coefficient α ($atm^{-1}\,m^{-1}$), the cell responsivity R ($V\,cm\,W^{-1}$), that for a given cell configuration is proportional to the microphone's sensitivity S_m ($V\,Pa^{-1}$), but is not gas dependent, and finally on the concentration C (atm) in units of partial pressure, i.e.

$S = PRC\alpha$. Instead of the absorption coefficient α, the molecular cross section σ (m^2 mol^{-1}) is frequently used. The quantities α and σ are related (Dewey *et al* 1973) through $C(\text{atm})\alpha(\text{atm}^{-1}\,\text{m}^{-1}) = N_A\sigma$ where N_A denotes the number of absorbing molecules per unit volume (mol m^{-3}).

It is a known fact that both the absorption coefficient of a gas and the sensitivity S_m of the microphone are functions of the ambient pressure (i.e. $\alpha = \alpha(p)$, $S_m = S_m(p)$ and therefore also $R = R(p)$). For this reason the relation $S = PRC\alpha$, stated above, is not *a priori* valid any longer at reduced pressure but has to be replaced by the more general expression $S(p) = PR(p)C\alpha(p)$.

Hence, in order to enable the experimentalist engaged in laser photoacoustic Stark-tuned spectroscopy to calculate the concentration C of a given pollutant, the measured voltage signal $S(p)$, the cell responsivity $R(p)$, the microphone sensitivity $S_m(p)$ and the absorption coefficient $\alpha(p)$ have to be known as functions of pressure.

Photoacoustic measurements of pressure-dependent absorption coefficients $\alpha(p)$ for test gases like C_2H_4 and NH_3 have been reported in the literature (Kavaya *et al* 1979). However, these data lack evidence for whether or not the effect of the microphone's sensitivity $S_m(p)$ has been included. Photoacoustic studies require the calibration of the detecting cell assembly and, in most experiments, the cell responsivity $R(p_{atm})$ at atmospheric pressure p_{atm} is determined by measuring the normalized photoacoustic signal S/P (p_{atm}) obtained with the test gas of a precisely known absorption coefficient $\alpha(p_{atm})$ present (concentration C) in the certified precision mixture, since

$$R(p_{atm}) = \frac{S(p_{atm})}{\alpha(p_{atm})}PC. \qquad (1)$$

The responsivity R is directly proportional to the microphone sensitivity S_m (which is normally specified at p_{atm}). As the next step, one calculates the pressure dependence of the absorption coefficient $\alpha(p)$ from equation (1) by measuring the normalized signals S/P (p) at varying pressures as:

$$\alpha(p) = \frac{S(p)}{PR(p_{atm})C} \qquad (2)$$

$$\alpha(p) = \frac{S(p)\alpha(p_{atm})}{S(p_{atm})}. \qquad (3)$$

Finally, in a realistic experiment carried out at some arbitrary pressure p, the values of $R(p_{atm})$ and of $\alpha(p)$ are used to derive the unknown concentration C from:

$$C = \frac{S(p)}{PR(p_{atm})\alpha(p)}. \qquad (4)$$

However, since S_m is pressure (and therefore R) dependent, equation (4) is incorrect whenever $p \neq p_{atm}$.

In the calibration procedure described above, the pressure effect of the microphone sensitivity S_m is hidden in $\alpha(p)$, i.e. $\alpha(p)$ is microphone dependent and cannot be separated. Consequently, use of the reported values of $\alpha(p)$ when calibrating the microphone's sensitivity $S_m(p)$ might lead to incorrect values of $R(p)$ and therefore also to the misinterpretation of concentration whenever working in the Stark-tuned mode. Knowing the operational principle of a microphone, one cannot but speculate on the effect of lowering the ambient pressure on its performance.

In this paper we therefore present a novel method by which the behaviour of the microphone $S_m(p)$ at reduced pressure can be determined directly without actually making use of a test gas. From the obtained value of $S_m(p)$ and a direct proportionality between $S_m(p)$ and $R(p)$ one has

$$\alpha(p) = \frac{S(p)}{PR(p)C} \qquad (5)$$

and finally

$$C = \frac{S(p)}{PR(p)\alpha(p)}. \qquad (6)$$

In equation (5) the absorption coefficient $\alpha(p)$ does not depend on S_m any longer, and hence relationship (6) is valid for $p \neq p_{atm}$.

Basically, the radiation from an intensity-modulated CO_2 laser impinges on an aluminium strip, of which one end was bolted to a brass plate (figure 1). The assembly was placed at a properly chosen location in the Stark photoacoustic cell. The non-reflected fraction of the energy is absorbed by a very thin layer within the material near to the surface of the strip. The penetrating thermal wave generates a bending moment causing the strip to vibrate and, hence, functions as the sound source. If its dimensions are selected properly the strip can be forced to vibrate (quality factor, Q_{strip}) at a frequency corresponding to that of modulation and of the cell's second longitudinal resonance. The amplitude of the strip's vibration is directly proportional to the amount of absorbed laser power and to the quality factor Q_{strip} of the excited resonance. The latter depends on the internal friction of the metal and damping due to air viscosity. For a freely vibrating strip with an experimentally determined intermediate Q value of 50–100 such as here, the damping effect of air viscosity
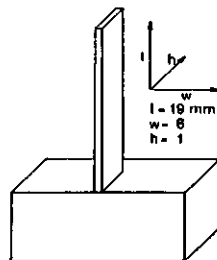

Figure 1. Aluminium strip used as the sound source. *l*, *h* and *w* refer to the length, height and width of the strip (all dimensions in mm).

is always smaller than that of internal friction. Therefore, the vibration amplitude and frequency may be regarded as being independent of the pressure in the photoacoustic cell. Provided the power of the laser is constant, the heat load and the sound energy generated by the strip will also be constant.

The second longitudinal resonance of the Stark cell is excited accordingly. The amplitude of the generated pressure wave (constant) is then measured by the miniature microphone (attached by tape to the bottom of the central section of the photoacoustic cell) at the modulation frequency using the lock-in technique. The amplitude of the pressure wave at a specified location of the microphone is, under given experimental conditions, solely dependent on the microphone sensitivity S_m. Thus, while decreasing the pressure in the cell, corresponding signal values provide direct information about $S_m(p)$. Since the microphone sensitivity specified by the manufacturer refers to the ambient pressure, absolute values $S_m(p)$ can be determined using the above data. Although basically a very simple device, the vibrating metal strip appears to be a suitable sound source for performing the microphone calibration measurement.

2. Theory

In order to determine the magnitude of the sound pressure generated by a vibrating strip placed within the photoacoustic cell, several physical processes must be taken into account. Only a qualitative description is needed here, since, as stated above, one is not interested in the exact relationship between the incident light intensity and the generated sound pressure. The one-dimensional thermal diffusion equation that governs the thermal wave generation is

$$\rho C_v \frac{\partial T}{\partial t} - K\Delta T = (1-R)\beta I \exp(-\beta x) \quad (7)$$

where the symbols ρ, C_v, K, R and β denote the density, specific heat at constant volume thermal conductivity, reflection and absorption coefficients of the strip material respectively; furthermore T is the absolute temperature of the strip and I ($W\,m^{-2}$) is the intensity of the incident radiation.

The time dependent solution of $T(x, t)$ of the above differential equation reads

$$T(x, t) = \frac{A}{i\omega + \chi\beta^2}$$
$$\times \left(\frac{\beta}{\gamma}\exp[-(1-i)\gamma x] - \exp(-\beta x)\right)\exp(-i\omega t) \quad (8)$$

with

$$A = (1-R)\beta I/\rho C_v, \quad (8a)$$

$$\gamma = (\omega/4\chi)^{1/2} \quad (8b)$$

and

$$\chi = K/\rho C_v. \quad (8c)$$

For metals the value of β is in the order of $10^7\,m^{-1}$ while γ at 1600 Hz has a value between 10^3 and $10^4\,m^{-1}$, ω is the mechanical chopping frequency. Therefore the second term of equation (8) can be neglected inside the strip so that

$$T(x, t) = T_0 \exp(-\gamma x) \exp i(\gamma x - \omega t)$$

with

$$T_0 = \frac{A(\beta/\gamma)}{i\omega + \chi\beta^2}. \quad (9)$$

The flexural vibrations of a thin strip are governed by the equation

$$\rho w h \frac{\partial^2 \zeta(z, t)}{\partial t^2} + B\frac{\partial^4 \zeta(z, t)}{\partial z^4} = \lambda w T_0 \exp(-i\omega t) \quad (10)$$

where λ ($Pa\,K^{-1}$) is the thermomechanical coefficient, $B(Pa\,m^4)$ is the cross sectional moment of the strip (rectangular bar) while $w(m)$ and $h(m)$ are the width and the thickness of the strip respectively. The term on the right-hand side of (10) represents the average mechanical stress caused by the heat expansion, while $\zeta(z, t)$ describes the displacement of the strip along the x axis and vanishes outside the illuminated region of the strip.

The periodic heating sets the metal strip into motion. Assuming $\zeta(z, t) = f(z)\exp(-i\omega t)$ and substituting this expression in (10) one obtains (Timoshenko *et al* 1974):

$$\frac{B}{\rho h w}\cdot\frac{\partial^4 f}{\partial z^4} - \omega^2 f = \frac{\lambda T_0}{\rho h}. \quad (11)$$

The general solution of this experiment is found in the literature. Since only the average displacement is of interest here one can write:

$$\langle \xi_\kappa \rangle \sim H\left((\omega_\kappa^2 - \omega^2)^2 + \frac{\omega^2\omega_\kappa^2}{Q_\kappa^2}\right)^{-1/2} \exp(-i\omega t) \quad (12)$$

and for the average velocity

$$\langle \dot{\xi} \rangle \sim -i\omega H((\omega_\kappa^2 - \omega^2)^2 + \omega^2\omega_\kappa^2/Q_\kappa^2)^{-1/2}\exp(-i\omega t) \quad (13)$$

with

$$H = \frac{\lambda T_0}{\rho h}. \quad (14)$$

The velocity amplitude v_k of the kth strip's resonance can be written as

$$v_k \sim \frac{\omega_\kappa H Q_\kappa}{\omega_\kappa^2} \sim \frac{\lambda T_0 Q_\kappa}{\rho h \omega_\kappa} \sim F_\kappa \cdot P\omega_\kappa^{-3/2}. \quad (15)$$

The quantity F_κ includes all the material and geometrical parameters but is independent of the ambient pressure and of the incident light power P. The absorbed energy causes an increase in strip temperature and, strictly speaking, the material constants might consequently change during the measurement. However, this temperature rise is, in general, very small and the above assumption is therefore justified.

959

60

The sound field inside a cavity can be determined by solving the lossless set of acoustic equations:

$$\rho_0 \frac{\partial u}{\partial t} + \text{grad } \Psi = 0 \qquad (16a)$$

and

$$\frac{1}{\rho_0 c_0^2} \frac{\partial \Psi}{\partial t} + \text{div } u = 0 \qquad (16b)$$

where ρ_0(kg m^{-3}) is the air density, Ψ(Pa) is the sound pressure, u(m s^{-1}) is the particle velocity and c_0(m s^{-1}) is the sound velocity. For a rectangular cavity with dimensions a, b, and c the eigensolutions are

$$\Psi = C \cos(kx) \cos(ly) \cos(mz) \cos(\omega t) \qquad (17a)$$

$$u_1 = (Ck/\rho\omega) \sin(kx) \cos(ly) \cos(nz) \sin(\omega t) \qquad (17b)$$

$$u_2 = (Cl/\rho\omega) \cos(kx) \sin(ly) \cos(mz) \sin(\omega t) \qquad (17c)$$

$$u_3 = (Cm/\rho\omega) \cos(kx) \cos(ly) \sin(mz) \sin(\omega t) \qquad (17d)$$

where C is the pressure amplitude, and the wavenumbers k, l, and m are calculated from the boundary conditions stating that the normal component of the velocity requires vanishing velocity (normal) component at the walls. Let q, r and s be integers so that the wavenumbers and the corresponding resonance frequencies are related through:

$$k = q\pi/a \qquad l = r\pi/b \qquad m = s\pi/c \qquad (18a)$$

with k, l and m satisfying

$$k^2 + l^2 + m^2 = \omega_{q,r,s}^2/c_0^2 \qquad (18b)$$

so that

$$\omega_{q,r,s} = c_0 \pi \left(\frac{q^2}{a^2} + \frac{r^2}{b^2} + \frac{s^2}{c^2} \right)^{1/2}. \qquad (18c)$$

In the Stark cell used in this study the second longitudinal resonance along the x axis is used for photoacoustic detection so that $q = 2$ and $r = s = 0$. The pressure depends solely on the x coordinate which characterizes the standing plane wave.

The vibrating metal strip sets the air into motion and the normal velocity of the gas at the strip's surface is equal to the strip velocity. With the strip dimensions being small compared with those of the cell, the velocity distribution along the strip may be neglected and an average value can be used instead. The vibrating strip is regarded as a small acoustic dipole radiating $W = |Z_m|\langle v \rangle^2$ of power into the cell (Z_m is the radiation impedance of the strip) that will sustain the oscillation of the sound field. The losses of the specific resonant mode can be characterized by the quality factor $Q_{q,r,s}$ defined as the ratio of the stored energy in the given mode per one cycle to the power lost during the same period. The quality factor $Q_{q,r,s}$ is determined experimentally by measuring the half-width of the acoustic resonance curve. Knowing the quality factor $Q_{q,r,s}$ of the excited mode the energy stored can be calculated as the temporal and spatial average of the energy density

multiplied by the volume V of the cell, i.e.

$$E = \tfrac{1}{2} \langle \rho_0 u^2 + \Psi^2/\rho_0 c_0^2 \rangle V = C^2 V/4\rho_0 c_0^2. \qquad (19)$$

Using the definition of the Q factor and $W = |Z_m|\langle v \rangle^2$ one obtains

$$E \sim Q_0 W 2\pi/\omega = Q_0 |Z_m|\langle v \rangle^2 2\pi/\omega. \qquad (20)$$

The amplitude of the sound pressure C can be determined from equations (19) and (20) as

$$C^2 = 8\pi\rho_0 c_0^2 Q_0 |Z_m|\langle v \rangle^2/\omega V \qquad (21)$$

with Q_0 denoting the quality factor of the excited (2, 0, 0) mode. The sound pressure generated by the vibrating strip is proportional to the average velocity of the strip which, in turn, is directly proportional to the incoming radiation power, i.e. $C \sim \rho_0 M P$.

All the material and geometrical constants for the given experimental arrangements excluding the pressure-dependent air density are included in M. The considerations above show that the sound pressure generated by a vibrating thin metal strip is proportional to the incident light power and to the density of the gas filling the cell. The M coefficient exhibits a very complicated dependence on different optical, elastic, acoustical and geometrical properties of the system, but it may be regarded as a constant for a given experimental arrangement and ambient temperature. Since the density is proportional to the ambient pressure the sound pressure generated by a vibrating strip will be proportional to the product of the ambient pressure p_0 and to the incident radiation intensity, provided the temperature' remains constant during the measurement. The voltage S measured by the microphone is the product of the microphone sensitivity S_m and the sound pressure $\Psi(x)$. Therefore the change in microphone sensitivity can be determined by measuring the voltage while evacuating the cell. Plotting the ratio $\Psi(0)S/\Psi S(0)$ of photoacoustic signals as a function of ambient pressure p provides the pressure characteristic of the normalized microphone sensitivity $S_m/S_m(0)$. $S_m(0)$ refers to the sensitivity specified at standard ambient conditions.

3. Experimental procedure

As indicated above the semi-clamped aluminium strip, instead of an actual test gas, served as the source for generating the sound wave. The resonating section of the original Stark cell (figure 2(a)) was removed and the rectangular strip (clamped at one end in the brass block) positioned (figures 2(b) and (c)) inside the cell (close to the entrance window) at a distance equal to one quarter of the acoustic wavelength (5 cm). In order to simulate the resonant behaviour of the Stark cell, the length of the strip was adjusted to match perfectly the cell's second longitudinal resonance (1608 Hz at STP). This adjustment has been accomplished by feeding a fixed stable frequency into the reference channel of a lock-in amplifier. The CO_2 laser was intensity modulated (chopped) at the frequency corresponding to the cell's second longitudinal
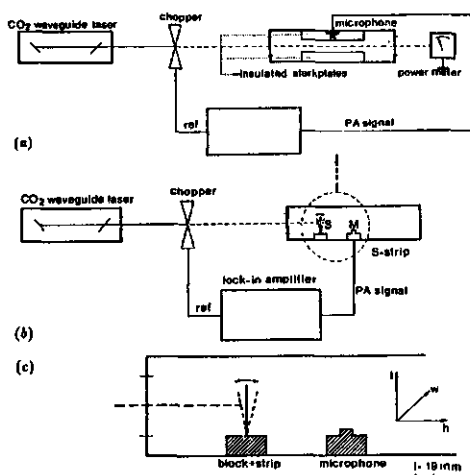
Figure 2. (a) Traditional CO_2 laser PA spectrometer for trace gas analysis (Sauren *et al* 1989a). Stark plates (forming an integral part of the demountable resonator unit that serves for generation as well as for detection of the acoustic resonance) occupy the middle section of the PA cell. The power meter behind the cell is used to normalize the PA signal. (b) The experimental set-up used in this study. Note that the resonator (encircled area) has been removed to accommodate the strip and the microphone. (c) Detailed drawing showing the combination of the clamped vibrating strip S (at $\lambda/4$ from the entrance window) and the electret microphone M (centred in the middle and taped to the bottom of the PA cell) replacing the 'traditional' resonator.

resonance at 1608 Hz. While observing the signal generated by the strip its length was altered until the maximum signal corresponding to the power frequency of 1608 Hz had been found.

The laser was tuned to the 10R(20) transition (maximum power emitted) and intensity modulated at the resonant frequency of 1608 Hz. For *test measurements* the pressure in the cell was reduced to that slightly below ambient (1000 mbar). At this pressure a Q value of 100 was found for the semi-clamped strip. Whilst gradually lowering the pressure from 1000 to 50 mbar the photoacoustic signal generated by the damped oscillator *(strip) was monitored as a function of pressure* using Microtel M37 electret microphone (nominal sensitivity 10 mV Pa^{-1} at 5000 Hz and ambient pressure). Repetitive pressure cycles (1000 mbar to 50 mbar and vice versa) revealed the relative error in the signal response of approximately 10%. One possible reason *for this relatively large error might be the free* (not actively stabilized in power) running laser. The output power of the laser displayed an oscillatory behaviour presumably due to misalignment of the laser tube. The time period of such oscillation was roughly 40 s. Furthermore, the ambient transient low-frequency noise of
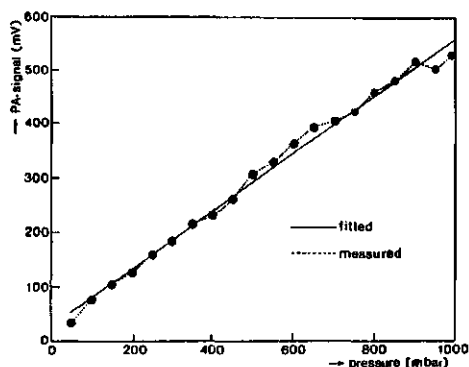
the laboratory air conditioning system occasionally overloaded the lock-in amplifier; to avoid this long integration times (10 s) had to be used.

4. Concluding remarks

The photoacoustic signal generated by laser-induced heating and subsequent oscillation of the strip clamped at one end is shown in figure 3. As expected the magnitude of the photoacoustic signal depends linearly on the pressure. From these data the sensitivity of the microphone $S_m(p)$ can be determined by measuring the signals S at some arbitrary pressure and at atmospheric pressure.
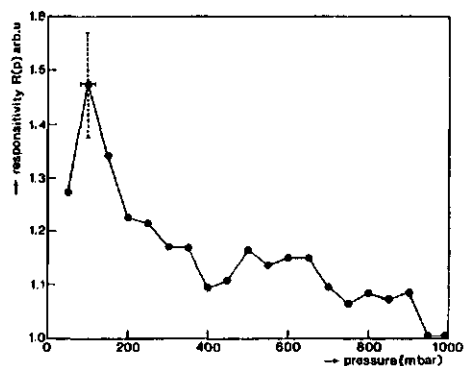
Figure 4. The sensitivity of the microphone $S_m(p)$ has been calculated according to $S_m(p) = [S(p_{atm}) \times p]/ [S(p) \times p_{atm}]$. The ratio $S(p_{atm})/S(p)$ is obtained from figure 3. The results are normalized to $S_m(p_{atm})$ specified by the manufacturer. Since $S_m(p)$ is proportional to $R(p)$, data shown in figure 4 enable the experimentalist to determine (equation (5)) the absolute values of the absorption coefficient $\alpha(p)$ and also the concentration C (equation (6)).

For example if the relevant pressure is 200 mbar then the corresponding microphone sensitivity $S_m(200)$ can be calculated as $S_m(200) = S(1000) \times (200 \text{ mbar})/(1000 \text{ mbar} \times S(200))$. The sensitivity of the microphone $S_m(p)$ obtained in such way is shown in figure 4; clearly the sensitivity slightly increases with decreasing pressure. The reason for the fairly large error bar in figure 4 is the fact that at low pressure the magnitude of the acoustic signal generated by the strip becomes comable to that of the ambient noise reaching the cell, causing a deterioration of the SN ratio CO_2 laser wavelengths.

Acknowledgments

References

Angeli G Z, Bozoki Z, Miklós A, Lőrincz A, Thöny A and Sigrist M W 1991 Design and characterization of a windowless resonant photoacoustic chamber with resonance locking circuitry *Rev. Sci. Instrum.* **62** 810–3

Dewey C F Jr, Kamm R D and Hackett C E 1973 Acoustic amplifier for detection of atmospheric pollutants *Appl. Phys. Lett.* **23** 633–5

Harren F 1988 The photoacoustic effect, refined and applied to biological problems *PhD Thesis Faculty of Sciences, Catholic University Nijmegen, The Netherlands*

Harren F, Reuss J, Woltering E and Bićanić D 1990 Photoacoustic measurements of agriculturally interesting gases and detection of ethylene below the PPB level *Appl. Spectrosc.* **44** 1360–70

Kavaya M J, Margolis J S and Shumate S 1979 Optoacoustic detection using Stark modulation *Appl. Opt.* **18** 2602–6

Meyer P L and Sigrist M W 1990 Atmospheric pollution monitoring using CO_2 laser photoacoustic spectroscopy and other techniques *Rev. Sci. Instrum.* **61** 1779–807

Miklós A and Lőrincz A 1989 Windowless resonant photoacoustic chamber for laser photoacoustic applications *Appl. Phys.* B **48** 213–8

Olafsson A 1990 Photoacoustic molecular spectroscopy with tunable waveguide CO_2 lasers. *PhD Thesis* Physics Laboratory, HC Orsted Institute, University of Copenhagen, Denmark

Sauren H, Bićanić D, Hillen W, Jalink H, van Asselt C, Quist J and Reuss J 1990 Resonant Stark spectrophone as an enhanced trace level ammonia detector: design and performance at CO_2 laser frequencies *Appl. Opt.* **29** 2679–81

Sauren H, Bićanić D, Jalink H and Reuss J 1989a High sensitivity, interference-free, Stark tuned CO_2 laser photoacoustic sensing of urban ammonia *J. Appl. Phys.* **66** 5085–8

Sauren H, van Hove B, Tonk W, Jalink H and Bićanić D 1989b *Monitoring of Gaseous Pollutants by Tunable Diode Lasers* eds R Grisar et al (Deventer: Kluwer)

Timoshenko S, Young D H, and Weaver W 1974 *Vibration Problems in Engineering* (New York: Wiley)

Vargas H and Miranda L C M 1988 Photoacoustic and related photothermal techniques *Phys. Rep.* **161** 43–101

Chapter 4   Intermodulated Photoacoustic Stark Spectroscopy (IMPASS) Applied to the Detection of Ammonia

4.1 Simplifying the Laser Photoacoustic Trace Detection of Ammonia by Effective Suppression of Water Vapour and of Carbon Dioxide as the Major Absorbing Atmospheric Constituents.

Hans Sauren[1], Tobi Regts[2], Cees van Asselt[1], and Dane Bićanić[1]

[1] Laser Photoacoustic Laboratory, Department of Agricultural Engineering and Physics, Agricultural University, Duivendaal 1, 6701 AP Wageningen, The Netherlands
[2] Laboratory for Atmospheric Physics, National Institute for Public Health and Environmental Hygiene, Antonie van Leeuwenhoeklaan, Bilthoven, The Netherlands

ABSTRACT

Highly sensitive (2-3 ppbv) interference-free photoacoustic and real time detection of ammonia in a matrix of absorbing gases (water vapour and carbon dioxide) at CO_2 laser wavelengths was accomplished by combining the mechanical modulation of the laser (frequency f_1) and the Stark modulation (frequency of the periodically varying electric field f_2). Ammonia was phase sensitive detected at either the sum or the difference frequency sidebands resulting in a dramatic suppression of the interfering absorption caused by water vapour and carbon dioxide.

INTRODUCTION

Atmospheric ammonia is presently the target of considerable interest due to its role in the environmental pollution. Next to the livestock breeding and high ammonia rates emitted by chemical plants, the excessive manure production causes the acidification of agricultural soils and threatens indirectly the ground water quality. The need for detecting atmospheric ammonia stimulates the development of a diversity of techniques including the spectroscopic ones too[1]. Various simple and sophisticated in-situ and remote ammonia monitors have been developed in the course of time. The most commonly encountered ammonia monitor in the practice is the one operating on the principle of catalytic conversion of ammonia to NO and NO_2 lacking fast response time (typical response time exceeds one minute) and adequate accuracy at low detection levels (ppbv) due to the presence of other

nitrous compounds in air (e.g. PAN) having NO and NO_2 as thermochemical end-products. Longpath measurements in conjunction with diode lasers and the introduction of differential optical absorption spectroscopy (DOAS) have helped to overcome the above mentioned problems to some extent, but these techniques are only useful when the average concentration measurements along the path are required.

Fast monitoring of ammonia fluxes is the issue currently receiving steadily more attention. Essentially, it requires the consecutive measurement of the air samples collected at different heights along a vertical line. For correlating the ammonia concentration at the different sampling points the availability of a sufficiently fast measuring system is an impetus when interference-free, real time detection is required (response time of the ammonia monitor should be faster than 1 Hz at a single sampling point). This last requirement can presumably be met with laser photoacoustic spectroscopy (LPAS) and other photothermal methods that measure the absorbed energy directly. Their intrinsic advantage is based upon the linearity between the signal and the concentration over more than 5 orders of magnitude (the signal is directly proportional to the measured gas concentration), its simplicity and high sensitivity[2] (sub-ppbv detection for various gases when combined with strong laser sources) and finally the reasonable selectivity[3]. Generally, the LPAS implies the periodical modulation of the laser radiation that is absorbed by a diluted gas inside the chamber (photoacoustic cell) causing temperature and pressure fluctuations detected by a microphone and a phase sensitive detector. Throughout the past 20 years large amounts of laboratory and field LPAS studies of different air pollutants have been reported in the scientific literature[4,5,6]. Results of several photoacoustic studies performed on ammonia in the air have been described, but the attempts met with success only at higher concentrations[7] due to the numerous practical problems associated with monitoring of gaseous ammonia. To start with due to its electronegative character ammonia is chemically highly reactive and forms chemical bonds with different materials ("adsorption") demanding materials with low adsorption affinity when constructing the photoacoustic cell and choosing the tubing. Another important phenomenon present in all gas mixtures involving CO_2 and N_2 is the kinetic cooling effect that influences the phase reversal of the measured photoacoustic signal. This effect becomes noticeable when the inverse of the modulating frequency of the laser becomes comparable to or is even smaller than the relaxation time of the CO_2-N_2 mixture and on the other hand is directly influenced by the amount of water being present. Unless this relationship is precisely known the measured photoacoustic signal, additive in character, leads to an erroneous interpretation of the concentration measurements. At last, many molecules exhibit absorption bands in the wavelength region (9-11 microns) covered by the CO_2 laser emission. Therefore, the photoacoustic signal generated by ammonia is affected by the simultaneouns absorption of major atmospheric constituents, in particular of water and carbon dioxide. Under normal conditions the standard atmosphere contains large quantities of water (partial pressure typically $2x10^{-2}$ atm) and of carbon dioxide ($3x10^{-4}$ atm) masking completely the signal due to the trace levels (ppbv) of ammonia.

The problem of adsorption is a drawback of all point source techniques. A thorough theoretical model enabling one to recover the concentration of ammonia present in the mixture of water vapour and carbon dioxide by analyzing the amplitude and phases of the photoacoustic signals measured at, at least two laser wavelengths, has been proposed and tested by Rooth *et al*[4].

An entirely different approach to selective detection of ammonia in a matrix of interfering

gases is based on the Stark effect that alters the absorption frequency of the absorbing species (having a non-vanishing dipole moment) upon the application of a transverse external electric field. Due to the large dipole moment (1.48 Debye in the ground state) of ammonia, a degree of spectral overlap between a properly chosen CO_2 laser emission frequency and an ammonia absorption line can be enhanced, while simultaneously "pushing" away the undesired constituents.

In this paper we report the on-line detection of ammonia as a first attempt towards the construction of a fast (1 Hz response time) candidate ammonia monitor. Sensitive detection of ammonia has been demonstrated in a series of experiments with simulated and controlled atmosphere using the novel Stark photoacoustic detection scheme suppressing effectively the contribution of water vapour and of carbon dioxide. Since the CO_2 molecule doesn't exhibit a permanent dipole moment the presence of an electric field will not perturb its energy levels, i.e. the Stark inactive CO_2 molecule cannot be shifted into (near) resonance with the CO_2 laser transition. Unlike carbon dioxide, water vapour possesses only a weak permanent dipole moment and, as it will be shown later, Stark effect due to water (taking place at the laser transition chosen for ammonia detection) was to small to be detected within the range of the applied electric field values. This experimental evidence justifies ignoring of the signal contribution due to the Stark splitting in water vapour. Either 10R(6) or 10R(8) laser transitions at 10.346 and 10.331 microns respectively could be used for monitoring ammonia in this study. In terms of absorption strength both these transitions are quite favourable. Previous experiments performed with the same set-up have shown moderate Stark shifts at 10R(6) and 10R(8) contrary to the 9R(30) laser transition at 9.217 microns (that nearly coincides with the strongest ammonia absorption frequency in the CO_2 laser region) which appeared Stark inactive within the range of accessible and applied electric field strength (3-5 kV/cm). In order to deal properly with the kinetic cooling effect and to suppress at the same time the effect of H_2O and CO_2 absorption, the CO_2 laser was amplitude modulated at a fixed frequency (f_1) of 40 Hz. The modulating frequency of the externally applied transverse Stark field (alternating in a symmetrical block wave form) was kept on either 1568 Hz (f_2) (in the sum frequency mode (f_1+f_2)) or 1648 Hz (f_2') (in the difference frequency mode ($f_2'-f_1$) corresponding to the second longitudinal resonance frequency (1608 Hz) of the photoacoustic Stark cell). In this detection scheme, a photoacoustic signal can only be generated by those molecules that interact constructively with both the modulated laser radiation and the electric Stark field (to the best of authors knowledge no molecule except ammonia, is known to exhibit both, a large Stark effect and large absorption of CO_2 laser radiation at the 10R(6) and 10R(8) laser lines). By tuning the detection frequency of the phase-sensitive detector (lock-in amplifier) to the second longitudinal resonance of the cell (f_2+f_1 or $f_2'-f_1$), spurious photoacoustic signals appearing at either the modulation frequency (f_1) of the CO_2 laser (e.g. the "background" absorption of H_2O and CO_2, the ambient noise and cell window noise) or at the Stark field modulation frequency (f_2 or f_2') (pick-up of the electric field by the microphones) were effectively suppressed by the lock-in amplifier resulting in a practically constant ("noiseless") photoacoustic signal due to ammonia (eliminating completely the coherent photoacoustic background). This innovative scheme making use of only a single laser wavelength, allowed selective ammonia detection in the low ppbv concentration range.

EXPERIMENTAL

The radiation from a home-made and stable CO_2 waveguide laser, interrupted periodically by a mechanical chopper, was focused, by a lens, into the photoacoustic Stark cell behind which a detector was positioned (for monitoring the laser power during the course of the experiments) as shown in Fig.4.1.1. The photoacoustic Stark cell (volume 300 cm^3) with three M37 Microtel electret microphones, was of the resonant type with a Q-factor of 24 and, and sealed by a pair of ZnSe windows provided with the antireflection coatings on both surfaces. Two of the three phase-locked voltage outputs from the home made electrical circuitry were used to drive simultaneously the chopper and the Stark high voltage power supply at the chosen frequencies. The third output, tuned to the cell's resonance, was fed into the reference channel of an Itaco 3961 two-phase lock-in amplifier. The photoacoustic signals detected at this frequency were acquired by a Hewlett-Packard data-logger (3 channels used for measuring the photoacoustic signal, the laser power and the pressure in the cell were used; sampling frequency of one channel was 1 sec) and stored into an IBM-XT for further processing. The recorder output from the lock-in was connected to a Kipp and Zonen flat bed two pens recorder ensuring parallel control during the entire course of the experiments.
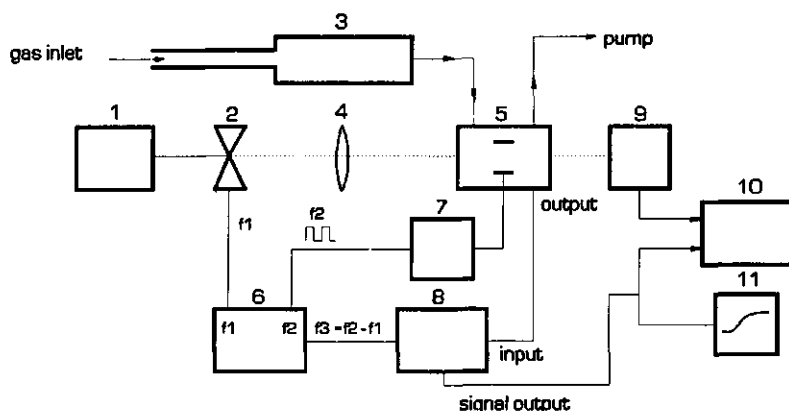

Fig. 4.1.1
1. CO_2 cw waveguide laser; 2. chopper; 3. critical capillary; 4. lens f=190 mm; 5. PA resonant Stark cell; 6. mixer; 7. Stark high voltage power supply; 8. lock-in amplifier; 9 power meter; 10. IBM-PC; 11. chartrecorder.

Prior to the experiments the feed line and the Stark cell were flushed for cleaning purposes using the "zero" gas mixture containing 160 ppmv carbon dioxide (in the ambient air the concentration of this gas is about 350 ppmv) and the natural abundance of nitrogen, oxygen, helium and water vapour. The concentration of the latter could be varied between 0% and 80% relative humidity at 20°C (for example a relative humidity (R.H.) of 50% at 20°C corresponds to an absolute water vapour concentration of 1%). Air of such varying

composition was mixed with ammonia, the concentration of which could be adjusted to any value between 0 and 360 ppbv. The gas inlet port of the Stark cell (the cell was used in the flow-through mode) was connected to the gas handling (manifold) system by means of the critical capillary that maintained the constant gas flow of 0.50 l/min through the cell. A suction pump of sufficient capacity connected to the gas outlet of the Stark cell provided the subatmospheric pressure (pressure drop across the capillary should exceed 500 mbar in order to achieve the calibrated gas flow) necessary for proper working conditions of the capillary. The line-width of the gas absorption lines is a function of pressure and becomes narrower at decreasing pressure. The optimal degree of spectral overlap between the CO_2 laser and the Stark shifted ammonia absorption frequencies at 10R(6) and 10R(8) can be achieved by working at reduced pressure. However, lowering the pressure inside the cell unlimitedly is not possible, since working at reduced gas pressures results in a smaller magnitude of the photoacoustic signal (when compared to that obtainable at standard pressure). As a compromise the pressure in the Stark cell was kept constant at the absolute pressure of 200 mbar; at this operating pressure field strengths as high as 5 kV/cm could easily be maintained without the occurrence of electric discharges between the Stark plates. For comparison reasons the Philips NO_x monitor was also connected to the manifold for simultaneous ammonia measurements (the time interval needed to achieve the steady state ammonia concentration in the manifold system was also recorded by this monitor).

RESULTS

Initially the laser, tuned to the 10R(6) line, was mechanically amplitude modulated at 40 Hz while driving the Stark high voltage power supply at 1648 Hz. Lock-in detection found place in the difference frequency mode f_2-f_1 equalling the second longitudinal resonance of the cell. In order to study the influence of the water concentration on the photoacoustic signal, water vapour (in concentration between 10% and 80% relative humidity) in a mixture of 160 ppmv CO_2, N_2, O_2 and He ("zero" air) was passed (0.50 lit/min) through the photoacoustic cell (no ammonia was admitted in this case). Other measuring conditions include 200 mbar pressure inside the cell, the transverse electric field strength of 4 kV/cm and the integration time of the lock-in (RC-time) amplifier of 3 sec. The detected photoacoustic signal was small and found constant within 10 % across the entire range of the water vapour concentrations as seen in Table I displaying the normalized signals at the 10R(6) and 10R(8) laser transitions.

	10R(6)	10R(8)
"zero air + 20% H_2O (R.H.)	38 nV/W	42 nV/W
+ 40% H_2O (R.H.)	41 nV/W	41 nV/W
+ 60% H_2O (R.H.)	44 nV/W	44 nV/W
+ 80% H_2O (R.H.)	36 nV/W	40 nV/W

Table I Normalized IMPASS signals at the 10R(6) and 10R(8) laser lines

When blocking the laser, thereby preventing the radiation from reaching the cell, it was found that the remaining signal originated from the electric pick-up of the modulating Stark field by the microphones. The magnitude and phase of this "background" signal were found independent of the water vapour concentration. The experimental evidence of major importance was the absence of any Stark effect due to the water under the used experimental conditions proving that the interference effect of strongly absorbing carbon dioxide and water vapour at 10R(6) and 10R(8) was completely suppressed in the difference frequency side band mode of detection.

Secondly, in another experiment, a constant 200 ppbv ammonia concentration was dynamically mixed with the zero air and the water vapour concentration varied within 50% to 80% relative humidity. The photoacoustic signal recorded at 10R(6) in the difference frequency mode, increases gradually before reaching its steady state concentration (Fig. 4.1.2A; gas flow = 0.50 l/min in all cases).
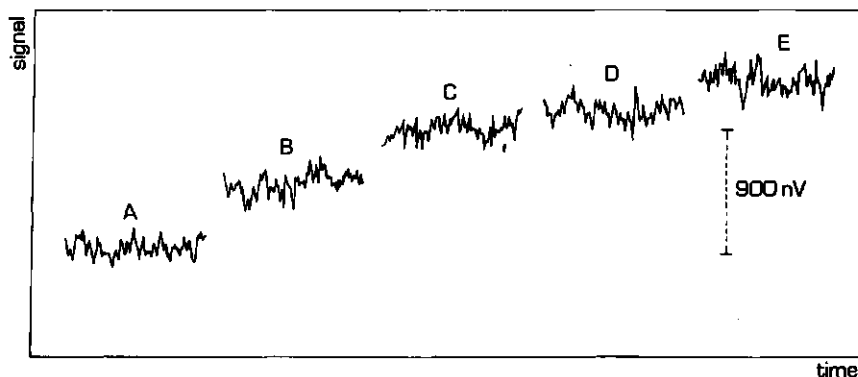

Fig. 4.1.2
2A: 50% R.H. H_2O + zero air + 0 ppbv NH_3; 2B: 50% R.H. H_2O + zero air + 200 ppbv NH_3 (inlet); 2C: 50% R.H. H_2O + zero air + 200 ppbv NH_3 (steady state situation); 2D: 60% R.H. H_2O + zero air + 200 ppbv NH_3 (steady state situation); 2E: 80% R.H. H_2O + zero air + 200 ppbv NH_3 (steady state situation)

The signal due to ammonia is clearly independent of the water vapour concentration (Fig. 4.1.2C). However, a small effect due to the interaction of H_2O and NH_3 present on the walls of the cell can be seen (Fig. 4.1.2E), without causing any deterioration of the recorded photoacoustic signal. The ammonia molecule is known to exhibit a second order Stark effect, meaning that the magnitude of the Stark signal is proportional to the second power of the applied electric field. This test was consistently performed with all gaseous mixtures used and satisfactory agreement between the experiment and theory was obtained. These measurements provided final and convincing evidence for the interference free detection of ammonia in a matrix of absorbing gases. The noise atop the recorded signal was fairly large during this initial phase of experiment. The entire photoacoustic set-up was constructed and mounted in

a temperature controlled and noisy calibration room. Substantial level (as high as 80 dB) of acoustic noise originated from the air-conditioning system maintaining the room temperature at a constant value of 20°C. Furthermore, the oven for catalytic conversion of NH_3 to NO and NO_2 of the Philips NO_x monitor, introduced electric transient signals on the lock-in amplifier whenever its heating coil was switched either on or off. A similar effect was observed for the pump that regulates the constant concentration of water vapour. Finally, an impedance mismatch between the data-logger and the lock-in amplifier caused a fast but small periodic decrease in the magnitude of the photoacoustic signal. For these reasons, at the later stages of this experiment, it was necessary to use longer integration times (10 to 30 sec) in order to achieve 2-3 ppbv detection sensitivity for ammonia.

In conclusion, this experiment clearly demonstrated the feasibility of the proposed method in simplifying substantially the task of photoacoustic detection of ammonia in realistic air samples. Current detection limit (at present (2-3 ppbv)) can be enhanced by boosting the laser output power at the 10R(6) and 10R(8) ammonia absorption lines and certainly by increasing the applied electric field strength. As far as the latter is concerned, the authors anticipate that higher electric Stark fields can be accomplished using a new, carefully designed, small volume (few cm^3) photoacoustic cell. Work on this matter is already in progress. The method presented here can, in principle, be extended to other pollutants (exhibiting permanent dipole moments) of potential interest. It also provides a valuable proof that development of a relatively inexpensive and unique, automated CO_2 laser Stark photoacoustic device should be continued towards its final design, technology and engineering stage before being used for its ultimate goal-the routine atmospheric measurements.

REFERENCES

1. van Pul, A. (1991), Ph.D. thesis, Agricultural University Wageningen.
2. Woltering, E. (1990), Ph.D. thesis, Agricultural University Wageningen.
3. Olafsson, A. (1990), Ph.D. thesis, Institute of Physics, Oersted Laboratory, University of Copenhagen.
4. Rooth, R., Verhage, A., and Wouters, L., (1990), Appl.Optics, **29**.
5. Sauren, H., Bićanić, D., Hillen, W., Jalink, H., van Asselt, C., Quist, J., and Reuss,J., (1990), Appl.Optics **29**.
6. Sauren, H. Bićanić, D., Jalink, H., and Reuss, J., (1989), J.Appl.Phys. **66**.
7. Henningsen, J. Olafsson, A. Hammerich, M., (1990), Trace gas detection with Infrared Gas Lasers, in "Applied Laser Spectroscopy", Eds.Inguscio and Demtröder.

4.2   PHOTOACOUSTIC DETECTION OF AMMONIA IN A SIMULATED ATMOSPHERE OF VARYING WATER VAPOUR CONTENT

Hans Sauren and Dane Bićanić

Laser Photoacoustic Laboratory

Department of Agricultural Engineering & Physics

Agricultural University, Duivendaal 1

NL-6701 AP, Wageningen, The Netherlands

ABSTRACT

Specific detection of ammonia present at trace level concentrations in a simulated atmosphere was attempted through the combined use of intermodulation CO_2 laser photoacoustic Stark spectroscopy and phase-sensitive detection at the sum and difference sidebands of the modulating laser and Stark electric fields. Results of experiments performed at both 10R(6) and 10R(8) laser lines indicate the signal dependence on the water vapor concentration present in the used gas mixture.

Adhering of ammonia to the cell walls was found also to be a function of the amount of water vapour in the simulated atmosphere.

INTRODUCTION

The analysis of pollutants discharged into the ambient air has become of major concern to environmental scientists. Detection of ammonia (NH_3) in particular has received much attention over recent years. This constituent is the most abundant alkaline component found in the atmosphere and is known to play an essential role in the neutralization of acids (e.g. H_2SO_4, HNO_3 and HCl) generated by the oxidation of sulphur dioxide and nitrogen oxides (e.g. $NH_{3(g)} + HNO_3 \leftrightarrow NH_4NO_{3(s)}$ and $HCl_{(g)} + NH_{3(g)} \leftrightarrow NH_4Cl_{(s)}$, where the indices g and s refer to the gas and the solid phase respectively). On the other hand, high ammonia deposition rates (produced by for example intensive livestock breeding and chemical plants) cause nitrification of soil, i.e.: $NH_3 + H_2O \leftrightarrow NH_4^+ + OH^-$ and $NH_4^+ + 2O_2 \rightarrow 2H^+ + NO_3^- + H_2O$, resulting in a leaching of potassium, magnesium and calcium from the soil[1]. The net upward and downward fluxes of atmospheric NH_3 are modelled by calculating its spatial distribution using data gathered by a series of ammonia concentration measurements performed at different sampling points along a vertical line. For accurate data correlation the detection system (i.e. the point sensor) used in the practice must be capable of rapidly scanning each sampling point with sufficient accuracy (normally in the low ppbv regime). To surmount the problems encountered whenever chemical (e.g. denuders) or thermochemical ammonia monitors (e.g. NO_x monitors) are used, CO_2 laser photoacoustic spectroscopy (LPA) has recently been tested as a possible technique for fast, interference-free, 'on-line' tracking of ammonia[2-5]. The main advantages of LPA above other spectroscopic techniques are its

sensitivity in the sub-ppbv level, the linearity between the signal and gas concentration over more than 5 orders of magnitude, its reasonable selectivity and the relatively simple apparatus needed. Moreover, large NH_3 absorption cross-sections α are found in the frequency range covered by the CO_2 laser; the three largest are observed at the 9R(30) (α=56 atm^{-1}cm^{-1}), the 10R(8) (α=26.0 atm^{-1}cm^{-1}) and the 10R(6) (α=20.6 atm^{-1}cm^{-1}) laser lines. Various articles dealing with the photoacoustic detection of ammonia employing the 9R(30) CO_2 laser line have recently been published. Olafsson *et al*[6]. used a grating tunable $^{12}C^{16}O_2$ laser (tunability 500 MHz) and a non resonant photoacoustic cell for 'on-line' monitoring of ammonia at ppmv-level in the stack-gases of a chemical plant in the presence of amounts of CO_2 as high as 15%. Rooth *et al*[?]. developed a specific methodology for photoacoustic detection of ammonia trace levels in a matrix of absorbing gases, such as CO_2 and H_2O, present at ambient concentration levels. However, to deduce the proper concentrations of ammonia present in the gas sample, the measured photoacoustic signals had to be corrected for interference effects due to water vapor and carbon dioxide as well as for the phase reversal resulting from the kinetic cooling effect. A different approach based on combined use of Stark and photoacoustic spectroscopy as a means to enhance the specificity when detecting ammonia concentrations in air samples has been suggested[7,8]. In a recent experiment both, the selectivity and sensitivity were increased[9] by means of the InterModulated PhotoAcoustic Stark Spectroscopy (IMPASS). The IMPASS utilizes the Stark effect induced at reduced pressure ($\approx$ 200 mbar) in the polar gas to shift the relevant ammonia transition into the resonance with the desired CO_2 laser line. With the fixed frequency laser radiation, being intensity modulated (f_{chop}), passing through the Stark photoacoustic cell, and the applied electrostatic field alternating at f_{Stark}, the phase sensitive technique is used to measure the IMPASS signal (due to ammonia) at $f_{det}=f_{chop}\pm f_{Stark}$ in the cell having acoustical resonance f_{res} at $f_{det.}$, i.e. $f_{det}=f_{res}$.

This paper is concerned with the investigation of the IMPASS's (designed to detect ammonia) immunity to the spectral interference resulting from the absorption of water vapor and carbon dioxide in the $^{12}C^{16}O_2$ laser region. The magnitude of the Stark effect in ammonia (present at trace levels in a simulated atmosphere) was therefore studied as a function of both the applied electric field (0-5 kV/cm) and the water vapor concentration (ranging from 10% R.H. to 60% R.H. at 20°C).

It was further shown that the rate of adsorption (and also the desorption) of ammonia to the cell walls depends on the changes of the water vapor concentration in the simulated atmosphere.

EXPERIMENTAL

The normal ambient atmosphere was accurately simulated in a gas handling system (Fig.4.2.1) by mixing carbon dioxide at a fixed concentration of 160 ppmv, water vapour (concentrations ranging from 10% to 80% relative humidity (R.H.) at 20°C) and the natural abundances of nitrogen, oxygen and helium (such a gas composition being called "zero" air) with ammonia at trace levels in the concentration range from 0 to 360 ppbv. The mixing was done in a well controlled and reproducible manner.
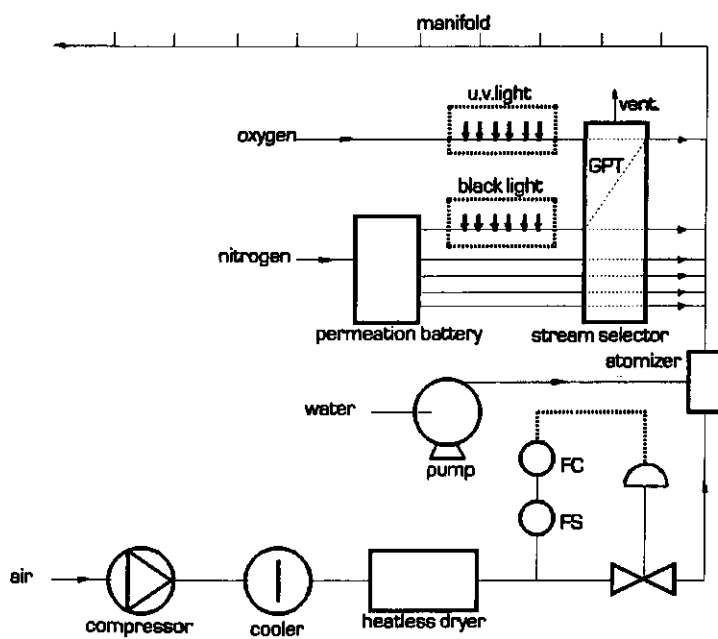
73

Fig. 4.2.1 The gas handling system

Following compression and cooling down to 2°C, air is purified in a heatless dryer consisting of two separate columns filled with silica gel (FS) and charcoal (FC). The dried, controlled flow is mixed with a known water flow in an atomizer. Trace constituents and diluted air are mixed in a static mixer and passed at a flow rate of 0.50 l/min, via the PTFE-teflon manifold to the Stark cell. A detailed description of the set-up used for the photoacoustic tracking of ammonia in the simulated atmosphere employing detection at both the sum and difference sidebands $f_{Stark} \pm f_{chop}$ (IMPASS) has been extensively described in a previous article[10]. Briefly, the standard IMPASS set-up (Fig.4.2.2) consists of the water cooled cw $^{12}C^{16}O_2$ waveguide laser (1), a mechanical chopper (2), a critical capillary (3), a ZnSe lens (f=190 mm) (4), a resonant photoacoustic cell provided with Stark plates (5), a triple frequency phase-locked loop (PLL) (used to modulate the Stark electric field at frequency f_{Stark}, to drive the chopper at a frequency f_{chop} and to provide the frequency $f_{det.}$ for phase-sensitive detection) (6), a high voltage power supply (output voltages ranging from 0 kV to 3 kV) (7), an Ithaco 3961 two-phase lock-in amplifier (8), a home-made thermopile laser power meter (9), a Hewlett and Packard data acquisition unit (10), and a IBM-XT computer for automated data processing (11).
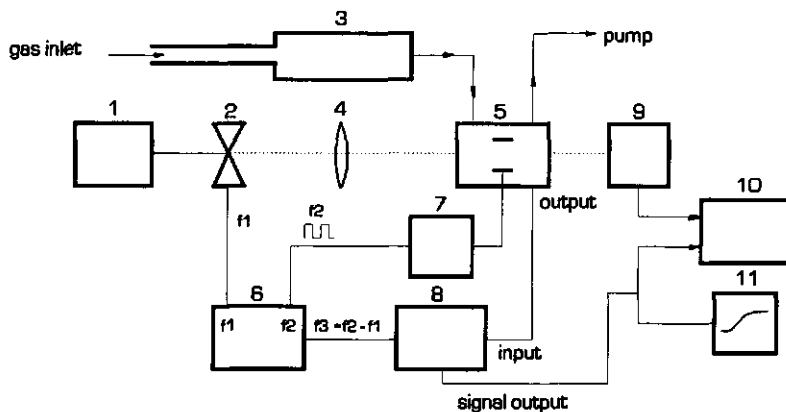
Fig. 4.2.2 The IMPASS system for detection of ammonia

When switching from IMPASS to the traditional CO_2 laser photoacoustic Stark spectroscopy (CLPAS) detection mode, both the PLL and the Stark high voltage power supply were disconnected from the apparatus. Instead, a Wavetek generator (Model 142 HV VCG Generator) and a stable FUG 7E-12500 HV unit were used for application of a Stark field in a periodic manner such as the "square-wave" variation (at a frequency $f_{Stark}=0.1$ Hz).

Fig. 4.2.3 The CLPAS system in the "slow" Stark modulation mode ($f_{Stark}=0.1$ Hz; $f_{det}=f_{res}=1608$ Hz) for detection of ammonia.

RESULTS AND DISCUSSION

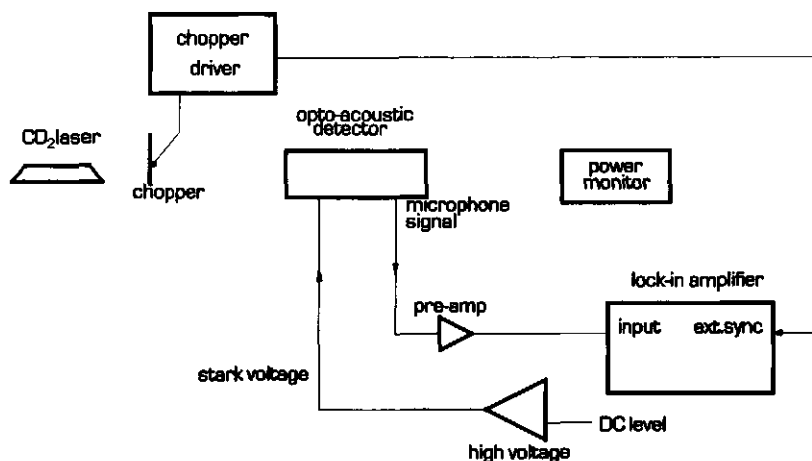Prior to testing the specificity of the IMPASS scheme in detecting ammonia (present in a matrix of absorbing gases i.e. CO_2 and H_2O) the IMPASS background signal was recorded by admitting a mixture of zero air (containing a water vapor concentration of 20% R.H. and a fixed CO_2 concentration of 160 ppmv) to the photoacoustic Stark cell. The background signal in the IMPASS mode was observed at the difference frequency sideband ($f_{Stark}-f_{chop}=f_{res.cell}$) with the amplitude modulated CO_2 waveguide laser (chopping frequency $f_{chop}=40$ Hz) tuned to the 10R(8) line (ammonia exhibits a near-coincidence at this laser transition). The modulation frequency of the Stark high voltage power supply was set to 1648 Hz; the maximum (calculated) strength of the electric Stark field was 4.5 kV/cm for a plate spacing of 5 mm. Employing the cell in the flow-through mode (0.50 l/min) the pressure was kept constant at about 200 mbar and the lock-in integration time fixed (i.e. RC-time=3 sec). Fig.4.2.4a displays the recorder trace of the IMPASS background signal, obtained with the "zero-gas" mixture containing 20% R.H. H_2O and 160 ppmv CO_2 and the natural abundances of N_2, O_2 and He. An ammonia concentration of 50 ppbv was subsequently mixed with the very same "zero-gas" and passed to the photoacoustic cell. The increase in IMPASS signal following the admission of ammonia is clearly seen (Fig.4.2.4b). The ammonia concentration was then increased gradually from 50 ppbv to 200 ppbv (Fig.4.2.4c). Since a direct proportionality between the photoacoustic IMPASS signal and the admitted NH_3 concentration is expected, the plot shown in Fig.4.2.4c indicates that the NH_3 steady-state concentration in the photoacoustic cell had not been reached yet: the magnitude of the IMPASS signal only doubled while the ammonia concentration was quadrupled.
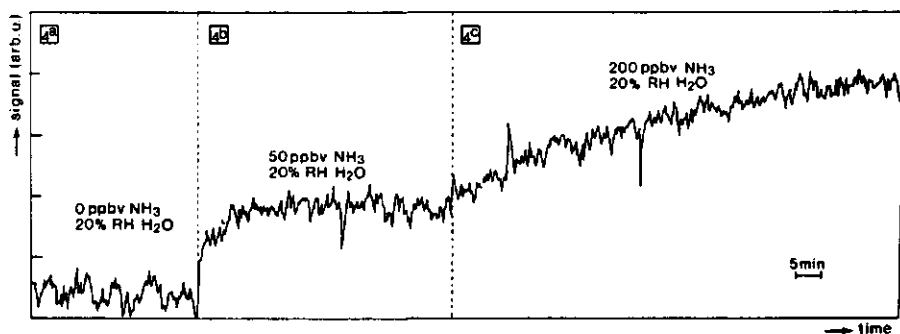
Fig. 4.2.4 IMPASS signal as a function of NH_3 concentration

The IMPASS signal rise time τ (defined as the ratio of the gas flow f (0.50 l/min) to the cell volume V (0.3 l), i.e. $\tau=V/f=36$ sec is the time interval needed for the IMPASS signal to reach 68% of its end value in the absence of any adsorption) of the photoacoustic cell increases to a value $\tau_{NH3}>\tau$. In our experiment τ_{NH3} increased to about 2 min. This

indicates that, presumably due to adsorption of ammonia to the cell walls, a longer period of time is needed to reach the steady-state signal level[11-13]

The effect of adding water vapor to the gaseous mixture appeared worthy of closer study. Initially 200 ppbv of NH_3 was mixed with the "zero-air" containing a water vapor concentration of 10% R.H., and passed to the photoacoustic Stark cell. The laser was tuned to the 10R(6) ammonia absorption line and the IMPASS signal was recorded accordingly in the difference frequency mode $f_{det} = f_{Stark} - f_{chop}$ (Fig.4.2.5a displays the chart recorder trace of IMPASS signal). Remaining experimental conditions were as follows: cell pressure 200 mbar, flow 0.50 l/min, and lock-in integration time (RC-time) 3 sec. The next step was to increase the water vapor concentration to 80%. As seen in Fig.4.2.5b., the IMPASS-signal increases following the admission of the sample into the cell. Since the NH_3 concentration in the gas mixture stream was kept constant (200 ppbv) the large increase of the IMPASS signal can only be attributed to the previously adsorbed NH_3 now being released (desorbed) from the cell walls and replaced by water vapor, thereby increasing the NH_3 concentration present in the gas phase.
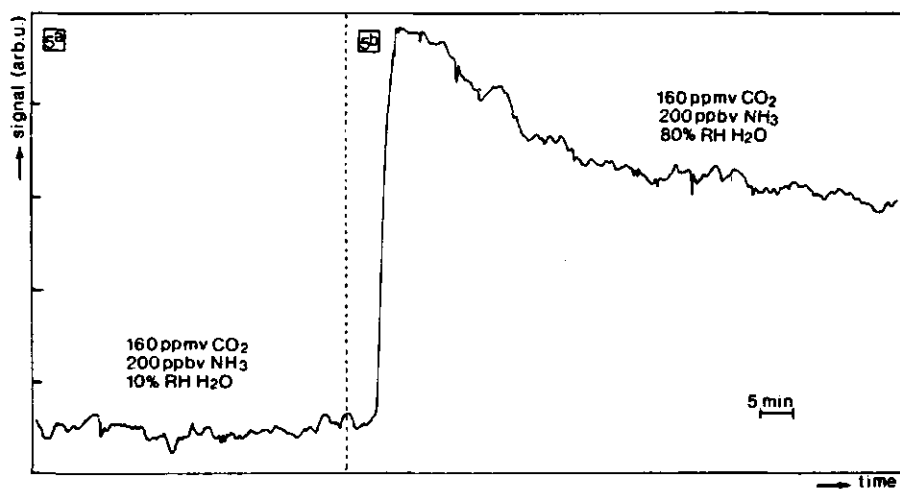
Fig.4.2.5 Effect of water vapor concentration on the recorded NH_3 IMPASS signal

The established chemical equilibrium existing in the cell between gaseous H_2O, NH_3 and CO_2 is initially disturbed by such a dramatic rise in water vapor content, but is then gradually restored, as seen by the levelling off of the time-dependent curve of the IMPASS signal. Experimentally it was proved that the IMPASS signal (using the very same gas mixture containing 80% R.H. H_2O, 200 ppbv NH_3, and 160 ppmv CO_2) gradually decreased to the former signal level as measured in Fig.4.2.5a. Although such sudden abrupt changes of water vapor concentration rarely occur in the ambient air, it is a good reason when tracking

77

ambient ammonia to simultaneously monitor the changes in the ambient water vapor concentration. This is needed in order to correctly account for fluctuations observed in the recorded NH_3 IMPASS signal.

In a subsequent experiment the effect of the presence of water vapour on the IMPASS signal was studied using only the "zero-gas" with no NH_3 admitted. The water vapor concentration was varied from 10% to 30% and then to 70% R.H. and passed together with a fixed CO_2 concentration of 160 ppmv and nitrogen to the photoacoustic cell. As stated above, the rise in the IMPASS signal, observed when increasing the water vapor concentration in the cell (from 10% (Fig.4.2.6a) to 30% (Fig.4.2.6b) and 70% R.H. (Fig.4.2.6c) can only be accounted for by assuming the apparent increase of gaseous NH_3 concentration to originate from the effect of H_2O adsorbing to the solid surface, thereby removing the previously adsorbed NH_3.
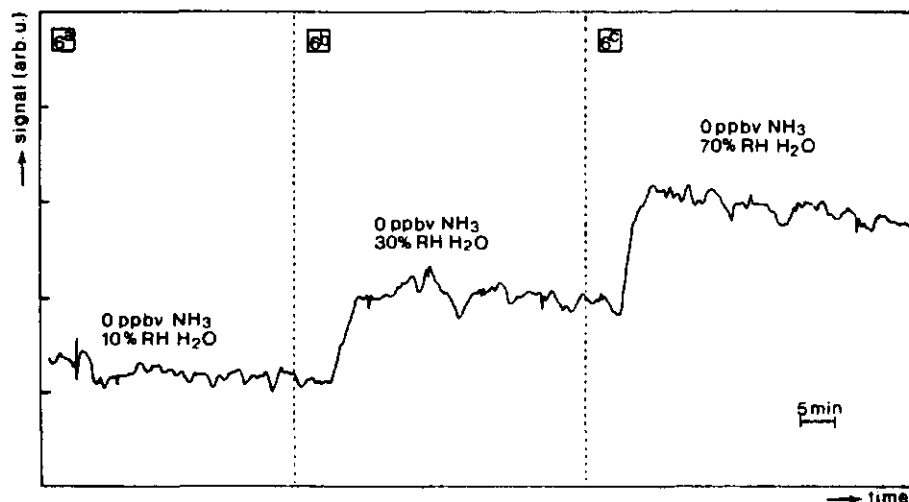
Fig.4.2.6 NH_3 memory effects as a function of water vapour concentration

The levelling off of the IMPASS signal after the abrupt admission of water vapor was experimentally proven to occur faster in gaseous mixtures containing no ammonia.
From Figs. 6a, to 6c, it is clear that, when working with a cell "polluted" with adsorbed ammonia, the changes in H_2O concentration will affect the IMPASS signal substantially ("memory-effect") even at a very low content of ambient ammonia. Such "contamination" can be minimized by employing a photoacoustic cell entirely constructed from chemically inert materials, such as glass or different kinds of teflon or by treating their surface (i.e. reduction of pores, increase of the operating temperature).

After using the simulated atmosphere of varying water vapor content to demonstrate how the IMPASS signal is affected by chemical-physical reactions occurring at the gas-solid

interface (i.e. the adsorption and desorption of ammonia to the walls of the photoacoustic cell in the presence of water), the effect of different water vapor concentrations on the magnitude of the Stark shift induced in ammonia was studied. Since the IMPASS detection of ammonia is based upon the application of a modulated electric field (Stark effect) the immunity of the detection system to water vapor interference at the chosen 10R(6) and 10R(8) ammonia absorption lines was experimentally checked.

In our previous papers[9,10] it was reported that a Stark shift in H_2O at the 10R(6) and 10R(8) laser lines was not observed when employing the IMPASS NH_3 detection scheme and the very same experimental conditions as described in this paper. Although the spectral absorption of H_2O and CO_2 at the laser lines used is suppressed when employing detection at the sum and difference sidebands ($f_{det}=f_{Stark}\pm f_{chop}$), other molecular (chemical-physical) effects disturbing the NH_3 IMPASS signal were experimentally verified. To do so, initially, fixed concentrations of CO_2 (160 ppmv), NH_3 (200 ppbv) and H_2O (20% R.H.) were mixed homogeneously in the gas handling system prior to passing the mixture to the photoacoustic Stark cell. Upon reaching the steady-state concentration, the IMPASS ammonia signal S was recorded as a function of the applied electric Stark field E. The observed IMPASS signals S_n (normalized to incident laser power) are presented in Table 1.

IMPASS 10R(8)

calculated E-field (kV/cm)	$S_n(E)$ (nV/W)
4.7	388
4.3	329
4.0	120
2.2	79
0.0	38

Fit: $S_n(E)=(0.04\pm0.03)+(-0.11\pm0.10)*E+(0.28\pm0.07)*E^2$

Table 1

The IMPASS ammonia signal as a function of the applied electric field strength E. $C_{NH3}=200$ ppbv; $C_{H2O}=20\%$ R.H. at 20°C; 10R(8) CO_2 laser line; cell pressure 200 mbar;

Fitting the experimental data yields (as predicted by theory[14]) a quadratic dependence of the recorded IMPASS ammonia signal $S_n(E)$ on the applied electric Stark field E (kV/cm).

However, when including the calculated standard deviation σ in the fitted parabolic expression for $S_n(E)$ a purely quadratic expression for the power series $S_n(E) = E^n$ is obtained.

In order to investigate more carefully the effect of the modulated electric field strength E on the ammonia signal S, both the Stark power supply and the PLL were removed from the apparatus and replaced by a very stable FUG 12500 high voltage power supply. The laser was mechanically chopped at the cell's actual acoustical resonance ($f_{chop} = 1608$ Hz) whilst driving the FUG power supply (in the square wave form) by a Wavetek generator at a frequency $f_{Stark} = 0.1$ Hz.

Whilst increasing the water vapor concentration from 30% to 40%, and then to 60% R.H., the photoacoustic signal S due to Stark shifting the ammonia molecule was recorded as a function of applied electric field E by tuning the CO_2 laser successively to the 10R(6) and 10R(8) ammonia absorption lines. The results of this study are presented in Table 2. The parabolic function $S_n(E) = a + b*E + c*E^2$ was used to fit the normalized CLPAS ammonia signals $S_n(nV/W)$ to the applied electric Stark field $E(kV/cm)$. The standard deviation σ is also calculated. It is clear that, at the 10R(8) CO_2 laser line, the magnitude of the linear coefficient exceeds that of the quadratic term. However the ratio of the coefficients b/c decreases at higher water vapor concentrations. At the 10R(6) CO_2 laser line the situation is less clear. Including the standard deviation σ in the fitted values for the linear and quadratic coefficients at both laser lines and performing straightforward calculations shows the quadratic dependence to vanish, apparently suggesting only a linear Stark effect at higher water vapor contents.

10R(6)	b	c	b/c
0% R.H.	0.053±0.017	0.1086±0.007	0.488
40% R.H.	0.257±0.07	0.068±0.03	3.78
60% R.H.	0.074±0.04	0.068±0.015	1.09
10R(8)	b	c	b/c
30% R.H.	0.146±0.033	0.04±0.013	3.65
40% R.H.	0.259±0.07	0.078±0.03	3.32
60% R.H.	0.127±0.05	0.052±0.018	2.44

Table 2 CLPAS-mode; zero air + 200 ppbv NH_3

Further, it was experimentally observed that the magnitude of the measured ammonia CLPAS-signals at both the 10R(6) and 10R(8) CO_2 laser lines decreased at increasing water vapor concentrations. There are several possible explanations for this observation as well as for the results of the measurements presented in Table 2. One cause for the variation in signal response might be the occurrence of chemical reactions between water and ammonia at high H_2O concentrations (i.e. $H_2O + NH_{3(g)} \leftrightarrow NH_4OH_{(aq)}$) that reduce the actual ammonia concentration in the gas phase. Just as acid droplets were found important in studies of HCl in the clouds, there might also be water droplets present in our samples, containing varying amounts of dissolved ammonia. Although increasing the relative humidity of the mixture

affects the dielectric constant ϵ of the medium filling the space between the Stark plates (ϵ is 1 for dry air and around 3.5 for air of 100% relative humidity at room temperature), the electric field does not change. For this reason the values of E calculated by taking the ratio of the Stark voltage (V) to the gap spacing (d) (i.e. E=V/d) are also correct for fitting the data in Fig.4.2.5.

Furthermore, at high relative humidity the pressure broadening increases substantially and it therefore becomes more difficult to recover the ammonia selectively via the Stark splitting at the 10R(6) and 10R(8) CO_2 laser lines using the same value of the square wave potential. At present the range of Stark voltages is restricted by the high voltage power supply available. Additional modifications in cell design are required if higher electric fields are desired. The results of our measurements justify the continuation of this study at high relative humidity in order to determine precisely the extent of the immunity degree of the IMPASS method when detecting ambient ammonia. Work on this matter is already in progress.

ACKNOWLEDGEMENT

REFERENCES

1. W.Asman, Ph.D. thesis, Agricultural University Wageningen, The Netherlands (1987).
2. R.Rooth, A.Verhage and L.Wouters, Appl.Opt., **29**, 3643,(1990).
3. A.Olafsson, M.Hammerich, J.Bülow and J.Henningsen, Appl.Phys.B, **49**, 91, (1989).
4. H.Sauren, D.Bićanić, E.Gerkema, submitted to Atm.Environm. (1991).
5. M.Sigrist, Rev.Sci.Instr., **61**, 1179, (1990).
6. A.Olaffson, Ph.D. thesis, Oersted Institute, University of Copenhagen ISSN 0906-0286 (1990).
7. H.Sauren, D.Bićanić, H.Jalink, J.Reuss, J.Appl.Phys. **66**, 5085-5087, (1989).
8. H.Sauren, D.Bićanić, W.Hillen, H.Jalink, K.van Asselt, J.Quist, J.Reuss, Appl.Opt. **29**, 2679, (1990).

9. H.Sauren, T.Regts, K.van Asselt, D.Bićanić, **12**, 719-724, Environm. Techn. Lett. (1991).

10. H.Sauren, D.Bićanić, and K.van Asselt, Infrared Phys. **8**, 475-484 (1991).

11. S.M.Beck, Appl.Opt., **24**, 1761, (1985).

12. G.Cooper, G.Gelbwachs, S.Beck, "Progress Report FY 1985/86" Aerospace Corp. El Segundo, California, USA.

13. H.Sauren, B.van Hove, W.Tonk, H.Jalink, D.Bićanić, In "Monitoring of Gaseous Pollutants by Tunable Diode Lasers", Eds. R.Grisar *et al.* Kluwer Academic Publisher ISBN 0-7923-03334-2 (1989)

14. H.Sauren Ph.D. thesis, Agricultural University Wageningen (1991).

4.3 PHOTOACOUSTIC DETECTION OF AMMONIA AT THE SUM AND DIFFERENCE SIDEBANDS OF THE MODULATING LASER AND STARK ELECTRIC FIELDS

HANS SAUREN, DANE BIĆANIĆ and KEES VAN ASSELT

Laser Photoacoustic Laboratory, Department of Agricultural Engineering and Physics, Agricultural University, Duivendaal 1, 6701 AP Wageningen, The Netherlands

Abstract—A novel scheme for on-line ammonia trace-gas detection, based on CO_2 laser intermodulation photoacoustic spectroscopy incorporating high voltage Stark modulation (IMPASS), is described and its sensitivity and specificity tested in a simulated atmosphere. The complete suppression of water vapour and carbon dioxide interferences was achieved resulting in a true "on-line" detection system capable of 3 ppbv NH_3 sensitivity in air. Performance of this new detection scheme (in the flowing regime) was found superior to that of the conventional photoacoustics (beam chopping mode).

1. INTRODUCTION

The net upward and downward transport rates of trace gases like ozone (O_3), sulphur dioxide (SO_2), nitrogen oxide (NO_2) and, in particular, of ammonia (NH_3) play an important role in the modelling and the understanding of photo-smog and air pollution.[1] A variety of models based on the successive measurements of gas concentrations along a vertical line at different sampling points have been suggested but lack sufficient data accuracy. This is partly due to the fact that in point sampling techniques one and the same gas concentration monitor is used to scan all sampling points. In order to correlate the experimental data the response time of the monitor has to be sufficiently fast. In general, the accuracy of the calculated gas concentration gradient decreases when the time needed for a complete scan of all sample points along the vertical line exceeds 10 s. This is, however a technical problem inherent to all types of gas monitors. The response time of a gas monitor depends also on the chemical and/or the physical properties of the gas.

Among the trace gases ambient ammonia is one of the most difficult to monitor. Its important role in the air pollution is well documented in a number of reports published in the last decade. Being the principal chemical compound emitted in intensive livestock breeding, gas stacks (chemical plants), and car gas exhausts (as one of the catalytical end products) its inclusion in atmospheric pollution models makes monitoring an important issue. The chemical properties of ammonia make it difficult to avoid its chemical reduction (from the gas phase into the solid phase). At first, due to its electronegative character ammonia is highly reactive and forms strong chemical bonds (adsorption) on electropositive sites of different materials. Secondly, the reduction of gaseous ammonia in the presence of excessive quantities of water vapour is known from literature.[2] High water vapour concentrations present in the atmosphere and the consequent reduction of gaseous ammonia pose a problem in low level flux detection to which no satisfactory solution has been found yet.

Methods for detection of ambient NH_3 are either chemical or physical ones. Among the chemical methods annular denuder systems (ADS) and gas monitors (operating on the principle of catalytic conversion of NH_3 in a high temperature oven to NO and NO_2) are most frequently used.

The latest generation of ADS are made out of glass in a 3-channel concentric geometry encased in a stainless steel sheath. The glass-surface is coated with chemicals to adsorb acidic and basic gases like SO_2, HNO_3 and NH_3. After a sampling period of 24 or 48 h aqueous extracts are analyzed by ion chromatography, as well as by colorimetric and pH electrode methodologies.[3] Although a sensitive technique for multi-component analysis, the extensive sampling time limits the flexibility of ADS when used in on-line gas flux studies.

83

At trace concentration level the ammonia monitor exhibits a lower intrinsic accuracy when used as fast sampling device (response time less than 1 min). An even larger problem (when monitoring ambient air with these monitors) is the interference of ammonia with other nitrogen-containing compounds. Detailed cross-sensitivity studies show that the accuracy in ammonia detection is mainly influenced by PAN, ethyl-nitrate, ethyl-nitrate and n-propyl-nitrate.[4,5] Like ammonia, all these molecules are thermo-chemically reduced to NO_x as the ultimate product. Research in the area of NH_3 detection by chemical means is a very active field and substantial improvements were made without however changing the basic detection principle. The variety of problems one faces while on-line measuring ammonia fluxes has also stimulated developments towards new physical techniques. So led the introduction of high power, continuous tunable light sources (lasers and broadband lamps in conjunction with monochromators) to a diversity of optical methodologies that were tested in practice. Differential optical absorption spectroscopy[6] (DOAS) and diode laser systems[7] (TDLAS) have been used in long-path atmospheric pollution monitoring. Both are based on the measurement of the attenuation (linear absorption) of a light beam caused by molecules absorbing along the optical path. A pronounced advantage of these techniques is the absence of actual contact of ammonia with the sensor (these methods do not make use of any feed-line tubing needed for transportation of the gas to the monitor or cells to perform spectroscopic identification). Nevertheless, atmospheric scattering of the light beam, low laser output powers (TDLAS), and spectral interferences caused by molecules absorbing at the same wavelength as the gas of interest (specially water vapour and carbon dioxide) limit their use in practice. The DOAS and TDLAS systems are suitable for monitoring average gas concentrations over long distances, rather than gas fluxes.

Laser photoacoustic spectroscopy (LPAS) was introduced as a new tool in point sampling measurements of air pollution by Kreuzer some 20 years ago.[8] The availability of powerful, tunable light sources (e.g. like the CO_2 laser), offers the experimentalist a highly sensitive (detection limit sub-ppbv level) and versatile technique with the possibility to overcome most of the previously mentioned problems encountered in trace gas detection. Briefly, the physical principle of LPAS is as follows: the radiation from a modulated laser is absorbed by gas molecules in a confined volume (i.e. a photoacoustic cell). The collisional deactivation of the excited molecules inside the cell, results in a pressure change detectable by a microphone. For a given cell, the resultant electric microphone signal S, processed by a phase sensitive detector, is directly proportional to the molecular absorption coefficient α ($atm^{-1} cm^{-1}$) laser power P (Watts) and the gas concentration C (in units of partial pressure), i.e. $S \propto \alpha PC$. Therefore a high output power level (several Watts) provided by (in these experiments a CO_2 cw waveguide) a laser radiation source is of benefit in trace detection.

The infrared region around $10 \mu m$ is very suited for characterizing a trace gas by optical absorption as the vibration-rotation spectra of many molecules are sufficiently rich with specific spectral signatures to allow monitoring. Atmospheric absorption of $^{12}C^{16}O_2$ laser radiation in the spectral window extending from 9 to $11 \mu m$ is primarily due to water vapour and carbon dioxide.[9,10] Although both are weak absorbers, their large abundance can impose operational limits (the "kinetic cooling" effect) on the photoacoustic detection of trace gases absorbing in the same spectral region. In the traditional beam chopped CO_2 laser photoacoustics (CLPAS) the presence of spectrally interfering gases (e.g. H_2O and CO_2) limits the sensitivity (the minimum detectable concentration) of a pollutant. Since the photoacoustic signal is a vector sum (magnitudes and phases) of all absorbing constituents present in the photoacoustic cell, the measured total signal S varies as a consequence of the fluctuations of water vapour and carbon dioxide concentrations in the ambient air. Lacking the precise data on the molecular processes involved in $H_2O-CO_2-N_2-NH_3$ gas mixtures leads to an erroneous interpretation of the desired signal due to ammonia and hence also of its concentration.

A phenomenon related to this problem (when working in CLPAS) is the kinetic cooling effect present in all gas mixtures containing CO_2 and N_2. It becomes noticeable when the inverse of the laser modulation frequency becomes comparable to (or is smaller than) the relaxation time in the CO_2-N_2 system. In a photoacoustic set-up the kinetic cooling effect manifests itself by a phase reversal, affecting the magnitude of the detected signal. However, the kinetic cooling effect critically depends on the amount of water vapour present (H_2O accelerates the relaxation of the excited N_2

molecules to the ground state) and becomes negligible at high water vapour concentrations.[11] This phenomenon is of major importance in on-line photoacoustic monitoring of air pollutants. To derive correct values of a trace gas from the measured photoacoustic signals, the effect of kinetic cooling on the molecular relaxation processes present in the gas mixture (and therefore on the magnitudes and phases of the recorded photoacoustic signals) must be known and accounted for in the signal interpretation and concentration analysis. Alternatively, the inverse of the laser modulation frequency has to be sufficiently large, compared to the molecular relaxation time, to avoid the effect of kinetic cooling on the photoacoustic signal.

The use of a cw CO_2 waveguide laser for photoacoustic monitoring of NH_3 is quite favourable, as ammonia exhibits several strong absorption lines in the CO_2 laser region with the three strongest being the 9R(30) ($\alpha = 56$ atm^{-1}cm^{-1}), 10R(6) ($\alpha = 26$ atm^{-1}cm^{-1} and the 10R(8) ($\alpha = 20.6$ atm^{-1} cm^{-1}). Several *in situ*, conventional CLPAS studies of gaseous ammonia have been performed so far, both in the low- (ppbv-level) and high-concentration (ppmv-level) ranges. Results of NH_3 monitoring at the ppmv-level have recently been published by Olaffson *et al.*[12,13] who used a 500 MHz tunable CO_2 waveguide laser photoacoustic spectrometer for ammonia detection in power plant emission. To avoid the problem of the CO_2 interference the measurements were performed at 12 mbar pressure in the cell. At this reduced pressure the molecular linewidth approaches the Doppler-limit and the gases were identified from the line-positions (known from laboratory studies) within the 500 MHz tuning window. When both the magnitudes and the phases (resulting from the kinetic cooling effect) of the recorded photoacoustic signals were taken in the analysis, interference free ammonia monitoring was possible to at 1 ppmv in the presence of 15% CO_2. As stated already, monitoring NH_3 in the ambient air becomes substantially more difficult in the low concentration range (ppbv). However, Rooth *et al.*[14] recently suggested a methodology by which the NH_3 concentration in a matrix of absorbing gases could be deduced from the proper interpretation of phases and signal strengths obtained at several prudently selected CO_2 laser wavelengths. Briefly, the method implies the consecutive recording of the magnitude and the phase of the photoacoustic signals (generated in a resonant "organ pipe" cell operated at atmospheric pressure) while admitting well controlled quantities of water vapour to a CO_2/N_2 gas mixture. The set-up was accordingly calibrated by adding trace level ammonia concentrations to the $H_2O/CO_2/N_2$ system. Since the ambient CO_2 concentration is fairly constant (around 350 ppmv), only the magnitudes and phases of the photoacoustic signal as a function of the water vapour concentration have to be found in order to completely determine all the physical parameters involved in this detection scheme.

Reducing the water vapour and carbon dioxide concentrations in the air by chemical means (for example H_3PO_4, KOH scrubbers) prior to the admission of the flowing sample air into the photoacoustic cell is rather risky as it introduces a number of additional uncontrollable parameters (in particular aging and saturation of the scrubber requires perpetual calibration procedures). Moreover, the adsorptive behaviour of ammonia to scrubbers in the presence of H_2O and CO_2 has so far not been studied with sufficient precision. A physical, rather than a chemical method is favoured to supress simultaneously the kinetic cooling effect and the absorption of water vapour at CO_2 laser wavelengths.

Apart from its chemical properties, ammonia, being a symmetric top molecule possesses a large dipole moment (1.48 Debye) in the ground state. Laboratory studies on ammonia[15] have shown Stark splitting of its rovibronic energy states in an externally applied electric field. This physical phenomena was used for the first time by Sauren *et al.* to determine directly photoacoustic NH_3 trace levels in the ambient air.[16] In this paper we report on the progress made with the Stark-tuned CO_2 photoacoustic spectrometer during the last 2 years. Different techniques were combined in an attempt to construct a photoacoustic monitor, with the ultimate goal the on-line interference-free tracking of ambient ammonia exhibiting signal responses fast enough to enable determination of ammonia deposition rates data. The new method essentially implies the reduction of the spectral ambient interferences at CO_2 laser wavelengths, the supression of the cell window noise and the decrease of the electronical noise (due to the pick-up by the detecting microphones of the Stark high voltage modulation).

The marked difference, with respect to the detection scheme used and published in 1989 is the utilization of a resonant photoacoustic Stark cell (resonance frequency $f_{res.cell} = 1608$ Hz at STP)

acting simultaneously as a frequency mixer and detecting spectrophone. This was achieved by directing the radiation of a mechanically modulated (f_{chop}) CO_2 laser into the Stark cell accomodating the gas sample at reduced pressure. A high electric Stark field (parallel to the E-field direction of the laser) was applied in a periodic way (f_{Stark}) to shift the ammonia molecules into resonance with the laser thereby enhancing the NH_3 cross-section for CO_2 laser radiation absorption. The interaction between the absorbing NH_3 molecules and the two modulated fields [i.e. the CO_2 laser (f_{chop}) and the Stark field (f_{Stark}), both in a block (square)-wave form] generates photoacoustic signals at the sum $[f_{chop} + f_{Stark} = f_{res.cell} = f_{detect.}; f_{detect.} > f_{Stark} \gg f_{chop}; f_{detect.}$ is the detection frequency to which a phase-sensitive detector (i.e. lock-in amplifier) is tuned to] and at the difference $(f_{Stark} - f_{chop} = f_{res.cell} = f_{detect.}; f_{Stark} > f_{detect.} \gg f_{chop})$ frequency (and their respective harmonics) sidebands. The interaction between the NH_3 molecule and the two modulating fields results in the generation of an acoustic sound wave (signal S) detected by the lock-in amplifier at $f_{detect.}$ that equals the resonant frequency (f_{res}) of the cell. Such an interaction can mathematically be expressed as a product of the Fourier series F of both square waves: $S \propto F(f_{chop}) * F(f_{Stark})$. Taking into account only the first order coefficients, gives: $S \propto A + B_1 \cos(f_{chop}t) + B_2 \cos(f_{Stark}t) + C \cos[(f_{Stark} + f_{chop})t] + C \cos[(f_{Stark} - f_{chop})t]$, ($t$ = time). Using a narrow bandwidth (1 Hz) phase-sensitive detection at $f_{detect.}$ photoacoustic signals at the sum or difference frequency sidebands can be found. Performing the experiments in a resonant photoacoustic cell is advantageous over the use of a non-resonant one mainly because of the acoustic signal amplification at the cell's resonance frequency ($f_{res.cell}$) and the simultaneous suppression of the acoustic off-resonance signals (arising for example at f_{chop} and f_{Stark}) with respect to the resonance frequency.

The absorption of CO_2 laser radiation in the ambient air is considered to be the result of molecular processes involving H_2O, CO_2 and NH_3. Two of these gases, i.e. H_2O and NH_3, are polar molecules with large permanent dipole moments. Carbon dioxide, being a linear molecule, does not exhibit a permanent dipole moment and therefore the application of an electric field does not perturb its energy levels; CO_2 is said to be Stark inactive. As shown, in several of our previous experiments,[16,18] a Stark shift (at the laser frequencies chosen for detection of ammonia [10R(6) and 10R(8)] of the asymmetric top molecule H_2O in an external electric field was not observed employing essentially the same photoacoustic set-up as in this study. This implies that water, like CO_2, is Stark-inactive under the used experimental conditions. In the case of ammonia however [as shown in an experiment using the 10R(6) and 10R(8) CO_2 laser transitions and slow Stark modulation in a block wave form[16]] the absorption coefficient α of NH_3 at these two laser lines depends on the magnitude of an applied electric field. An alternating electric field gives rise to modulation of the absorption coefficient and, of the intensity of the laser radiation passing through the gas. The degree of modulation of the laser radiation and the Stark field is proportional to the NH_3 concentration. This physical phenomenon forms the basis for interference-free detection of ammonia in the ambient air. In the set-up described here, only small, spurious electric pick-up by the microphones, due to the application of the modulated Stark field (maximum field strength in this experiment was $E = 5 \, kV/cm$ at 200 mbar) at a frequency $f_{Stark} + f_{detect.}$ were detected in the phase-sensitive mode. The magnitude and the phase of this signal appeared to be constant and independent of the gas concentrations used. For proper ammonia concentration evaluation the spurious Stark signal was vectorially subtracted from the signal recorded by the employed single-phase lock-in amplifier. Optically inducing heating, caused by the absorption of the modulated CO_2 laser radiation, generates a photoacoustic signal at a frequency f_{chop} which is rejected by the lock-in amplifier since $f_{detect.} \gg f_{chop}$. Additional contributions to the signals due to spectral interferences (H_2O, CO_2), are totally suppressed when working in the sum- or difference frequency detection mode, leading to an almost noise-free photoacoustic signal. Through the proper choice of the laser modulation frequency kinetic cooling can be avoided fulfilling thereby the condition $f_{chop} \ll f_{kin.cool}$ (calculated figures are $f_{kin.cool} = 48 \, Hz$ for 0% R.H. H_2O, and $f_{kin.cool} = 1410 \, Hz$ for 50% R.H. H_2O).

As it will be shown in the combination of CO_2 laser Intermodulation Photoacoustic Stark Spectroscopy (IMPASS) is a novel, powerful tool for direct interference-free detection of ammonia in the (simulated) air down to the low ppbv-level, and forms an important step towards the completion of an automated, fast, on-line ammonia monitor suited for gas concentration measurements.

86

2. EXPERIMENTAL

The IMPASS study on ammonia was performed at the National Institute of Environmental Protection and Public Health (RIVM), in Bilthoven (The Netherlands), in a specially designed calibration room. The ambient atmosphere was accurately simulated by mixing water vapour, carbon dioxide, and nitrogen with ammonia at trace level concentration in a well controlled and reproducible manner followed by specificity tests for on-line detection of NH_3 present in a matrix of interfering gases. The generation of test atmospheres was based on the dynamic dilution of known amounts of different pollutants at a specified humidity level. Figure 1 presents a simplified scheme of the test gas generator. Compressed air is cooled down to $+2°C$ and the liquid water separated from the gas stream. A heatless dryer, consisting of two columns filled with a suitable adsorbent, purifies the air. The active columns filled with silica-gel retained H_2O, CO_2, NO_2, SO_2, O_3, mercaptanes and oxygenated hydrocarbons present in the ambient air. The purified air contains less than 40 ppm moisture (dew-point lower than $-50°C$), about 160 ppm CO_2 and the natural abundance of N_2, O_2, and rare gases. The amount of SO_2, NO_2, O_3, unsaturated hydrocarbons, oxygated hydrocarbons and mercaptanes after purification is negligible. An additional dust filter retained all particles with a diameter larger than $0.01\ \mu m$. The mass of the dried, purified air (zero air) is mixed with a known mass of water. The mass flow controller enables the water concentrations to be set anywhere within the 0% to 90% R.H. range at 20°C. (a water concentration of 50% R.H. at 20°C corresponds to the absolute water concentration of 1%; the conversion of R.H. to the absolute water concentration is a linear one). Trace constituents and the purified air were mixed in a static mixer. The "polluted" air of a well controlled, known composition is passed to the PA Stark cell via the teflon-PTFE-lined manifold. Throughout the experiments with the $NH_3/H_2O/CO_2/N_2$ mixtures the ammonia concentration in the manifold feedline (ranging from 0 to 360 ppbv) was maintained constant by means of permeation tubes.

2.1. The CO_2 laser Intermodulation Photoacoustic Stark Spectroscopy system (IMPASS)

The scheme of the intermodulated photoacoustic Stark set-up is schematically presented by Fig. 2. The photoacoustic signal was recorded (by a single phase lock-in amplifier) at either the sum $(f_{chop} + f_{Stark} = f_{detect.} = f_{res.cell})$ or difference $(f_{Stark} - f_{chop} = f_{detect.} = f_{res.cell})$ frequency side-band. The $^{12}C^{16}O_2$ cw waveguide laser is a home-made model of improved design. Through the inner tube a gas mixture (consisting of 65% He, 22% N_2 and 13% CO_2) is continuously flown through a 2.8 mm dia. and 40 cm long plasma tube to produce a constant working pressure (ranges from 50 to 65 mbar). The plasma tube is water cooled (15°C) to maintain a constant temperature of three
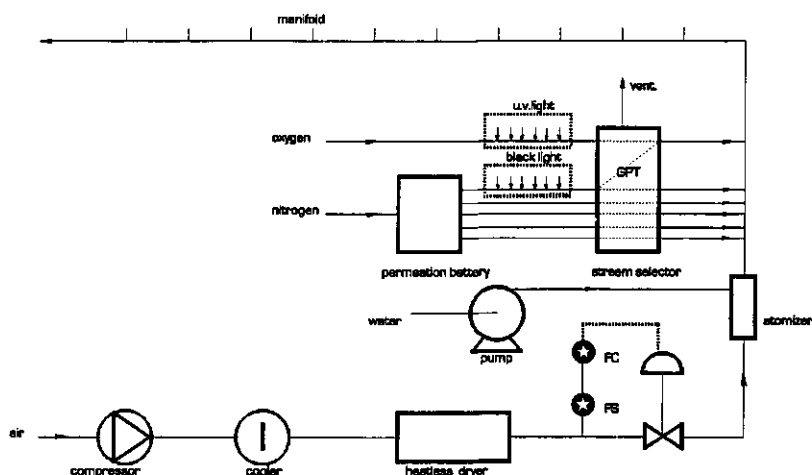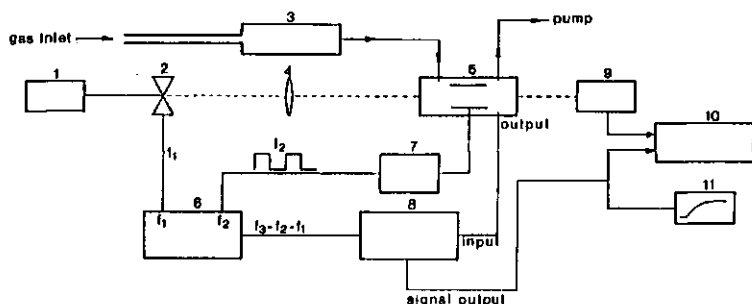

Fig. 1. The test gas generator.

Fig. 2. Block diagram of the IMPASS system. 1. cw CO_2 waveguide laser; 2. chopper; 3. critical capillary; 4. lens $f = 190$ mm; 5. PA resonant Stark cell; 6. phase-locked loop (FPhL); 7. Stark high voltage power supply; 8. lock-in amplifier; 9. power meter; 10. IBM-PC; 11. chart recorder.

tungsten pin-shaped electrodes. A PTR grating (150 lines/mm) was used for selective wavelength tuning. The grating was optimized for laser operation in the 10-μm bands (10P and 10R); the 10R band contains the strong 10R(6) and 10R(8) NH_3 absorption lines. The laser provided stable (long term stability better than 0.5%) output powers of about 2.5 W on the 10R(6) and some 3 W on the 10R(8) line over extended periods (more than 6 h) of continuous operation.

The Stark cell used in this experiment is of the resonant type, with a total active volume of 0.3 l. The housing of the cell was manufactured from aluminum (Alpase Aluplus). The photoacoustic sound wave is generated in a PTFE-teflon (polytetrafluorethylene) block of 10 cm length that serves as a longitudinal organ pipe resonator of length $l = \lambda/2$ corresponding to a second longitudinal frequency of 1608 Hz at STP. The teflon block is centered in the middle of the cell, fitting closely into the aluminum housing. The cell, designed for operation in the flow-through mode, is further equipped with two carefully designed baffles volumes on either side of the teflon block that accomodates three identical channels of 5.0 mm * 5.0 mm cross-section and 10 cm length. The cell is completed by two rectangular, polished aluminum plates (i.e. the Stark plates) separated by two teflon spacers. In each channel at the site of the pressure maximum a miniature Microtel M37 microphone (10 mV/Pa at 1608 Hz) with a flat signal response (1000–4000 Hz) is mounted flush with the inner wall of the top aluminum Stark plate. Only the middle channel is illuminated by the laser radiation. The microphones in the side channels (B and C) serve for averaging the noise signals (flow noise and electric pick-up by the microphones due to the application of the high voltage Stark modulation) prior to subtraction from the signal recorded by the microphone in the middle channel (A) as shown in Fig. 3. Assuming that the magnitude of the overall noise and electric pick-up due to the high voltage Stark field are equal in all three channels, the subtraction $[A_{micr} - (B_{micr} + C_{micr})/2 = A_{total}$ termed the total signal output; A_{micr}, B_{micr}, and C_{micr} are the respective magnitudes of the signals detected in the middle and the side-channels recorded by the M37 microphones) improved the S/N ratio after lock-in detection (with respect to the noise measured with A_{micr} only) by a factor 4. More important, the electric pick-up at the cell's output
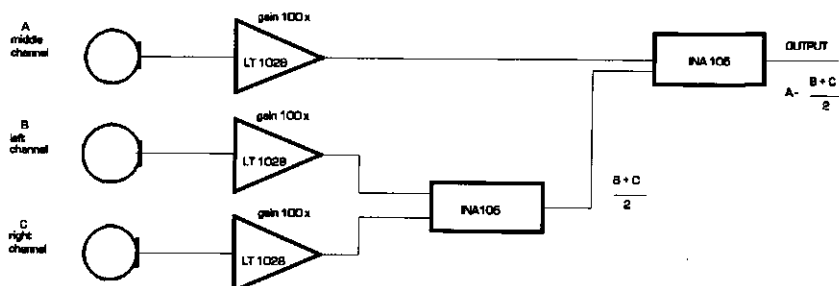

Fig. 3. Electronic preprocessing circuit. A, B, and C refer to the microphones in the Stark cell.

88

could be substantially suppressed allowing detection of the photoacoustic signal at a sensitive scale without overloading the input stage of the lock-in amplifier. In addition, the low Q-factor ($Q = 24$) made the cell rather insensitive to changes in gas temperature or small chopper frequency drifts (maximum shift 1 Hz at the resonance frequency) maintaining, however the advantage of an acoustical amplifier. A (calibrated range 10–1000 mbar) Motorola MPX-1000 sensor was mounted inside the cell for pressure control. A critical capillary inserted between the manifold and the gas inlet port of the Stark cell maintained a constant, calibrated gas flow (0.50 l/min) through the cell. With the capillary in place, pressure fluctuations were less than 0.1 mbar at a total pressure of 200 mbar. A suction pump of sufficient capacity connected to the gas outlet of the cell provided subatmospheric pressure (the pressure drop across the capillary should exceed 500 mbar in order to achieve the calibrated gas flow) necessary for proper working conditions of the capillary. A detailed description of this cell is given elsewhere.[17]

A high voltage Stark field (in the square block-wave form) was generated by a home-made power supply and modulator. Voltages between 0 and 2.5 kV (corresponding to electric field strengths of 0 to 5 kV/cm) could be selected by a 10-turn potentiometer. The high voltage was supplied to the bottom aluminum Stark plate; the upper plate carrying the microphones was grounded. A homemade 3 frequencies-phase-locked (FPhL) loop was used to drive simultaneously the chopper (f_{chop}) and the high voltage Stark power supply (f_{Stark}). The frequency phase-locked output ($f_{chop} + f_{Stark} = f_{res.cell}$ in the sum-mode; $f_{Stark} - f_{chop} = f_{res.cell}$ in the difference mode) was used as the reference frequency for phase sensitive detection (PAR 126 single phase lock-in amplifier). A lens ($f = 190$ mm), positioned at a distance ($v_d = 2f$) twice its focal length (i.e. 380 mm) from the output coupling mirror of the laser, directed the laser radiation through the middle channel without hitting the walls. Power saturation of the v_2 transition in NH_3 was avoided by this lens geometry resulting in an unitary mapping of the laser beam spot size in the middle of the cell ($v_d = b_d = 2f_{lens}$, magnification $|b_d/v_d| = 1$; b_d is the distance from the lens to the middle of the cell). The laser power was monitored by a power meter positioned behind the cell. A mechanical chopper modulating the CO_2 waveguide laser was positioned in front and as close as possible to the Stark cell. At this position the noise resulting from chopping the finite, slightly focussed laser beam was experimentally found to be at minimum. The generated photoacoustic signal was detected in the phase-sensitive mode by a PAR model 126 single-phase lock-in amplifier. The total signal output $A_{total} = A_{micr} - [(B_{micr} + C_{micr})/2]$ was fed into the lock-in's input channel. A bandpass filter, composed of a low-pass at 300 Hz and a high-pass filter at 10 kHz (both with a 3-dB roll-off) prefiltered the microphone signal, without affecting its magnitude, prior to phase-sensitive detection. Initially, 1 and 3 s lock-in integration times (RC-time) were selected. Due to electric transients longer integration times (up to 30 s) were used at a later stage in order to achieve a 3 ppbv detection limit for ammonia in a matrix of absorbing gases. A Hewlett-Packard 3421A 10-channel data acquisition/control unit, with a sampling frequency of 1 Hz per channel, was used for data acquisition. The output signal of the lock-in, the power meter and the pressure meter were acquired by this device and processed by an IBM-XT computer. A Kipp & Zonen flat bed two pens chart recorder was connected to the recorder output of the lock-in amplifier for visual signal control during the measurements. A calibrated Philips NH_3 gas monitor was connected (in parallel with the Stark cell) to the gas manifold. The admission of ammonia and its steady state concentration in the manifold was consistently controlled by this monitor. The instrument also served to compare mutually the IMPASS signals.

As explained in a previous article[18] the cell was operated at a subatmospheric pressure of about 200 mbar to narrow the molecular linewidth and to increase the ammonia Stark shift. Further, previous experiments showed[19] a maximum response of M37 Mircrotel microphone close to that pressure. Therefore, in all following experiments the pressure in the cell was kept constant at 200 mbar.

To test the specifity of the IMPASS system in detecting NH_3 in a mixture of other absorbing gases, high ammonia concentration (200 ppbv) was admitted together with the zero air into the cell. After reaching the steady-state concentration in the manifold (monitored by the Philips NO_x-analyzer), the IMPASS ammonia signal was recorded in the difference-frequency mode ($f_{Stark} - f_{chop} = f_{res.cell}$) as a function of different water vapour concentrations (10%, and from 50 to 90% R.H.). The laser was tuned to the 10R(6) NH_3 absorption line and chopped at a frequency

89

Table 1

H$_2$O concentration (R.H.),%	Signal = nV/W
10	40
50	390
60	412
70	471
80	517

Table 2

f_{Stark} (Hz)	f_{st} (Hz)	f_{chop} (Hz)	Signal = nV/W
1791	1608	183	40
1700	1608	92	100
1658	1608	50	181
1648	1608	40	205
1633	1608	25	210

50 ppbv NH$_3$, zero air. 10% R.H. H$_2$O; pressure 200 mbar; 10R(8) CO$_2$ laser line; IMPASS signal as function of laser modulation frequency f_{chop}.

of 183 Hz. The modulation frequency of the Stark HV power supply was fixed (to 1791 Hz); the calculated value of the electric field strength between the Stark plates was 4.3 kV/cm. The results, normalized to laser power, are listed in Table 1.

Although the recorded IMPASS signals are weak ($\approx 1.2 \mu$V for 200 ppbv NH$_3$ in the used gas mixture) two tests were performed to verify whether the recorded IMPASS signal was indeed due to the interaction between ammonia and the modulated laser and Stark field. At first decreasing gradually the Stark field led to the observance of quadratic dependence of the recorded signal on the applied electric field [at the 10R(6) line]. This evidence confirms the second order Stark splitting in ammonia predicted by theory [on the 10R(8) laser line a linear dependence of the signal on the applied field was found[20]]. Secondly, altering the admitted ammonia concentration was followed by the changes in the recorded photoacoustic IMPASS signals. Knowing that H$_2$O does not exhibit a measurable Stark effect under the conditions used, it was concluded that in this experiment the recorded signal originated from ammonia present in the simulated atmosphere. The large experimentally found noise atop the recorded signal is due to different acoustic and electric sources outside the set-up. The noise level of the air-conditioning system maintaining the temperature inside the calibration room at a constant temperature of 20°C was as high as 80 dB. Furthermore, the heating of the oven in the Phillips NH$_3$ ammonia monitor (to convert thermochemically NH$_3$ to NO$_x$) introduced spike-signals in the lock-in amplifier whenever engaging the temperature servo-system. The electric transients resulting from opening or closing the valve of the pump controlling the admission of water vapour had a similar deteriorating effect on the recorded photoacoustic signal. Finally, an impedance mismatch between the data logger and the lock-in amplifier caused a fast but small periodic decrease in the magnitude of the recorded IMPASS ammonia signal. To avoid these problems and to achieve a 3 ppbv ammonia detection sensitivity, at later stages of this study longer lock-in integration were used.

The quenching effect of water vapour on the relaxation of the exited N$_2$ becomes apparent at high concentrations (above 50% R.H.): the photoacoustic signal is constant, and independent of water vapour concentrations in the range from 50 to 80% R.H. Experiments have unambiguously proved[20] that the increase observed in the IMPASS NH$_3$ signals (as a function of increasing water vapour concentration) can be attributed to the alpase–aluplus aluminum–ammonia chemical interaction, rather than to admission of water vapour. The ammonia adsorbed on the walls of the feedline tubing and the cell is replaced by water molecules causing a release of the previously adsorbed ammonia that leads to a higher NH$_3$ concentration in the gas phase; this "memory effect" has been reported before.[21,22] The decrease observed in the magnitude of the recorded photoacoustic signal at 10% R.H. is a manifestation of the kinetic cooling effect occurring in the gas mixture used. Experimentally it appeared that at low water vapour concentrations the signals from carbon dioxide and ammonia contributing to the total additive photoacoustic signal were almost 180 degrees out of phase, resulting in a decrease of the total vector sum detected by the lock-in. A direct proof of this assumption was found by chopping the laser at half of the frequency ($f_{chop} = 92$ Hz; $f_{Stark} = 1700$ Hz) used in the previous experiment. An increase in the magnitude of the IMPASS ammonia signal was found confirming the above stated assumption.

Initially, an experimental attempt was made (in a low content water vapour environment) to find the laser chopping frequency below which the kinetic cooling effect vanishes. To do so the cell was filled with zero air (consisting of 160 ppmv CO$_2$, the natural abundances of N$_2$, O$_2$, and the rare gases), 50 ppbv NH$_3$ and water vapour at a constant concentration of 10% R.H. The photoacoustic

signal was recorded in the difference side-band mode ($f_{Stark} - f_{chop} = f_{res.cell}$) as a function of the laser chopping frequency; upon changing f_{chop} the difference frequency ($f_{Stark} - f_{chop}$) was automatically corrected in order to match the resonance frequency ($f_{res.cell}$) of the cell. The laser was tuned to the ammonia absorption frequency coinciding with the 10R(6) laser line and the results (normalized to laser power) are listed in Table 2.

The dependence of the photoacoustic signal on the laser modulation frequency is clearly seen. Below 40 Hz the IMPASS signal is not affected by the amount of water vapour present in the cell any longer providing the evidence that the kinetic cooling effect does not manifest itself below this frequency. Once determined, this modulation frequency was used consistently in all experiments. No accurate experimental study of the dependence of the kinetic cooling effect on the modulation frequency of the laser and the water vapour concentration could be performed due to the limited frequency operational range of the FPhL.

In a final phase of this experiment the performance in detection of ammonia of the conventional CO_2 laser photoacoustic (CLPAS) system using the simulated atmosphere was studied. In this mode of detection (without the Stark high voltage modulation) the laser was modulated by the chopper at a frequency corresponding to the resonance frequency of the cell (i.e. $f_{chop} = 1608$ Hz). Photoacoustic signals were recorded in the phase-sensitive mode using zero air, 50 ppbv NH_3, and a water vapour concentration varying from 10 to 90% R.H. Further experimental conditions were: 10R(6) CO_2 laser line, cell's pressure 200 mbar, lock-in integration time 3 s, and a gas flow 0.50 l/min. The normalized signals, calculated from this experiment, are listed in Table 3. In the CLPAS-mode, the decrease of the magnitude and the phase shifts of the photoacoustic signal as a function of increasing water vapour concentration are worth mentioning. Apparently, when employing high laser modulation frequencies the total vector sum representing the contribution of all the individual gases is at a minimum for water concentrations close to 50% R.H., and increases only slightly for water vapour concentrations exceeding 50% R.H.

The same signal behaviour was found when using only zero air and a varying concentration of water vapour (no NH_3 was admitted). In Table 3 the normalized photoacoustic signals recorded at the strongest H_2O adsorption line [10R(20)] are given too.

For comparison purposes the H_2O absorption at this line [10R(20)] was also measured in the IMPASS difference mode using a water vapour concentration of 70% R.H. and zero air (no ammonia was admitted). Further experimental conditions were: $f_{chop} = 40$ Hz, $f_{Stark} = 1648$ Hz, $E_{Stark} = 4.3$ kV/cm, and a cell pressure of 200 mbar. After several repetitive measurements the largest signal found was approximately 17 nV/W, indicating the potential of the IMPASS system in the suppression of water vapour and carbon dioxide adsorption at CO_2 laser frequencies. It is believed however that this signal is more likely due to the noisy surrounding in which the experiments were performed, rather than to that of water vapour absorption itself. The experiments, performed in the CLPAS-mode (Table 3) confirm the influence of the laser modulation frequency on the molecular relaxation processes (kinetic cooling) in CO_2–N_2 gas mixtures and the quenching capacity of water vapour (no drastic phase change above 50% R.H.). Further, the CLPAS-experiments illustrate clearly the necessity for knowing precisely the physical parameters involved in the kinetic cooling process whenever employing

Table 3

CLPAS-mode	H_2O concentration (R.H.), %	Signal = μV/W	Phase
10R(8)	40	1.0	312
50 ppbv	50	0.64	10
NH_3	60	0.68	31
	70	1.75	47
10R(20)	0	5.0	253
0 ppbv NH_3	10	7.0	79
200 mbar	20	16.5	80
	30	26.0	83
	40	37.0	80
	50	52.0	81
	60	80.0	81
	70	145.0	85

91

a classical photoacoustic system as a trace gas detector. From the figures given in Table 3 (i.e. the normalized photoacoustic signal) the ammonia concentration cannot be derived directly without additional spectral information (to be obtained from measurements at different laser lines). This limitation is a severe drawback when attempting to construct an on-line gas monitor.

3. CONCLUSION

In this article the potential of a CO_2 laser IMPASS system in the on-line detection of NH_3 trace levels, present in a matrix of absorbing gases, has been demonstrated. Complete suppression of absorption signals due to the interfering gases H_2O and CO_2 and window noise has been achieved without deteriorating the detected 3 ppbv NH_3 IMPASS signal (in the flowing mode). The ultimate detection sensitivity can further be improved by employing a more powerful laser and by developing another photoacoustic cell for which a direct contact between the Stark plates and the gas is avoided. Since the recorded IMPASS signal, at the 10R(6) laser line depends quadratically on the magnitude of the electric field, the application of higher electric field strengths might lead to a NH_3 detection limit below the ppbv level for realistic air samples. As far as the interpretation of signal (in the IMPASS mode the recorded lock-in signal is directly proportional to the ammonia concentration present) is considered, the conventional beam chopped CO_2 laser photoacoustic spectroscopy is clearly inferior to the presented detection scheme at low NH_3 concentration levels. Although at the time of writing this report the problem of ammonia adsorption to the cell walls has not been adequately solved yet, the authors believe that this problem might eventually be surmounted by utilizing other materials and a small volume photoacoustic cell (few cm^3) of a special geometrical design. Work on this matter is already in progress.

REFERENCES

1. A. van Pul, Ph.D. thesis, Agricultural Univ. Wageningen (1991).
2. B. van Hove, Ph.D. thesis, Agricultural Univ. Wageningen (1989).
3. T. L. Vossler, R. K. Stevens, R. J. Paur, R. E. Baumgardner and J. P. Bell, *Atm. Environ.* 22, 1729 (1988).
4. A. M. Winer, *Environ. Sci. Tech.* 8, 1118 (1974).
5. D. W. Joseph and C. W. Spicer, *Analyt. Chem.* 50, 1400, (1978).
6. U. Platt, D. Perner and H. W. Pätz, *J. Geophys. Res.* 84, 10 (1979).
7. H. I. Schiff and G. I. MacKay, in *Monitoring of Gaseous Pollutants by Tunable Diode Lasers* (Edited by R. Grisar *et al.*). Kluwer Academic, Dordrecht (1989).
8. L. B. Kreuzer, *J. appl. Phys.* 42, 2937 (1971).
9. J. Hinderling, M. W. Sigrist and F. K. Kneubühl, *Int. J. infrared Phys. millimeter Waves* 7, 683 (1986).
10. L. S. Rothman, R. R. Gamache, A. Barbe, A. Goldman, J. R. Gillis, L. R. Brown, R. A. Toth, J.-M. Flaud and C. Camy-Peyret, *Appl. Opt.* 26, 4058 (1987).
11. A. D. Wood, M. Camac and E. T. Gerry, *Appl. Opt.* 10, 1877 (1971).
12. A. Olaffson, M. Hammerich, J. Bülow and J. Henningsen, *Appl. Phys. B* 49, 91 (1989).
13. A. Olaffson, M. Hammerich and J. Henningsen, *Springer Series in Optical Sciences* (Edited by J. C. Murphy *et al.*) Vol. 62 (1989).
14. R. A. Rooth, A. J. L. Verhage and L. M. Wouters, *Appl. Opt.* 29, 3643 (1990).
15. J. Reijnders, Ph.D. thesis, Catholic Univ. Nijmegen (1978).
16. H. Sauren, D. Bićanić, H. Jalink and J. Reuss, *J. appl. Phys.* 66, 5085 (1989).
17. H. Sauren, D. Bićanić, W. Hillen, H. Jalink, K. van Asselt, J. Quist and J. Reuss, *Appl. Opt.* 29, 2679 (1990).
18. H. Sauren, T. Regts, K. van Asselt and D. Bićanić, *Environ. Tech. Lett.* (1991). In press.
19. A. Miklós, H. Sauren and D. Bićanić, *Meas. Sci. Techn.* (1991). In press.
20. H. Sauren, D. Bićanić, *Appl. Spectrosc.* To be published.
21. B. van Hove, W. Tonk, G. Pieters, E. Adema and W. Vredenberg, *Atm. Environ.* 22, 2515 (1988).
22. H. Sauren, B. van Hove, W. Tonk, H. Jalink and D. Bićanić, in *Monitoring of Gaseous Pollutants by Tunable Diode Lasers* (Edited by R. Grisar *et al.*). Kluwer Academic, Dordrecht (1989).

4.4 IN SITU INTERMODULATION PHOTOACOUSTIC STARK SPECTROSCOPY FOR THE CONTINUOUS DETERMINATION OF GASEOUS AMMONIA CONCENTRATIONS IN THE ATMOSPHERE

Hans Sauren, Edo Gerkema, and Dane Bićanić

Laser Photoacoustic Laboratory
Department of Agricultural Engineering & Physics
Agricultural University
Duivendaal 1
NL-6701 Wageningen
The Netherlands

Abstract-A concept of Intermodulated Photoacoustic Stark Spectroscopy (IMPASS) was used in an attempt to perform the interference-free field measurement of trace ammonia concentration levels in the air.

INTRODUCTION

The spatial distribution of gaseous ammonia (NH_3) in the lower atmosphere is a critical parameter in understanding the role and significance of this species in chemical reactions and the environmental acidification problem. The difficulties, associated with detection of NH_3 concentration levels in the 0.1-10 ppbv (Ferm 1979, Abbas and Tanner 1981) when using dry and wet chemical techniques, have stimulated the development of an ammonia sensor solely based on principles of optical detection. One of these, the CO_2 laser photoacoustic spectroscopy, has attracted considerable attention from the scientific community ever since McClenney and Bennet (1979) and McClenney *et al.* (1980) achieved respectable NH_3 detection levels in the air. Following this initial success, several attempts have been made during the last decade to develop a photoacoustic monitor suited for direct and in-situ detection of atmospheric ammonia (Meyer and Sigrist 1988, Rooth *et al.* 1990, Olafsson 1990, Sauren *et al.* 1989, Sauren and Bićanić 1991). The research towards the development of potential optical NH_3 monitoring techniques has been particularly intensive in the Netherlands, as the deposition is found the highest among the West-European countries (Asman 1987, van Hove 1989, Erisman *et al.* 1989). The control of ammonia emission rates by means of a reliable instrument has therefore become a necessity. So far, none of the photoacoustic sensors reported in the literature has met all the requirements imposed by the air pollution practice.

Spectral interferences in the CO_2 laser emission region (9-11 μm), resulting from the absorption of atmospheric water vapor (H_2O) and carbon dioxide (CO_2) (Hinderling *et al.*1986, Rothman *et al.*1987), as well as the kinetic cooling effect (Wood *et al.*1971) impede the direct and on-line detection of ammonia trace levels when working in the traditional photoacoustic detection mode. However, CO_2 laser photoacoustic spectroscopy combined with Stark modulation and frequency mixing (InterModulated PhotoAcoustic Stark Spectroscopy, abbreviated IMPASS) has recently proved to be a technique with potential to surmount most of the difficulties stated above (Sauren *et al.* 1991a,b). In this paper we report on the first direct, in-situ field measurements of ammonia at trace levels applying the improved (IMPASS) CO_2 laser photoacoustic design.

EXPERIMENTAL

The constructional details of the photoacoustic set-up used in this study (IMPASS) have been described extensively in a number of recently published articles (Sauren *et al.*1989, Sauren *et al.* 1991a,b Sauren and Bićanić). Fig.4.4.1 gives a schematic view of the IMPASS detection set-up. It makes use of a modulated (high voltage) electric field to shift the absorption line of the ammonia molecule into resonance with the chosen transition (10R(6) and 10R(8)) of the CO_2 waveguide laser. It was shown experimentally that the major atmospheric constituents (i.e. H_2O and CO_2) do not exhibit a Stark effect under the given experimental conditions used. Therefore, when working in the IMPASS detection mode, a photoacoustic signal can only be generated by those molecules (to the best of the authors knowledge no molecule, except ammonia, is known to exhibit both a large Stark effect and large CO_2 laser radiation absorption at the laser lines used) interacting constructively with both, the modulated laser radiation and the Stark electric fields.
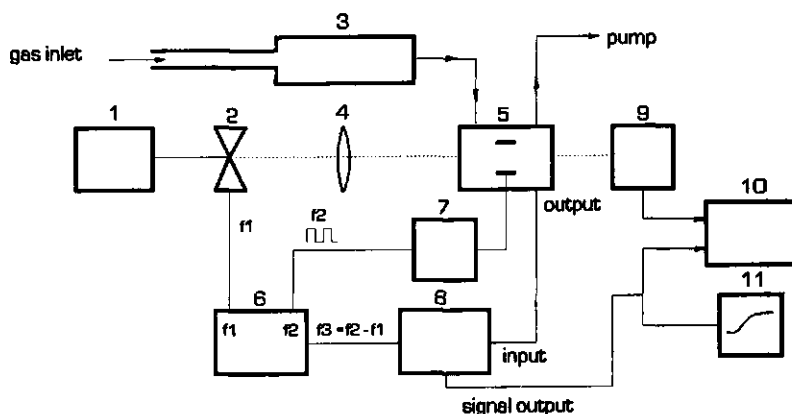

Fig.4.4.1 The intermodulated photoacoustic Stark spectroscopy apparatus used in this study

The radiation of a $^{12}C^{16}O_2$ waveguide laser (1) was mechanically chopped (2) at a frequency $f_{chop}=40$ Hz and directed unobstructively through the resonant photoacoustic Stark cell (5) (resonance frequency $f_{res.cell}=1608$ Hz) by a ZnSe lens (4) (f=190 mm). The cell was used in the flow-through mode (gas flow 500 ml/min) by inserting a calibrated glass-made critical capillary (3) (Euroglass) in the PTFE teflon gas feedline. A suction pump of sufficient capacity was used to ensure the sub-atmospheric pressure drop along the capillary necessary to maintain the calibrated gas flow during the course of the experiment. In order to reduce the undesired effects caused by adsorption of ammonia to the walls, anodized Alpase-aluplus aluminum and PTFE teflon were used as construction materials for the cell. The cell, with a total active volume of 300 ml, incorporated two separated (5 mm) Stark plates, three miniature M37 microphones (Microtel Amsterdam) and a calibrated (10-1000 mbar) miniature Motorola pressure sensor.

The Stark field (used in the positive block-wave form, i.e. here $f_{Stark}=1648$ Hz) was generated by a home-made power supply and a modulator (7). Applied electric field strengths ranged from 0 to 6 kV/cm. The high voltage was supplied to the bottom aluminum Stark plate; the upper plate carrying the microphones was grounded. A specially designed phase-locked loop (PLL) (6) was used to simultaneously drive the chopper (at a frequency f_{chop}) and the high voltage power supply (at a frequency f_{Stark}). The third frequency (f_{det}) was used as a reference frequency for phase-sensitive detection and was kept equal to the resonance frequency of the cell ($f_{det}=f_{res}$) during the experiment. The interaction between the gas sample flown through the cell and the two modulated electric fields (i.e. the CO_2 waveguide laser at frequency f_{chop} and the Stark field at frequency f_{Stark}) generates photoacoustic signals at the sum ($f_{chop}+f_{Stark}=f_{res}=f_{det}$) and difference ($f_{Stark}-f_{chop}=f_{res}=f_{det}$) frequency (and their respective harmonics) sidebands. The microphone signal and the reference frequency were fed into an Ithaco 3961-A two phase lock-in amplifier (8) that converted the photoacoustic signal into a d.c. voltage, which in turn is proportional to the ammonia concentration. During the entire course of this study a lock-in integration time of 10 sec (RC-time) was used.

Using phase-sensitive detection at a frequency $f_{res}=f_{det} \neq f_{Stark} \neq f_{chop}$ spurious photoacoustic signals appearing at either the laser modulation frequency f_{chop} (e.g. the absorption due to H_2O and CO_2, ambient noise and cell window noise) or at the modulation frequency of the Stark field f_{Stark} (pick-up of the electric field by the microphones) were effectively suppressed by the lock-in amplifier, resulting in a photoacoustic signal solely due to ammonia. The relevant data in the IMPASS measurements were acquired by a Hewlett and Packard 3421 A data logger (10) and processed by an IBM-PC/XT (11).

RESULTS AND DISCUSSION

The $^{12}C^{16}O_2$ waveguide laser, mechanically chopped at a frequency of 40 Hz, was tuned to the 10R(6) ammonia absorption line at 10.346 μm. The high voltage unit was driven by the modulator at 1648 Hz, while the detection frequency (f_{det}) of the Ithaco two-phase lock-in amplifier was set to the cell's longitudinal resonance (f_{res}) at 1608 Hz. Detection of the photoacoustic signal was performed at the generated difference frequency sideband ($f_{res}=f_{Stark}-f_{chop}=f_{det}$). Since the discharge voltage between the Stark plates depends on the

water vapor content of the gas sample as well as on the pressure in the cell, arcing was avoided using electric field strengths not exceeding 4.6 kV/cm. The resonant photoacoustic cell was operated at a reduced pressure of 200 mbar. Experimentally it was proved that at this working pressure the signal to noise ratio of the photoacoustic signal was at the optimum. Prior to the experiments described in this study the IMPASS set-up was calibrated in the laboratory using the homogeneous mixture of ammonia in a closely simulated atmosphere (Sauren *et al.*1991a). Further, a comparison measurement performed in the lab between the IMPASS system and a NO_x-monitor (equipped with a catalytic converter) showed mutually satisfactory agreement in recorded NH_3 concentration levels.

Sampling was performed 0.5 m above ground level at the site of the department of Physics of the Agricultural University during March and April 1991. The IMPASS set-up was operated 'stand-alone' during working hours from 8.00 am till 6.00 pm. Ambient air was drawn (at a flow rate of 500 ml/min) through a 4 meter long PTFE-telfon tubing prior to being admitted into the photoacoustic cell. The magnitude of the photoacoustic signal S, and its phase ϕ, the laser power P, the cell's operating pressure P_{pres} and the Stark high voltage V were all consecutively processed by the IBM-computer. The time needed to complete a single measuring cycle of all 5 parameters was about 8 sec. After five cycles the average and the standard deviations of the above parameters S, ϕ, P, P_{pres}, and V, were calculated by the computer and the mean values were stored. Deviations in the laser output power P, the pressure P_{pres} in the cell and the magnitude of the applied Stark voltage were less than 0.5%. The standard deviation of the photoacoustic signal magnitude and its phase was around 7%. Fig.4.4.2 presents half-hourly mean NH_3 concentration levels (measured in March 1991 during working hours) calculated from the above 40 sec values.
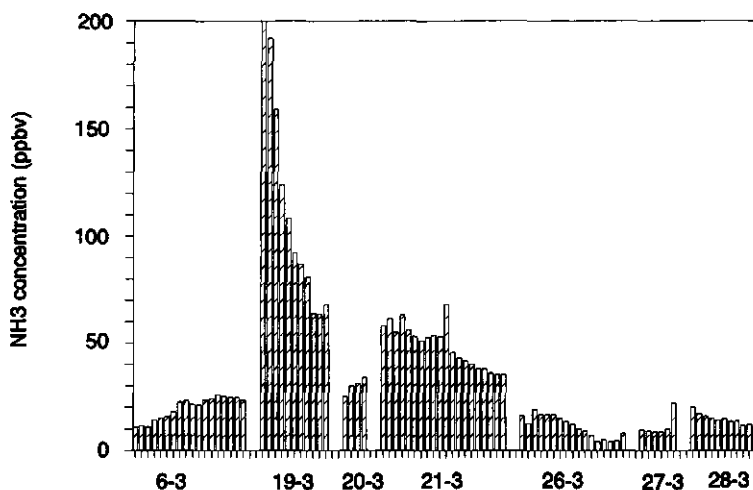

Fig.4.4.2 IMPASS ambient ammonia concentration levels recorded in March 1991. Figure represents half-hourly averages

96

Fig.4.4.2 shows that ammonia levels were generally below 30 ppbv except those measured on March 19 and March 21. However, Fig.4.4.2 does not reveal the IMPASS system's real-time response as the shown values represent the half-hourly mean averages.

Ammonia concentration level slightly higher than the typical background concentration in The Netherlands (10 ppbv) might be anticipated from Fig.4.4.2.

As the output power of the laser (at the 10R(6) line) during the course of this study dropped below 1 Watt, the next suitable and Stark tunable ammonia absorption line (10R(8) at 10.331 μm) exhibiting higher output power and better long term stability, was selected and used consequently.

Fig.4.4.3 displays ammonia concentration levels (sampled at the same location as in the foregoing measurement) recorded (with the CO_2 laser tuned to the 10R(8) ammonia absorption line) during the first week of April 1991 on days when the relative humidity was low (60% R.H. or less).
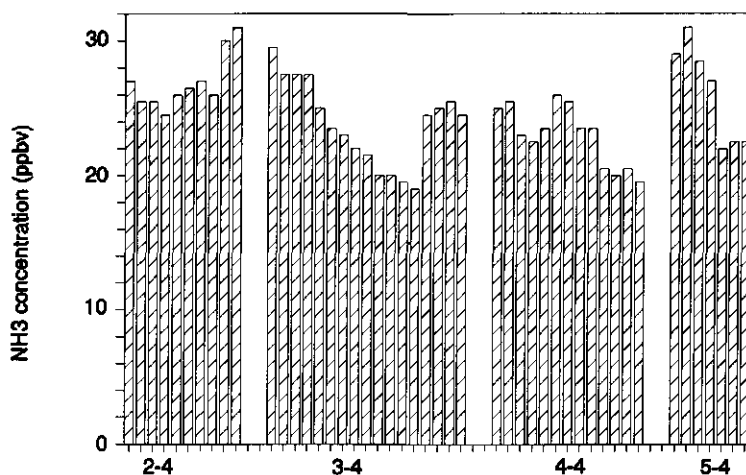

Fig.4.4.3 Ambient ammonia concentration levels recorded in April 1991. Figure represents half-hourly averages.

In order to enhance the S/N-ratio, the magnitude of the photoacoustic signal was increased by applying an electric field strength of 6 kV/cm. This was possible as neither arcing nor electric breakdown between the Stark plates were observed. Presumably, the discharge voltage between the Stark plates can be related to the amount of water vapor present in the gas sample. As the sampled air between the Stark plates resembles a dielectric of a capacitor, varying water vapor content affects the maximum voltage value that can be applied without causing an electric breakdown. A NH_3 concentration pattern similarly varying as in the case

with the CO_2 laser tuned to the 10R(6) line is found.

In order to study the daily variation in more detail, ammonia concentrations using the 40 sec mean values are depicted in the figures 4.4.4-4.4.6.

In Fig.4.4.4 (recorded on Wednesday March 5, 1991) large NH_3 concentration fluctuations can be seen.
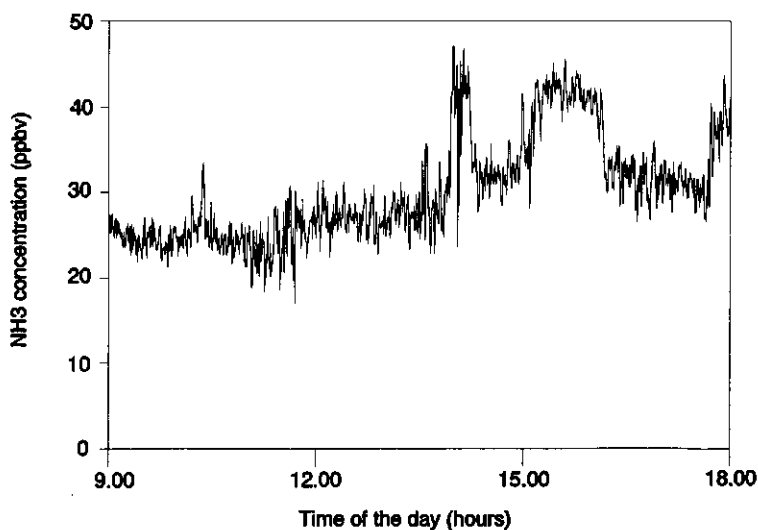

Fig.4.4.4 Ambient ammonia concentration levels recorded on March 5, 1991

Interesting variations in the ambient ammonia concentration were also found on Wednesday March 19 (Fig.4.4.5), and Friday March 21 (Fig.4.4.6). Fluctuations in the NH_3 concentration were generally small during the day (a typical example is presented in Fig.4.4.7). It is a well known fact that the ambient temperature, water vapor concentration and wind direction affect the ambient ammonia concentration. Specially rainfall seems to have a large impact, ranging from the production of ammonia from dry soils to scavenging of large amounts of ammonia from the air. It must be emphasized that in presented study no correlation between the ambient temperature, absolute water vapor concentration and wind direction, and the observed ammonia concentration pattern was performed as no meteorological recordings were available.
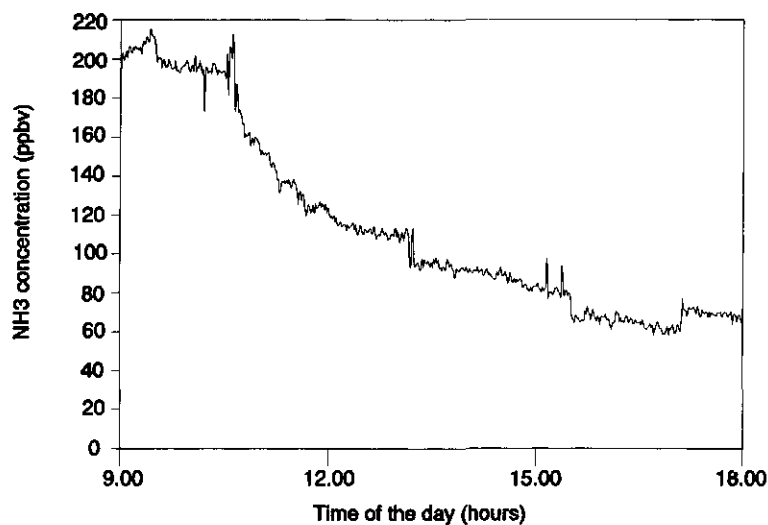
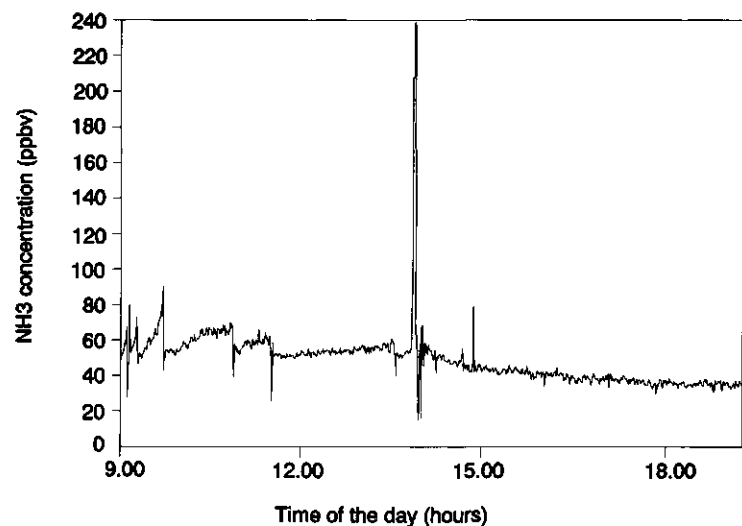**Fig.4.4.5** Ambient ammonia concentration recorded on March 19, 1991

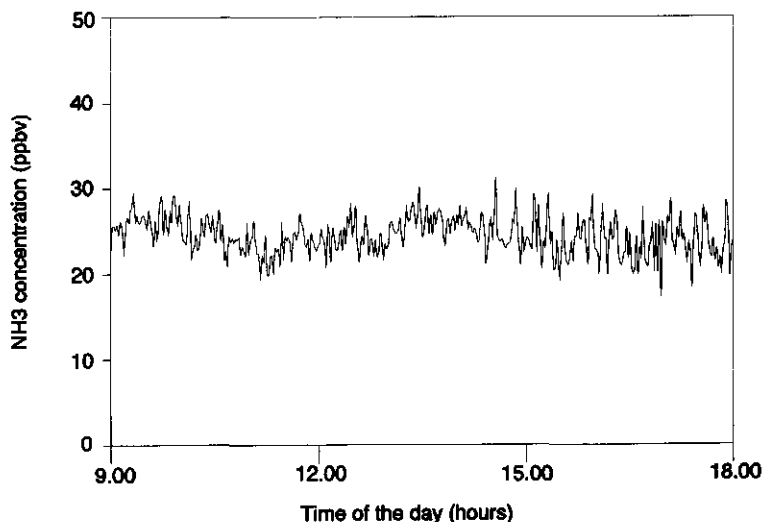**Fig.4.4.6** Ambient ammonia concentration recorded on March 21, 1991

Fig.4.4.7 Ambient ammonia concentration recorded on April 4, 1991

CONCLUSIONS

Intermodulated photoacoustic Stark spectroscopy (IMPASS) was demonstrated a versatile technique for measuring ambient ammonia levels in the 3-200 ppbv concentration range. A distinct feature of the IMPASS system (when compared to conventional optical and chemical techniques) is its capability to determine NH_3 levels with a time resolution (or transit time, i.e. the minimal time scale on which fluctuations in the ammonia concentration can be detected) of 40 sec. The notorious adsorptive behaviour of ammonia limiting the response-time of the present Stark cell might be substantially improved by using a specially designed, small volume (few ml) photoacoustic cell entirely constructed from high quality glass. At present, the detection limit achieved (2-3ppbv NH_3) can, presumably, be improved by increasing both the output power, as well as the applied Stark high voltage. Work on this matter is currently under study.

A pronounced advantage of the IMPASS-technique is the combination of Stark modulation and CO_2 laser photoacoustic spectroscopy, which enables drastic reduction of possible (gaseous) interfering components, a fact that, at present poses a tedious task to chemical and optical NH_3 detection techniques employed in the practice. As ammonia is Stark-tunable on both the 10R(6) and 10R(8) CO_2 laser lines, the occurrence at trace levels of an interfering component exhibiting large CO_2 laser absorption cross-section and induced

100

Stark effect can be overcome by monitoring ammonia at the non-interfering laser line.

In order to correlate and to interpretate the fluctuations in the ammonia concentrations obtained with this technique, it is necessary to consider meteorological parameters as absolute water vapor concentration, temperature, windspeed and wind direction.

The ambient water vapor concentration in particular is important when tracking ammonia since, various reports suggest that the ammonia concentration is found to decrease at increasing water vapor concentration (Loper *et al.* 1986). The effect of water vapor concentration on the ambient ammonia concentration can be studied by a Lyman-α water vapor sensor. Work on this matter is already in progress.

ACKNOWLEDGEMENT

REFERENCES

Abbas R. and Tanner R.L.(1981) Continuous determination of gaseous ammonia in the ambient atmosphere using fluorescence derivatization. *Atmospheric Environment* **15**, 277-281.

Asman W.A.H.(1987) Atmospheric behaviour of ammonia and ammonium. Ph.D. thesis Wageningen Agricultural University The Netherlands ISN 299632.

Erisman J.W., De Leeuw F.A.A.M. and van Aalst R.M.(1989). Deposition of the most acidifying components in The Netherlands during the period 1980-1986. *Atmospheric Environment* **23**, 1051-1062.

Ferm M.(1979). Method for determination of atmospheric ammonia *Atmospheric Environment* **13**, 1358-1393.

Hinderling J., Sigrist M.W. and Kneubuhl F.K.(1986). Field laboratory experiments on the 8 to 14 μm spectral window of the terrestrial atmosphere *Int.J.Infrared Phys. Millimeter Waves* **7**, 683-713.

Hove L.W.A.van(1989). The mechanism of NH_3 and SO_2 uptake by leaves and its physiological effects. Ph.D. thesis Wageningen Agricultural University The Netherlands.

Loper G., Gelbwachs J. and Beck S.(1986). Progressive Report FY 1985/1986 Aerospace Cooperation, El Segundo, CA, USA.

McClenney W.A. and Bennett C.A.Jr.(1980). Integrative technique for detection of atmospheric ammonia. *Atmospheric Environment* **14**, 641-645.

McClenney W.A., Bennett C.A.Jr., Russwurm G.M. and Richmond R.(1979). Optoacoustic cell design for trace gas analysis using a Helmholtz Resonator. Proc. Topical Meeting of Photoacoustic Spectroscopy, 1-3 August, WB11P 1-4.

Meyer P.L. and Sigrist M.W.(1988) Air-pollution monitoring with mobile CO_2-laser photoacoustic system. PhD-thesis 8651 ETH Zurich Switzerland.

Olafsson A.(1990). Photoacoustic molecular spectroscopy with tunable waveguide CO_2 lasers. Ph.D. thesis H.C.Ørsted Institute University of Copenhagen ISSN 0906-0286.

Rooth R.A., Verhage A.J.L. and Wouters L.W.(1990). Photoacoustic measurement of ammonia in the atmosphere: influence of water vapor and carbon dioxide. *Appl.Opt.***29**, 3643-3652.

L.S.Rothman *et al.*(1987). The HITRAN Data Base: 1986 edition *Appl.Opt.***26**, 4058-4097.

Sauren H., Bićanić D., Jalink H. and Reuss J.(1989). High-sensitivity, interference-free, Stark-tuned CO_2 laser photoacoustic sensing of urban ammonia. *J.Appl.Phys.***66**, 5085-5087.

Sauren H., Bićanić D., Hillen W., Jalink H., van Asselt K., Quist J. and Reuss J.(1990). Resonant Stark spectrophone as an enhanced trace level ammonia concentration detector: design and performance at CO_2 laser frequencies. *Appl.Opt.***29**, 2679-2681.

Sauren H., Regts T., van Asselt K. and Bićanić D.(1991a). Simplifying the laser photoacoustic trace detection of ammonia by effective suppression of water vapor and carbon dioxide as the major absorbing atmospheric constituents. *Environmental Technology* **12**, 719-724.

Sauren H., Bićanić D. and van Asselt K.(1991b). Enhanced specificity in sensing of gaseous ammonia at trace levels by the optoacoustic detection at the sum and difference sidebands of the modulating laser and Stark electric fields. *J.Infrared Phys.*,**31**, 475-484.

Sauren H. and Bićanić D.(1991). Photoacoustic detection of ammonia in a simulated atmosphere of varying water vapor content. *Analytical Instrumentation* (1991) in press.

Wood A.D., Camac M. and Gerry E.T.(1971). Effects of 10.6 μm laser induced air chemistry on the atmospheric refractive index *Appl.Opt.***10**, 1877-1884.

Chapter 5   Closing Remarks

Although a considerable amount of theoretical and experimental work has been carried out, the possibilities for improving the overall performance are not exhausted yet. Future experiments can benefit from the improvements summarized below.

1)
The important feature of any laser is the degree of its power and frequency stabilization. The laser used in this experiment was run in an unstabilized, "free-running" mode. In a future design frequency stabilization will be achieved by means of the photoacoustic signal generated in an isolated photoacoustic cell containing pure ammonia at low pressure (0.1 Torr or less). The laser is initially tuned to the molecular absorption frequency of interest. The photoacoustic signal generated in the low-pressure cell is fed into a feed-back loop and the laser stabilized using a first derivative technique.
Power stability of the laser can be improved by stabilizing the current of the laser high voltage power supply using the optogalvanic effect[1].

2)
The measurements described in Chapter 3 have shown that the choice of material for construction of the photoacoustic Stark cell is of crucial importance in minimizing the adsorption of ammonia to the cell walls. The experiments performed with the Stark cell composed of components manufactured from aluminum and PTFE-teflon, indicated pronounced affinity of these materials for adsorption of ammonia. For this reason it is worthy trying to develop a resonant photoacoustic Stark cell constructed from high quality glass. Choosing a cell geometry that prevents the Stark plates from coming into actual contact with the gas, might help to reduce the adsorption. Likewise, mounting the microphone farther away from the Stark plates is thought to be effective in reducing electric pick-up and stray-radiation.
The location of the gas inlet and outlet ports with regard to the standing acoustic wave (as well as their geometrical shape) is assumed to be of major importance in reducing the noise due to the gas flow. The use of cone-shaped gas ports (with the larger opening facing the cell) might prove superior to the currently used right-angle shaped ports.
A more sensitive microphone (presently 10 mV/Pa at STP) will allow the reduction of the total working pressure in the cell to values below 0.1 Torr. In this pressure regime higher electric field strengths are achievable without transient sparking or electric discharges. This in turn leads to a higher probability for enhancing the spectral overlap between the laser emission frequency and the absorption frequency of Stark tuned ammonia. It should be experimentally verified whether or not a decrease in the amount of absorbing molecules will be compensated by the availability of higher electric fields and increased spectral coincidence.

3)
Lock-in amplifiers are sensitive to very low frequency noise (1-10 Hz) that deteriorates the measured photoacoustic signal. Incoherent noise in this frequency range

mainly arises from transients such as ambient traffic, slamming of doors etc. A solution to this problem is a personal computer (interfaced with an electronic memory buffer) used as a high speed sampling device. Knowing exactly the frequency of the generated photoacoustic sound wave, the microphone signal is sampled (sampling period 2^6 or 2^7 times the sound wave frequency) and accordingly digitized using high-speed analogue-digital converters before being transmitted to an electronic buffer. From a buffer the digitized signal is then transferred to the computer and processed employing FFT (Fast Fourier Transform) algorithms. Longer sampling period and the process averaging interval increases the S/N-ratio proportional to the square root of the number of sampling runs.

4)

In the infrared region around 10 μm the ammonia molecule exhibits 14 absorption lines with absorption coefficients α larger than 1.0 atm^{-1}cm^{-1}. Enhancement of the spectral overlap between the $^{12}CO_2$ waveguide laser and the Stark tuned ammonia absorption lines might be anticipated when using absorption lines that are in near coincidence with the CO_2 laser at zero-field. Application of low electric field strengths leads then to a substantial improvement in spectral overlap. For this purpose the sa9R(30) | J=5,K=5,M> NH_3 absorption multiplet located near 1084.63 cm^{-1} appears most interesting.

5)

As stated in Chapter 1 the photoacoustic signal S and hence the IMPASS signal depend linearly on the laser output power P_{laser} (at present the maximum available output power at the 10R(8) CO_2 laser NH_3 line is about 3 Watts) and the amount of absorbing molecules C (fractional concentration). Consequently, increasing the laser power P_{laser} leads to a larger photoacoustic signal S and therefore to an improved value for the minimum detectable concentration C_{min}.

Higher detection limits can be achieved by either positioning the photoacoustic cell inside the laser cavity (intracavity set-up), or combining the present IMPASS set-up with boosted laser power.

In CO_2 laser intracavity arrangement typical laser power may reach 30-70 Watt[2]. However, at these power levels saturation might occur in which case the generated photoacoustic signal S no longer increases linearly with laser power P_{laser}. For intracavity experiments this causes a need for determining the threshold value of the laser power at which saturation occurs. This can be achieved by using appropriate optical laser beam attenuator and subsequent measurement of the signal S as a function of the laser power P.

An alternative is to use a more powerful laser (laser power should exceed the present power levels of the used CO_2 waveguide laser, i.e. about 3 Watts at 10R(8) laser line and some 2.5 Watts at 10R(6) transition) combined with the present extra-cavity IMPASS set-up. Higher output powers can be achieved by employing a CO_2 laser amplifier inserted between the CO_2 waveguide laser and the Stark cell. The amplifier is nothing but a second CO_2 laser pumped by the waveguide laser. The amplifier consists of a laser tube filled with the same gas medium and is terminated by ZnSe windows. This technique appears quite promising as demonstrated by the Nijmegen group (a 3-5 times higher total output power).

6)

The present IMPASS monitor lacks an active frequency tracking system capable of simultaneously controlling the chopper speed and the Stark high voltage modulation so that the sum or difference of both frequencies always matches the instantaneous resonant

frequency of the photoacoustic Stark cell. This latter is mainly dependent on the operating temperature.

The $^{12}C^{16}O_2$ laser photoacoustic spectroscopy, the Stark effect, and the intermodulation technique were combined to demonstrate the feasibility of such an approach in real time tracking of ambient ammonia. At present the monitor's sensitivity is about 2 ppbv. This encouraging result suggests further pursuing a development of this method. Since the entire photoacoustic monitor has not reached its final stage of development yet, the ultimate detection sensitivity and signal response time cannot be estimated at present. Nevertheless, further optimization (material choice and cell design) will most likely push the currently achieved limits.

The construction, and testing of the PA NH_3 monitor described in this thesis may be regarded as an important step towards a definite development of an 'on-line,' automated instrument for measurement of ammonia concentrations.

References

1. W.Demtröder, Laser Spectroscopy, Springer Series in Chemical Physics Vol.5, New York (1982).
2. F.J.M.Harren, F.G.C.Bijnen, J.Reuss, L.A.C.J.Voesenek and C.W.P.M.Blom, Appl.Phys.B, **50**, 137-144, (1990).

Summary

One of the causes of the acidification of the environment are high ammonia (NH_3) emission rates. In environmental research it is an impetus to measure the ammonia concentration sufficiently accurate and fast. This thesis describes the development, construction and testing of a $^{12}C^{16}O_2$ laser photoacoustic monitor for trace detection of ambient ammonia. It is for the first time that hyphenated photoacoustics has been applied to the direct detection of ambient ammonia.

The difficulties met in the practice with NH_3 monitors based on chemical or physical-chemical detection has stimulated the research towards the development of a monitor based on physical detection principles.

Gas-phase photoacoustic spectroscopy has proven a sensitive and feasible technique for detection of pollutants. Owing to the availability of powerful, collimated, monochromatic and tunable light sources (such as the CO_2 (waveguide) laser) the detection of trace gases at ppbv and even at pptv levels appears within reach.

Although a sensitive technique, classical photoacoustic spectroscopy is limited by the complex interpretation and additive character of signal resulting from spectral interferences (when dealing with mixtures), occurring in the wavelength region of the emitting light source. Especially in the infrared (2-20 μm), molecular fingerprints of important trace gas molecules frequently overlap or are masked by water vapor and carbon dioxide absorption. Spectral interference from the previously mentioned and largely abundant ambient species impedes the unique determination of ambient ammonia in the $^{12}C^{16}O_2$ laser emission frequency region.

Using the Stark effect induced in ammonia and subsequent detection of the generated photoacoustic signal at the sum and difference sidebands of the modulated laser and Stark electric fields, detection of ammonia at trace levels employing the 10R(8) and 10R(6) CO_2 laser lines has been successfully achieved. The sensitivity of the method was tested in a simulated atmosphere (present limit 2 ppbv NH_3). Although materials exhibiting a low NH_3 adsorption affinity have been used to construct the photoacoustic Stark cell, signal response time of the system is at present limited to 40 sec.

In addition to a brief historical review Chapter 1 contains an outline of the methods used in detecting ammonia. Intrinsic difficulties associated with the different chemical and photoacoustic methods are described, as well as an experimental and theoretical description of the method employed in this thesis (InterModulated PhotoAcoustic Stark Spectroscopy or IMPASS). The theory of infrared rotational-vibrational transitions as well as the Stark effect applied to the case of symmetric rotators exhibiting inversion doubling are presented in Chapter 2. Details of the photoacoustic Stark cell, the three frequency phase-locked loop, progress and improvements made on the $^{12}C^{16}O_2$ waveguide laser as well as a new method for calibrating photoacoustic cells are given in Chapter 3. Experiments performed on detection of ammonia in a closely simulated atmosphere and in realistic air samples are discussed in Chapter 4.

Finally, Chapter 5 presents closing remarks concerning suggestions for improving the performance of the present instrument.

Samenvatting

De verzuring van het milieu is o.a. een gevolg van de grote uitstoot van ammoniak (NH_3). Ten behoeve van het milieu-technisch onderzoek is het van belang de ammoniak concentratie snel en nauwkeurig te kunnen meten. Dit proefschrift beschrijft de ontwikkeling, de bouw en de prestaties van een op fotoakoestische principes gebaseerde ammoniak monitor. Het is voor het eerst dat fotoakoestiek in combinatie met andere fysische technieken wordt gebruikt voor de direkte detectie van atmosferisch ammoniak.

De gevoeligheid en de responstijd van de gebruikelijke NH_3-meetmethoden, gebaseerd op chemisch en fysisch-chemische technieken worden in de praktijk niet toereikend geacht. In het luchtverontreinigingsonderzoek kent ook de traditionele fotoakoestiek zijn beperkingen. Deze beperkingen zijn een gevolg van spectrale interferenties van de verschillende in de atmosfeer aanwezige gassen. In de traditionele fotoakoestiek wordt veelal gebruik gemaakt van een CO_2 laser. De CO_2 laser emitteert electromagnetische straling in het infrarode gebied van 9 tot 11 μm. In dit gebied vertonen naast NH_3 ook H_2O (water) en CO_2 (koolstofdioxide) absorptiebanden. De spectrale overlap van de bovengenoemde moleculen in het emissiegebied van de CO_2 laser bemoeilijkt een rechtstreekse en eenduidige bepaling van de NH_3 concentratie in de buitenlucht. In dit onderzoek worden luchtmonsters door een speciaal ontworpen meetcel gevoerd. In deze cel wordt over het gas een periodiek variërend hoogspanningsveld aangelegd, waardoor het Stark effect in ammoniak optreedt. De $^{12}C^{16}O_2$ laser straling wordt in amplitude gemoduleerd en vervolgens door de cel geleid. De combinatie van het periodiek geïnduceerde Stark effect en de gemoduleerde laser straling leidt tot som- en verschilfrequenties die met een fasegevoelige detector gemeten worden. Deze combinatie wordt InterModulated Photoacoustic Stark Spectroscopy genoemd (IMPASS). De IMPASS techniek onderdrukt de spectrale interferenties en meet de ammoniak concentratie in de buitenlucht rechtstreeks en interferentie-vrij. De IMPASS techniek bereikt in dit onderzoek een gevoeligheid van 2 ppbv NH_3 met een responsietijd van 40 seconden.

Naast een kort historisch overzicht van fotoakoestische metingen aan ammoniak bevat hoofdstuk 1 een algemene beschrijving van verschillende ammoniak detectie methoden. Ook worden de karakteristieke verschillen tussen chemische en fotoakoestische methodieken weergegeven. Tevens wordt de ontwikkelde IMPASS techniek theoretisch en experimenteel beschreven. Hoofdstuk 2 beschrijft de theorie van het Stark effect. Hoofdstuk 3 bespreekt de, details van de speciaal ontworpen fotoakoestische cel, de fase-gelockte loop, en de verbeteringen aangebracht op de $^{12}C^{16}O_2$ laser. Tevens wordt een nieuwe methode voor de ijking van een fotoakoestische cel theoretisch en experimenteel geëvalueerd. Hoofdstuk 4 bevat verscheidene publicaties van de IMPASS metingen aan ammoniak in een nagebootste atmosfeer en rechtstreeks in de buitenlucht.

Het laatste hoofdstuk geeft suggesties met betrekking tot toekomstige verbeteringen van de ontwikkelde monitor.

Curriculum Vitae

Johannes Joseph Anna Maria (Hans) Sauren was born in Simpelveld (province Limburg), The Netherlands, on April 13, 1963. After graduating from "Veluws College" secondary school (Atheneum B), Apeldoorn, he studied physics at the Catholic University in Nijmegen, where he obtained an M.Sc.-degree (majoring in Molecular and Laser physics) in 1987. Thereafter he worked as a research assistant on a governement grant at the Laser Photoacoustic Laboratory in the Department of Agricultural Engineering and Physics, Agricultural University Wageningen, The Netherlands, on the development and testing of a CO_2 laser photoacoustic monitor for the 'on-line' detection of atmospheric ammonia. As a graduate student he has worked at the US Environmental Protection Agency, Research Triangle Park North Carolina, USA, the Ecole Supérieure de Physique et de Chimie Industrielles in Paris, France, and at Cambridge University, England, in order to gain additional theoretical and experimental knowledge in chemical and optical detection of atmospheric pollutants, electrochemistry and laser physics, respectively. From January 1992 he will be working as a post-doctoral researcher in the Department of Chemistry, Queen's University, Kingston, Ontario, Canada. The fellowship is funded by a Centre of Excellence grant from the Natural Sciences and Engineering Research Council of Canada.